1995

Modelling The Motion Of Pulp Inside Wood-chip Disc Refiners

Xiaolin Fan

MODELLING THE MOTION OF PULP INSIDE WOOD-CHIP DISC REFINERS

by

Xiaolin Fan

Department of Applied Mathematics

Submitted in partial fulfillment
of the requirements for the degree of
Doctor of Philosophy

Faculty of Graduate Studies
The University of Western Ontario
London, Ontario
November 1994

ISBN 0-315-99253-0

ABSTRACT

The thesis studies the movement of wood pulp through a rotating disk refiner, by developing continuum and discrete models of the process. An existing continuum model of pulp movement for steady-state refining is first extended to include time-dependent effects, in order to study the dynamic aspects of refining operation. A system of hyperbolic P.D.E.'s is obtained, but it is shown to suffer from numerical instability. Attention is therefore shifted to a discrete model, and a stochastic model treating pulp as discontinuous flocs is developed. The prediction of the residence time distribution of pulp in a refiner is the first test for the model. The model treats pulp as individual flocs moving in three regions inside a refiner: the grooves in the stator, the gap between the plates, and the grooves in the rotor. As the pulp moves through the refiner, it changes regions stochastically. The model calculates the residence time by following each floc individually and then accumulating the results to obtain the distribution of the time. The model is also used to predict the treatment time, that is, the time that pulp spends between the refiner plates. The treatment time distribution shows a non-monotonic rise to a maximum, followed by a non-monotonic decay to zero. Several simple prototype simulations are analyzed to show that the behaviour is not due to errors in the numerical simulation, but is inherent in the class of models used. The model is then extended to a time-dependent one, by keeping track of all flocs in the refiner simultaneously. The fluctuation of the locally averaged densities of pulp inside the refiner are simulated. The trends in the treatment time and the residence time of pulp in the refiner, as well as the correlation between the locally averaged densities and the treatment time are also given. The stochastic model is improved by introducing formulas that calculate the probabilities for flocs to switch regions based on both the locally averaged densities and the densities of pulp flocs

averaged over the refining zone. A new set of residence-time and treatment-time distributions calculated using the probability formulas is given. Finally, the relation between the thrust load on the refiner and the plate gap is predicted by considering the forces supported by a single floc, and a mechanism is found to take into account all the flocs collectively.

To my parents.

ACKNOWLEDGEMENTS

I would like to express my sincere gratitude to all those who have assisted me during the course of this research. In particular, I felt indebted to the followings:

First, Prof. D. J. Jeffrey has always been an inspiration, and I really appreciate the opportunity to work under his guidance. His patience and encouragement, both for the research and the preparation of the thesis were invaluable. His enthusiasm and pursuance for knowledge set an example for me to follow. I would also thank him for the financial support since 1988.

Dr. D. Ouellet, in the Pulp and Paper Centre of UBC, has also been a great assistance especially for developing the stochastic models. As a matter of fact, without his cooperation, the new modelling would have not gone this far. I especially appreciate the numerous E-mail discussions with him, and admire his serious attitude towards academic work. I also cherish the friendship developed during the last two years of 'networking' for the Phase I of the Networks of Centres of Excellence (NCE) program under the Natural Sciences and Engineering Council of Canada (1989–1993).

It was pleasure to work with Dr. D. Stanford, in the Department of Statistical and Actuarial Sciences, in solving the non-monotonic behaviour problem of the treatment time distribution. His contribution to the solution of the problem was acknowledged.

I would thank Prof. A. I. Mcleod, in the Department of Statistical and Actuarial Sciences, for letting me use several his random subroutines to confirm the non-monotonic behaviour of the treatment time distribution.

I would also thank Mr. M. I. Stationwala, from the Pulp and Paper Research Institute of Canada, for letting me use his high-speed photographs to explain the assumptions made in developing the discrete model.

In addition, sincere thanks goes to NCE for providing partial funding of this research, and I appreciate the opportunity and the challenge to work on such an industrial project.

Last, but not the least, it is beyond any words to express my deep appreciation towards my family, particularly my wife Wenqing Liu, for their patience, encouragement and moral support.

TABLE OF CONTENTS

LIST OF TABLES

LIST OF FIGURES

Chapter 1

GENERAL INTRODUCTION

1.1 Pulp and Paper

Paper has traditionally been defined as a felted sheet of fibres formed on a fine screen from a fluid suspension (usually water), and pulp is the suspension containing fibrous raw material for papermaking. Usually, pulp fibres are of vegetable origin, commonly wood, but other materials such as animal, mineral or synthetic fibres may be used for special applications. Paper is an inexpensive product consumed in large quantities, and the pulp and paper industry is one of the largest industries in Canada. The modern pulp and paper industry utilizes lumber residuals as the basic raw material, and is characterized by large capital investment in its production facilities; Paper mills are no longer labour intensive, operations being highly automated.

The manufacture of paper takes place in two stages: the conversion of wood to pulp and the making of paper from pulp. In the first stage, wood is delivered to the mill, either as logs or as chips, for chemical or mechanical pulping. Chemical pulping takes place in large, usually continuous digesters, while mechanical pulping uses either grinders or refiners. The pulp is then cleaned and bleached. The pulp is further treated mechanically in a process known as 'beating', in which the flexibility of fibre is increased and the surface fibrillation is created. After beating, additives such as sizing agent and filler are added to the pulp slurry to improve the paper properties.

Then the beaten pulp is either dried for market or pumped to paper machines, where the sheet of paper is formed, pressed, and dried to the specification.

1.2 Pulping

The three major components of wood are cellulose (45% by weight), hemicellulose (25%-35%) and lignin (21%-25%) [1]. The polymer cellulose determines the characteristic of the fibre and permits its use in papermaking, while lignin is an organic glue, which cements the fibres together. Wood consists of fibres in the shape of hollow tubes, and exhibits a number of properties which fulfill the requirements of papermaking. In general, the best balance of papermaking properties occurs when most of the lignin is removed from the fibres while retaining substantial amounts of cellulose fibres. Properties are also greatly optimized by beating or refining, which causes the fibres to hydrate (i.e., pick up water) and swell, increasing their flexibility and bonding power.

The primary purpose of pulping is to separate fibres from each other, and the secondary purpose is to give the fibres optimal properties for their ultimate use. To achieve the two purposes in the most economical way, two main types of pulping processes have been developed [2]: Chemical and Mechanical pulping. The processes produce substantially different fibre characteristics, and the choice between them depends upon the wood species available and the end applications for the pulp produced. A combination of different chemical and mechanical pulping process is used in order to obtain the desired paper quality.

1.2.1 Chemical pulping

Chemical pulping uses a variety of chemicals to degrade and dissolve the lignin which binds the cellulose fibres together, and leave behind most of cellulose and hemicellulose in the form of intact fibres [3]. Usually it is considerably lower in yield than mechanical pulp, but it produces a more compact stronger sheet of paper. It is easily bleached, and the bleached brightness is considerably more stable than what can be obtained

from mechanical pulps. A serious problem is environmental pollution.

1.2.2 Mechanical pulping

Mechanical pulping uses mechanical forces to free cellulose fibre from lignin, and therefore differs from chemical pulping that it does not destroy the lignin [3]. Paper from mechanical pulp absorbs ink easily, rapidly and uniformly, giving it excellent printability. Because of its high yield (almost 100%), mechanical pulp has certain advantages over chemical pulp in areas of huge consumption, such as newsprint. On the other hand, it has undesirable properties such as low strength, harsh fell and lack of permanence, and does not develop strength during beating.

Developments in mechanical pulping, especially Thermal Mechanical Pulping, have improved the strength of the paper, and newer CTMP (Chemical-Thermal Mechanical Pulping) may serve as an adequate substitute for chemical pulping in some area in the near future [3, 4].

1.2.3 Mechanical pulping methods

Mechanical pulps are produced by two different processes: Grinding and Refining. In the grinding process, debarked logs are forced against a revolving abrasive stone, which in part grinds the fibres off the logs and also separates them from the lignin matrix. This happens in a process of compression and release when the stone passes over the individual fibres. In refining, wood chips are fed between two metal discs with at least one of them rotating. The wood fibres are separated by grooves and bars on the surfaces of the two discs acting on wood chips and fibre bundles.

The two types of mechanical pulps are significantly different. The groundwood pulp has a higher content of fine material owing to the abrasive action, whereas the refiner pulp has a smaller content of fine material and long fibres tend to be more ribbon-like. The principle of groundwood pulping is simple, but efficient production of a uniform, good quality pulp requires careful control of stone surface roughness, pressure, shower water temperature and flow rate. While the mechanism governing

refining is more complicated, it can produce a uniform quality of pulp and is more suitable for automation and computer control, thereby reducing labour costs. Furthermore, refiner pulp can use sawdust or hardwood, though not as easily as softwood, as raw material. At present, more than half of the mechanical pulp is made by refining [1] and this can only increase.

1.3 Wood-chip Refiner

Although the refining of chips was started by Asplund in 1931, it was not until the 1950's that work started on the production of papermaking pulp, and the first commercial refiner mechanical pulp (RMP) was produced in 1960 [5, 6]. The three basic types of refiners are schematically shown in Figure 1.1 [3]. In the first, one disc rotates; in the second, a centre disc rotates against two stationary discs; and in the third, the two discs counter rotate.

The plate clearance is of critical importance, with a typical size of the order 0.1 mm, and is accurately controlled by either an electro-mechanical or hydraulic loading system. The material to be refined is introduced by a screw feeder into the open eye of the refiner. As the material moves through the refining zone towards the periphery, the wood mass is progressively broken down into smaller particles and finally into fibres. Water is supplied to the eye of the refiner to control pulp consistency. Sometimes, chemicals are also added to achieve special purposes. Refiners are currently available with plates up to 76 inches in diameter with 30,000 hp of power supplied to each plate [1].

1.3.1 Refiner plate

The discs are faced with plates containing a pattern of bars and grooves. Generally refiner plates can be classified in two categories: first-stage refiner plates and second-stage refiner plates as shown in Figure 1.2. First-stage refiner plates have wide breaker bars close to the eye of the refiner that shred the chips and feed them to the 'refining zone'. The refining zone consists of progressively narrower bars and grooves where the

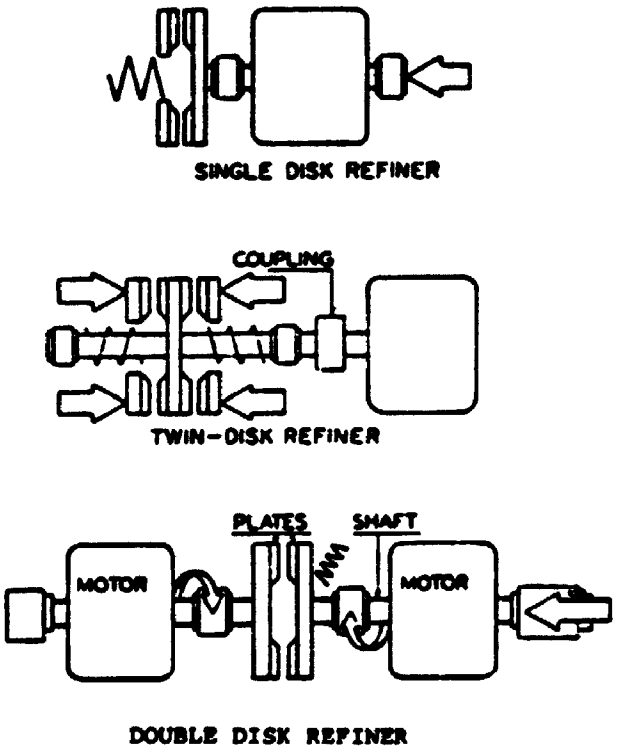

Figure 1.1: Schematic representation of the three most common refiner configurations.

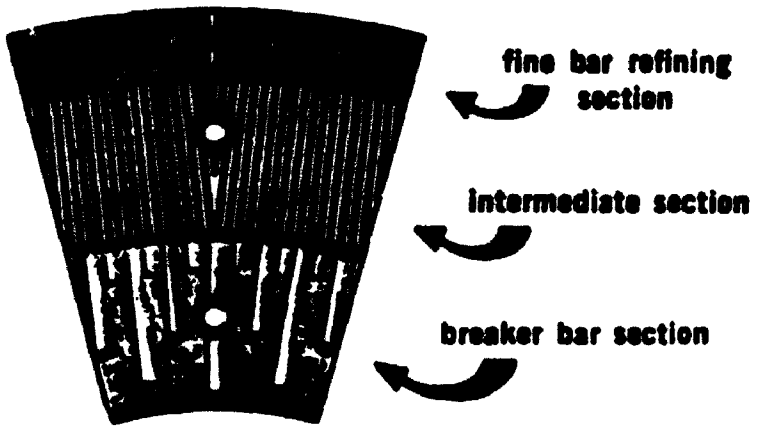

Segment of a disc refiner plate (Sprout Waldron Div., Koppers Co.).

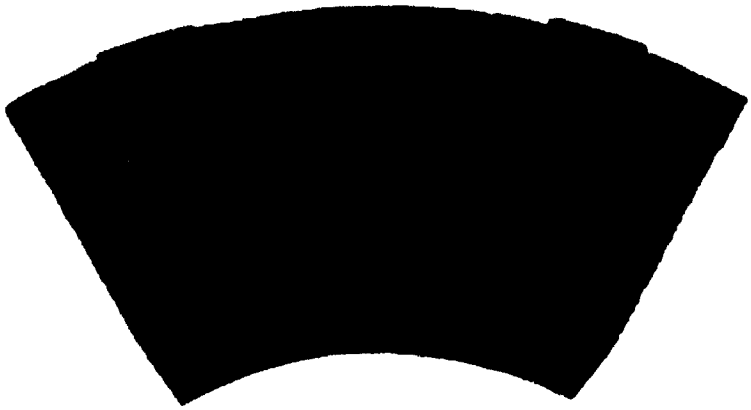

Segment of disc refiner plate (Sunds AB).

Figure 1.2: Typical refiner plates for first (above) and second (below) stage refining.

coarse material is converted to pulp. Usually the plates are tapered slightly (by 0.01 mm/mm or less) to ensure that the pulp moves evenly towards the periphery. Some plates are provided with dams to block the grooves at intervals and force the pulp to move over the bars. Plates may also be made with a peripheral rim to increase the retention time of pulp between the plates.

Second-stage refiner plates usually have a shorter breaker bar section and a larger portion of refining surface. The breaker bars are necessary to align and impart centrifugal force to the partly refined pulp. Figure 1.2 shows a typical first stage plate (above) and second stage plate.

At present, there are no rules for plate design, and it is strictly a method of trial-and-error. Design characters of the refiner plates include: Types of metal or alloy for the plate; Bar and groove dimensions, locations and the number; Dam shape, location and the number; And plate taper. A general refiner plate is shown in Figure 1.3 to define refiner plate terminology [5]. Apparently different demands of pulping methods and quality require different plate patterns. It is assumed that the bars are used to apply pressure to the fibres, while the grooves allow the fibres to expand and the excess steam and water to escape. The taper design depends on a lot of factors and has to be optimized case-by-case, but it is normally less for second-stage refining than for first-stage.

1.4 Control of Refining Process

For acceptable refining to take place, the plate gap between the bars has to be small, on the order of a few fibre diameters. It is observed that water alone can not support a compressive load exerted by refiner plates. When fibres are present in water, the load carrying capacity of the pulp is substantially higher than water alone [7, 8, 9]. As a matter of fact, the load carrying capacity of a refiner is quite enormous during refining. Furthermore, the load carrying capacity of stock to be refined is so high that it actually deforms the refiner plates [10].

There are many variables which affect the chip refining process and pulp quality it

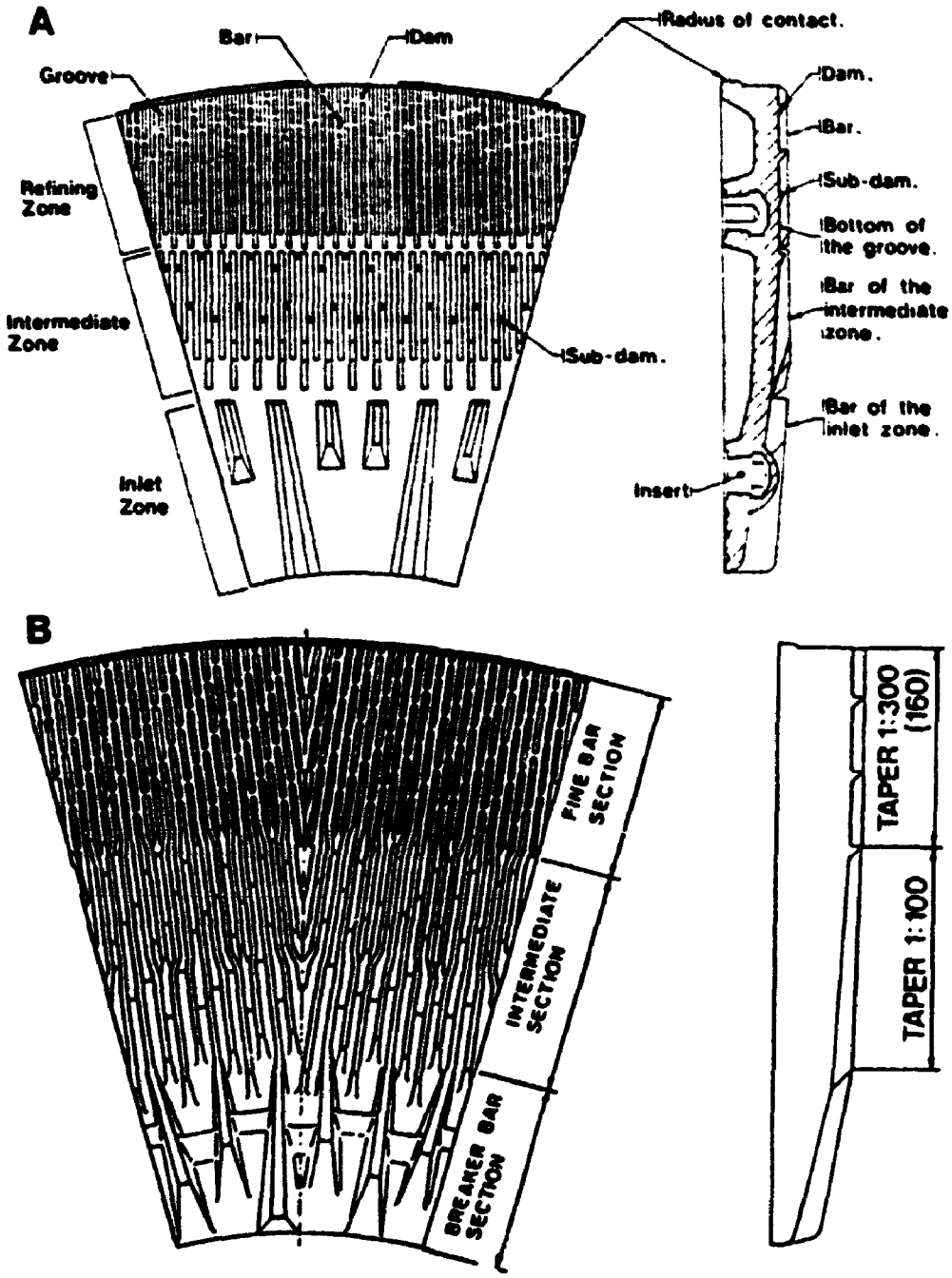

Figure 1.3: Refining plate terminology. A. View of the refining surface; B. Taper.

produces, but only few of them can be actively controlled during refining. Operating variables in refining are defined as the variables which have influence both on pulp quality and refining operation. The control variables mean that they can be directly controlled during the refining operation. According to Stationwala *et al.* [11], there are three primary operating control variables in most types of refiner mechanical pulping processes. They are dilution water rate, throughput and refiner plate gap setting, each of which can be adjusted separately in the process of refining. In turn, these variables, or some combination of them, control discharge consistency, specific energy and motor load, all of which in one way or in another are related to the pulp quality. In fact, these operating variables are interrelated in nature, which contributes another reason why there is no unified theory pertaining to refining process.

To maintain uniform operation, it is important that the steam be freely exhausted from the refining zone. Uneven steam exhaustion relates to 'blowback', which causes interruption of chip flow and corresponds to load fluctuations. Steam pressure development has been found to be affected by most of the operating variables, but is easily controlled by reducing the temperature and consistency of the feed. Chip quality is another important factor to influence the pulp quality, and it should be controlled before the refining stage.

Another important aspect of refining control is to prevent plate-clashing. Usually the pulp pad between the discs counter-balances the applied load and prevents destructive contact of plates. Should the pad break down, due to either process or machine disturbance, plate contact can occur, with resulting damage to the plates and interruption of normal production. Since no theory has been developed to describe the phenomenon, preventing plate-clashing relies only on sensor devices [12].

1.5 Mathematical Models of Refining

Although there are many papers in the literature describing the hypotheses and theories of refining [10, 13, 14, 15, 16, 17, 18, 19], very little work has been done on the theoretical analysis of the refining process, and only in recent years have some

mathematical models of refining been worked out to predict the relations between the parameters involved and pulp quality.

1.5.1 Steam flow models

A preliminary theory on steam flow in a chip refiner was put forward by Dana *et al.* [20]. With some restrictions, this work identified how the development of self-pressurization and steam flow in the refining zone could be predicted. The theoretically predicted level of self-pressurization was found to be only a fraction of that calculated from experimentally measured temperatures in the refining zone.

In recent work, Miles *et al.* incorporated the interaction between steam and pulp into the preliminary steam theory, resulting in a modified steam theory [21]. The new model assumed the pulp to be evenly distributed in the refining zone with the generated steam flowing through the porous pulp pad. By suitably choosing the values of the specific surface area of the pulp inside a refiner, the authors were able to fit the analytical result to practical measurements of the steam distribution within the refiner.

Newman *et al.* has simplified his numerical analysis and his recent modification of the preliminary steam theory appears to provide simplified solutions using more realistic levels of skin friction coefficient than those used earlier and under conditions which include the possibility of the steam attaining supersonic velocity, even though they were not certain whether this condition actually occurs in refining [22]. Predictions, using this newer model, compare favorably with experimental data.

A dynamic model of steam flow was developed by Aarni and Virkkunen [23]. To the best of our knowledge, this is the only modelling done for time-dependent effect of steam flow. It was claimed that the simulation can be used to optimize the operating point of the steady state operation of refining, and to study the effect of control variables on the refining operation. The simulation also showed that the fastest response time of the refiner is of the order of 30 microseconds and the time that a disturbance takes to travel through the refiner is one millisecond. But the model reported lacks some details such as setting of some important parameters, boundary

and initial conditions for the simulation.

1.5.2 Pulp flow (movement) models

Two theoretical models were developed more recently for pulp flow inside a refiner by Miles *et al.*[24] and Fan [25]. Although they interpreted pulp movement differently, the models are very similar in appearance. With some assumptions, the models predicted the pulp velocity profiles along a refiner radius, but no time-dependent effects of pulp flow were included. The features and the differences of the two models will be discussed in more detail later when we extend the current models into a time-dependent model.

1.6 Scope and Aims of the Thesis

This thesis describes a study of the pulp movement inside disc refiners by mathematical modelling and numerical simulations. The work attempts to answer the following questions:

- What is the time-dependent effect on pulp flow (movement)?
- What is the alternative for modelling pulp movement as a continuum?
- Is it possible to incorporate recent experimental observations into a relatively simple, but effective model?
- If such a model can be developed, what is the best example to test the model?
- Can we predict the residence time distribution and the treatment time distribution using the new model?
- How can this model take time-dependent effect of pulp movement?
- Can we relate the probability parameters to the local conditions of pulp movement?
- How can we calculate the forces supported by discontinuous flocs?

The work is presented in the subsequent six chapters.

Chapter 2 describes extending the previous pulp movement model into a time-dependent model without adding more forces. A simple system of hyperbolic partial differential equations is obtained, but instabilities hamper the numerical solutions.

Chapter 3 introduces modelling pulp movement as a discontinuous stochastic process. Predicting residence time distribution is a first test of the model, and some results are given for the numerical simulations of the new model.

Chapter 4 investigates the behaviour of the treatment time distribution found by using the model. The origin of the non-monotonic behaviour is identified by studying a simplified model, and a theoretical explanation is given for this phenomenon.

Chapter 5 deals with the time-dependent stochastic modelling of pulp movement in a refiner. Locally averaged pulp densities are used as an indication of local pulp property variation with time, and correlation between the locally averaged pulp density and the residence time as well as the treatment time are also presented.

Chapter 6 explains the derivation of the formulas that are used to calculate the probability expressions in the model. Several versions of the probability expressions are proposed to relate the probabilities to the averaged pulp densities based on the understanding (or assumptions) of the floc exchange mechanisms. Implementation of the model and some results of numerical simulations are also included.

The final Chapter illustrates the development of the relations among operating variables in refining, in particular, between varieties of the loads and the plate gap. The assumptions for a single floc to behave under repeated compression and relaxation are described, and the mechanism for the total load supported collectively by all the flocs inside refiners is speculated. Some simulation results are given at the end.

The thesis concludes with a section giving summary and contribution to knowledge, suggestions for further work.

Chapter 2

EXTENSION OF THE STEADY-STATE MODEL

2.1 Background

Several theoretical models have been developed describing the steady-state operation of a refiner [20, 21, 22, 24, 25]. One set of calculations has concentrated on the steam flow, largely ignoring the presence of pulp and dilution water except in as much as they justified putting terms in the equations to describe the generation of steam throughout the refiner [20, 21, 22]. A second set of calculations has attempted to model the movement of the pulp between the plates [24, 25]. The word *movement* is used rather than flow, because it is not clear to what extent the pulp does flow. The choice of the words *flow* and *move* is based on whether the internal deformation of the material is assumed to be important. Thus a block of wood *moves* from one place to another because any theoretical treatment will ignore things happening inside the wood. In contrast, water or oil *flows* because we cannot ignore internal processes, i.e., the internal velocity profile. Modern disc refiners operate at very high consistency levels, usually above 40 % (Consistency being defined as the wood fibre weight divided by the total weight of the wood fibre and water). High consistency pulp is considered to be a non-Newtonian fluid with a very high viscosity, if it is treated using the standard ideas of fluid mechanics [26]. To include equations for such flow in any model would make solution very cumbersome and time consuming and yet might return little in improving the agreement between theory and experiment.

Our first work has been a steady-state study of pulp movement in a refiner [25]. By assuming that the refiner is working with constant input and motor load, we

can exclude time-dependent terms from the equations and obtain a relatively simple solution. The difficulty with this strategy is that, because we have simplified the situation so much, the predictions available from such a model are inherently few. The model is basically not accurate enough to warrant making a quantitative comparison between the theory and experiment.

To extend the previous model, we have focused on generalizing the model to include time-dependent effects. The behaviour of a refiner under varying loads and inputs is important in its own right, because it is the basis of refiner control. The inclusion of time variation also opens up many useful possibilities for comparison between theory and experiment. Some of the behaviour of a refiner has a qualitative aspect that can be studied independently of the accuracy of individual numerical predictions. For example, pulp-pad collapse and the subsequent danger of plate clashing is something that requires an explanation in qualitative terms. At present, pulp-pad collapse is a condition that is *detected* by control programs but not explained.

To derive a set of equations that can model the movement of pulp inside a refiner, we must start with a mental picture of what is going on between the plates.

2.2 Basic Assumptions

The first assumption we would like to make is that the variations of pulp movement in the tangential direction are negligible due to the obvious symmetrical structure of the refiner disks. Fox *et al.* [27] observed that in a model refiner, the flow patterns in the tangential direction around the periphery are similar except near the exit area. Thus our model is axisymmetric in that all quantities vary only with r, the radial distance from the centre of the discs.

Pulp movement is assumed to be mainly confined to the grooves of the refiner plates, as has been observed in the high-speed ciné films and photographs of the refiner [28, 29]. The refining action is assumed to be concentrated on the bars and is the result of relatively small amounts of pulp being stapled on the bars for a short period of time. Thus the model takes the pulp in the grooves of refiner plates into

consideration while ignoring the pulp between the plates.

We shall lump the wood and water together as a single phase characterized by a velocity and a consistency. The steam will be a separate, second phase with its own velocity and density.

The hydraulic load is assumed to be uniformly distributed in the refining zone, and shared by the steam pressure and the pulp confined in the grooves. The pulp compressed between the refiner plates is ignored at the moment because of the small quantity of pulp compared with that inside the grooves.

2.3 Derivation of Governing Equations

We consider a plate containing a simple type of bar pattern. Let depth of grooves d and width w be constants with respect to radius r. Then the total number of grooves will increase towards periphery. The total number of grooves can be expressed as $n = \alpha 2\pi r/w$, where α is a fixed parameter to represent the width ratio of bars and grooves.

We now use cylindrical coordinates outlined in Figure 2.1, and consider an element ring of pulp in the refining zone. The governing equations consist of conservation of wood material in the element ring and conservation of momentum in the same element. The schematics of the pulp element in the refiner is shown in Figure 2.2.

2.3.1 Continuity equation (mass conservation of wood)

The amount of wood material in a unit volume is $(c\rho)$, where c is pulp consistency and ρ pulp density. Thus the conservation of wood in the element results in the following equation:

$$\frac{\partial}{\partial t}(c\rho) + \frac{1}{r}\frac{\partial}{\partial r}(c\rho r u) + \frac{1}{r}\frac{\partial}{\partial \theta}(c\rho v) + \frac{\partial}{\partial z}(c\rho w) = 0 \tag{2.1}$$

where v and w are pulp velocities in the directions of θ and z. If we ignore cross flow and tangential flow, i.e., $w = 0$ and $v = 0$, we end up with the following equation:

$$\frac{\partial}{\partial t}(c\rho) + \frac{1}{r}\frac{\partial}{\partial r}(c\rho r u) = 0. \tag{2.2}$$

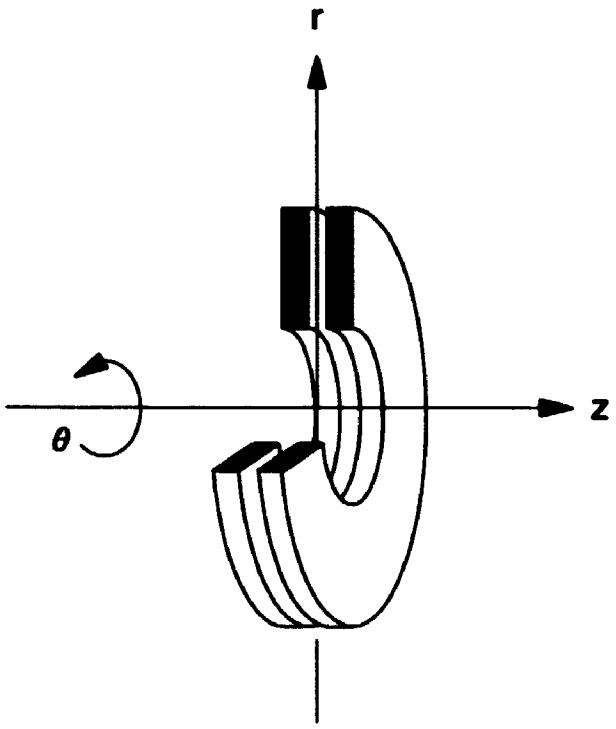

Figure 2.1: Cylindrical coordinates used for modelling of a disk refiner.

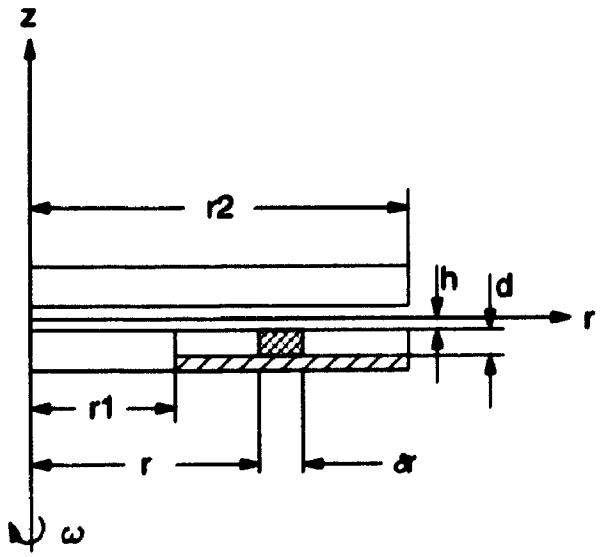

Figure 2.2: Schematics of a pulp element inside the grooves of the refiner.

Based on a sensitivity analysis of the dynamic model of steam flow [23], it was concluded that the effect of the consistency on dynamic operation of refining is insignificant. Also consistency was known to have a slowly increasing profile with respect to the refining radius r, as a result of water evaporation along r [23, 24]. Therefore, we approximate the pulp consistency $c = c(r)$ as linear along the refining zone radius r. In particular, we let $c = c_1 + b_1(r - r_1)$ where c_1 is inlet consistency and b_1 is a constant so that $dc/dr = b_1$. We have

$$\frac{\partial \rho}{\partial t} + \frac{\rho u}{c} b_1 + \frac{1}{r}\frac{\partial}{\partial r}(\rho r u) = 0 \tag{2.3}$$

where u is the pulp velocity. We see that pulp in the element is not conserved due to the fact that water evaporates inside a refiner at the rate of $(-\rho u b_1/c)$.

2.3.2 Conservation of momentum

To obtain an equation describing the force balance on the pulp, four possible forces should be considered.

1). Centrifugal Force

The force on the pulp element ring is

$$\delta F_\omega = (\delta m)\omega^2 r = \alpha 2\pi r d \cdot \delta r \rho \omega^2 r \tag{2.4}$$

where δr is the radial length of the element ring and ω is angular velocity of rotating discs.

2). Friction

Coulombic friction is assumed to exist between the pulp and groove. The friction force for the pulp element ring is

$$\delta F_c = \mu P_p \delta A = \mu P_p \delta r (2d + w)\frac{2\pi r d}{w} \tag{2.5}$$

where μ is friction coefficient between pulp and groove, and P_p is the internal pressure of pulp.

3). Pressure Gradients within the Pulp

If the outlet of the refiner is obstructed, it is obvious that the wood can not be fed into the refiner. The mechanism that would prevent the feeding would be the greater pressure inside the pulp resisting the pressure of the pulp being pushed. In a less extreme way, it is expected that the constriction at the fine-bar section would make itself felt in the dynamics of the pulp by creating a higher pressure there, building up a pressure gradient within the pulp. This force is hard to represent because we have little information about internal pressure distribution and compression characteristics of moving pulp. At the present time it does not appear to be an essential component of the model and will be neglected.

4). Steam Drag on Pulp

The magnitude of this quantity is also hard to assess, since it is not clear whether the steam flows through the pulp in the grooves or only through the pulp trapped between the plates. As with item 3) above, the steam force does not seem to be essential to the model, because the pulp clearly moves outwards to the steam pressure maximum in spite of having to move against the steam flow. Physically, this means that we model a non-pressurized small size refiner. The steam flow will obviously reduce the pulp velocity to some extent as it approaches the pressure maximum and increase it as it leaves.

Thus we take the first two contributions which involve simple mechanisms into consideration for the model, ignoring the last two contributions at the moment. It is unlikely that any new qualitative effect will emerge. Obviously, quantitative predictions will benefit from these ignored terms.

Now the momentum of the element of pulp is $\alpha 2\pi r d \cdot \delta r \rho u$, and the rate of change will be

$$\frac{D}{Dt} = \frac{\partial}{\partial t} + u \cdot \nabla = \frac{\partial}{\partial t} + u\frac{\partial}{\partial r} + \frac{v}{r}\frac{\partial}{\partial \theta} + w\frac{\partial}{\partial z}. \tag{2.6}$$

After taking into account the assumptions that $v = 0$ and $w = 0$, we get simplified form of the above equation:

$$\frac{D}{Dt}(\alpha 2\pi r d \cdot \delta r \rho u) = \frac{\partial}{\partial t}(\alpha 2\pi r d \cdot \delta r \rho u) + u\frac{\partial}{\partial r}(\alpha 2\pi r d \cdot \delta r \rho u). \tag{2.7}$$

Therefore, the force balance for the element of pulp is

$$\frac{\partial}{\partial t}(\alpha 2\pi r d\cdot\delta r\rho u)+u\frac{\partial}{\partial r}(\alpha 2\pi r d\cdot\delta r\rho u)=\alpha 2\pi r d\cdot\delta r\rho\omega^2 r-\mu P_p\delta r(1+2\frac{d}{w})2\pi r\alpha. \quad (2.8)$$

Then, after simplification we obtain

$$\frac{\partial}{\partial t}(\rho u)+\frac{u}{r}\frac{\partial}{\partial r}(r\rho u)=\rho\omega^2 r-\mu P_p\lambda, \quad (2.9)$$

where $\lambda = 1/d + 2/w$.

2.4 Equations in Matrix Form

Now if we substitute Equation (2.3)$\times u$ into Equation (2.9) and simplify Equation (2.3), we are able to obtain the system of equations governing the pulp movement in a refiner:

$$\frac{\partial\rho}{\partial t}+u\frac{\partial\rho}{\partial r}+\rho\frac{\partial u}{\partial r}+\frac{\rho u}{r}+\frac{\rho u}{c}b_1=0 \quad (2.10)$$

$$\frac{\partial u}{\partial t}-\frac{u^2}{c}b_1-\omega^2 r+\frac{\mu P_p\lambda}{\rho}=0. \quad (2.11)$$

The above equations can be rearranged into matrix form:

$$A_{ij}\frac{\partial u_j}{\partial t}+a_{ij}\frac{\partial u_j}{\partial r}+b_i=0, \quad (2.12)$$

or

$$\vec{A}\frac{\partial\vec{u}}{\partial t}+\vec{a}\frac{\partial\vec{u}}{\partial r}+\vec{b}=\vec{0}, \quad (2.13)$$

where in our case, $\vec{A}=\begin{bmatrix}1&0\\0&1\end{bmatrix}=\vec{I}$, $\vec{a}=\begin{bmatrix}u&\rho\\0&0\end{bmatrix}$, $\vec{u}=\begin{bmatrix}\rho\\u\end{bmatrix}$,

and $\vec{b}=\begin{bmatrix}\frac{\rho u}{r}+\frac{\rho u}{c}b_1\\-\frac{u^2}{c}b_1-\omega^2 r+\frac{\mu P_p\lambda}{\rho}\end{bmatrix}$.

Because the 2×2 coefficient matrix $\vec{a}$ has 2 real and distinct eigenvalues for all possible solutions of the system (2.13), then (2.13) is said to be hyperbolic type [30], or is classified as first order hyperbolic system with two independent variables [31].

The system is also called quasi-linear hyperbolic due to the fact that the coefficient matrix $\vec{a}$ is in the form of $\vec{a} = \vec{a}(\vec{u}, r, t)$ only, and independent of the derivatives of $\vec{u}$. According to [31, 32], the characteristic form of the above matrix system is

$$l_i \frac{du_i}{dt} + l_i b_i = 0 \qquad \text{on} \quad \frac{dr}{dt} = C \tag{2.14}$$

where l_i is the left eigenvector of coefficient matrix $\vec{a}$, while C is governed by the characteristic equation $l_i a_{ij} = l_j C$, or $|a_{ij} - C\delta_{ij}| = 0$,

i.e.,

$$\begin{vmatrix} u - C & \rho \\ 0 & -C \end{vmatrix} = 0, \tag{2.15}$$

which yields

$$(u - C)(-C) = 0. \tag{2.16}$$

Solving the above equation, we obtain the eigenvalues of the coefficient matrix $\vec{a}$ to be, $C = 0$ and $C = u$, which are the characteristic lines of the hyperbolic system.

1). Along characteristic line $C = 0$

The left eigenvector $\vec{l}$ is obtained by substituting $C = 0$ into the characteristic equation, i.e.,

$$\vec{l}(\vec{a} - C) = \vec{0}, \tag{2.17}$$

or

$$[l_1, l_2] \begin{bmatrix} u & \rho \\ 0 & 0 \end{bmatrix} = [0, 0]. \tag{2.18}$$

We solve the above matrix equation and put $\vec{l}$ into orthonormal form $\vec{l} = [0, 1]$. The resulting equations along the characteristic line $C = 0$ are

$$\frac{du}{dt} - \frac{u^2}{c} b_1 - \omega^2 r + \frac{\mu P_p \lambda}{\rho} = 0 \qquad \text{on} \quad \frac{dr}{dt} = 0. \tag{2.19}$$

2). Along the Characteristic Line $C = u$

Following the same steps used in 1), we are able to obtain the left eigenvector $\vec{l} = [1, \rho/u]$, and the resulting equations are

$$\frac{d\rho}{dt} + \frac{\rho}{u}\frac{du}{dt} + \frac{\rho u}{r} + \frac{\rho u}{c} b_1 + \frac{\rho}{u}\left(-\frac{u^2}{c} b_1 - \omega^2 + \frac{\mu P_p \lambda}{\rho}\right) = 0 \qquad \text{on} \quad \frac{dr}{dt} = u. \tag{2.20}$$

2.5 Solution Methods

There is no analytical solution for this system of hyperbolic equations. Thus a numerical scheme has to be employed to get a solution.

1). Method of Characteristics

The basic rationale underlying the use of characteristics is that by an appropriate choice of coordinates, the original system of hyperbolic first order P.D.E.'s can be replaced by a system expressed in characteristic coordinates. These are the 'natural' coordinates of the system in which P.D.E.'s reduce to O.D.E.'s. A knowledge of the characteristics is also important to the understanding of discontinuity and shocks present within the solution domain [33, 36]. This method involves two steps: The first is to locate the characteristic curves; and the second is to integrate the O.D.E.'s along the characteristic lines. The key for this method to be successful is the complexity of the characteristics concerned. For example, if the characteristic curves are straight lines, it is fairly easy to construct the characteristic coordinates. In our case, one of the characteristics is $C = u$ which is unknown, therefore it is not appropriate to use this method to build grids of characteristic coordinates for the numerical solution.

2). Finite Difference Method

The method of integrating along characteristics is usually the most accurate and convenient. However, for the hyperbolic system of no great complexity, whose solution is known to be well behaved, we can alternatively employ finite difference procedures. For the finite difference methods to be useful, we must take into account the characteristics of the system [35]. Since we do not know the behavior of the hyperbolic system, this method is also not practical.

3). 'Hybrid' Method

As the name suggests, 'hybrid' method is the one that uses characteristics method as a basis and then interpolates the results into spatial distributions of the dependent variables at a fixed time step. The method has the advantage of attempting to follow the characteristics as closely as possible (depending on the scheme for the interpolation) [34, 35]. Thus this method was chosen to perform the numerical solution for

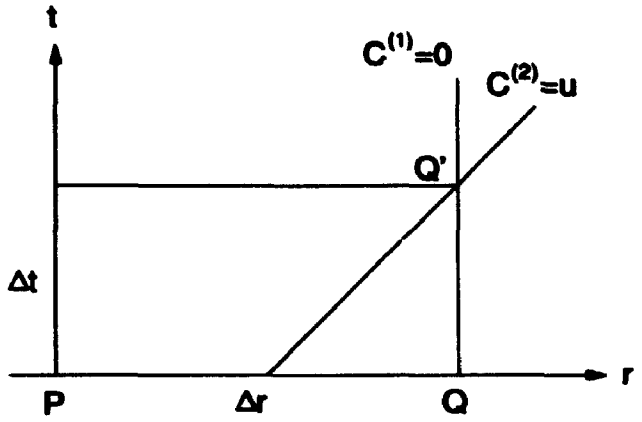

Figure 2.3: Layout of grid points for the numerical scheme.

the first order hyperbolic system.

2.6 Numerical Scheme

The numerical scheme is due to Courant *et al.* [38] and explained in detail by Jeffrey and Taniuti [37]. Their method has the advantage of being straight forward and general in its application, which is appropriate to the numerical solution for our hyperbolic system. The scheme is applicable to initial and boundary value problems for quasi-linear hyperbolic system in two independent variables.

The scheme uses a rectangular grid for time and space variables advancing from time t to $(t + \Delta t)$ by interpolating the results based on the characteristics of the hyperbolic system. The details are the following: Suppose that we know the solution up to time t with known grid point P and Q in Figure 2.3, and we want to advance the solution to Q' which corresponds to time $(t + \Delta t)$. The numerical scheme in matrix form is

$$\vec{l}^{(i)}(Q)\left[\frac{\vec{u}(Q') - \vec{u}(Q)}{\Delta t} + C^{(i)}(Q)\frac{\vec{u}(Q) - \vec{u}(P)}{\Delta r}\right] + \vec{l}^{(i)}(Q)\vec{b}(Q) = 0 \qquad (2.21)$$

where i is the index to indicate ith characteristic line, and in our case i is equal to 1 or 2.

To ensure that the domain of dependence of grid point Q' is contained between segment PQ, we have to select Δt and Δr such that all the characteristic lines through Q' when traced backwards in time intersect the line between grid point P and Q. This condition requires that the gradients of each of the characteristics at Q' should be bounded by the rays $Q'P$ and $Q'Q$. Or this may be expressed by the condition that

$$\max\left|C^{(i)}(Q')\right| < \frac{\Delta r}{\Delta t}, \qquad i = 1, 2 \tag{2.22}$$

for all points Q' under consideration. In our case the above condition becomes

$$|u| < \frac{\Delta r}{\Delta t}. \tag{2.23}$$

The convergence of the discrete valued vector $\vec{u}$ to the differentiable solution of the hyperbolic system as Δr and Δt tend to zero subject to condition (2.22) has also been established by Jeffrey *et al.* [37].

1). For $\vec{l}^{(1)} = [0, 1]$ and $C^{(1)} = 0$

Substituting the above relations into Equation (2.21), we get the numerical formula for u to advance from grid points P and Q to a new point Q'

$$u_{Q'} = u_Q + \Delta t \left[\frac{u^2}{c} b_1 + \omega^2 r - \frac{\mu P_p \lambda}{\rho}\right]_Q \tag{2.24}$$

where subscript Q outside of the square bracket indicates that the variables inside are evaluated at the point Q.

2). For $\vec{l}^{(2)} = [1, \rho/u]$ and $C^{(2)} = u$

We have a similar equation for ρ at point Q'

$$\begin{aligned} \rho_{Q'} \;=\; & 2\rho_Q - \rho_Q \frac{u_{Q'}}{u_Q} - \frac{\Delta t}{\Delta r} u_Q (\rho_Q - \rho_P) \\ & - \frac{\Delta t}{\Delta r} \rho_Q (u_Q - u_P) - \Delta t \left[\frac{\rho u}{r} - \frac{\rho}{u}\omega^2 r + \frac{\mu P_p \lambda}{u}\right]_Q . \end{aligned} \tag{2.25}$$

2.7 Initial and Boundary Conditions

1). Initial Conditions

Suppose that we start the calculation from a steady state of refining operation, i.e., when a refiner has reached the normal operation stage. Since the model is based on the

assumption that the material between the refiner discs is continuous, this assumption is violated before the machine reaches the normal operation stage. Naturally the initial conditions for the numerical scheme are the steady state solutions obtained from the previous model [25]. These are the profiles of u and ρ as functions of refiner radius r.

2). Boundary Conditions

The boundary conditions are based on the previous model for the steady state solution. Then a small change u_{1new} is given to the steady state boundary condition for inlet velocity u_1 to simulate the dynamic effect of changing the feed rate during the operation of refining. Here only the change in u_1 and ρ_1 are considered to be mainly responsible for the feed rate change because consistency is found to be insensitive to the operation of refining by Dana *et al.* [20]. We chose to change u_1 for testing the stability of the system, for the following reasons: First, from the steady state solution, u_1 and ρ_1 have a simple reciprocal relation for a fixed feed rate; Secondly, changing u_1 will result in a simple relation for the numerical scheme at the inlet boundary to start the simulation, so that it is less likely to introduce instabilities at the inlet. For example, from Equation (2.11), we can express ρ_1 in terms of u_1 and $\partial u/\partial t$ at r_1, but if we use ρ_1 to start, that will involve evaluating two more partial derivatives with respect to r in addition to the $\partial \rho/\partial t$ at r_1 to obtain u_1 using Equation (2.10).

2.8 Implementation of the Numerical Scheme

A program was written in Fortran to implement the numerical scheme discussed before. The same basic group of the refiner operating parameters in [25] was used to make relevant comparisons, in which internal pulp pressure is $P_p = 50$ kPa and the friction coefficient $\mu = 0.2$. The program requires three input parameters: u_1 pulp velocity at inlet radius r_1; total number of steps in time N; and increment of u_1 (linearly) as time increasing. The output variables are u and ρ with respect to radius r in different time steps. During a calculation, the values of u and ρ are plotted simultaneously for every 5th time step using the plotting subroutines

developed by Jeffrey [39]. The step sizes of Δr and Δt are chosen by the convergence condition (2.23), and the accuracy of the calculation required. The values of step sizes adopted in the program are: $\Delta r = 1 \times 10^{-3}$ m, and $\Delta t = 2.5 \times 10^{-5}$ s. In the graphs shown below, we chose to show only the results of the u profiles, because we found that for all the cases, the ρ profiles follow the trend of the u profiles closely for both steady and dynamic state simulations.

2.8.1 Steady state simulation

The steady state solution is obtained by using the boundary and initial conditions directly from the previous steady state model [25]. We approximate these profiles using the condition in the steady state that flux of wood is constant, or $\alpha 2\pi r d \cdot c\rho u = F$ where F is the feed rate of wood, or $rc\rho u$ = constant. We know from the solution of the previous model [25] that u is approximately proportional to $1/r$ so that we let $u = u_1 r_1/r$, then pulp density can be expressed as $\rho = \rho_1 c_1/c$, where u_1 and ρ_1 are inlet pulp velocity and pulp density predicted in the previous model.

The results are the steady state profiles of u and ρ as functions of r advanced in time, which are shown (only profiles of u as representatives) in Figures 2.4 to 2.6. A small deviation from the steady state curves is observed for $N = 80$. Then a certain degree of oscillations is observed when the number of time steps is above 80. The oscillations are intensified as N becomes larger. Notice that, for example in Figure 2.4, each line representing a steady profile in 5 time steps apart shifts up a little bit, resulting in an overall much thicker line of a profile except near the r_1. The profiles of ρ are very similar to that of u, and can be seen in Appendix A.

2.8.2 Dynamic state simulation

The largest number of time steps that produces a reasonably stable solution in steady state simulation is adopted to carry out the calculations. For most of the cases, we use total number of time steps $N = 80$. The initial conditions are kept the same as in the steady state solution. But the boundary condition u_1 is changed to u_{1new} to simulate

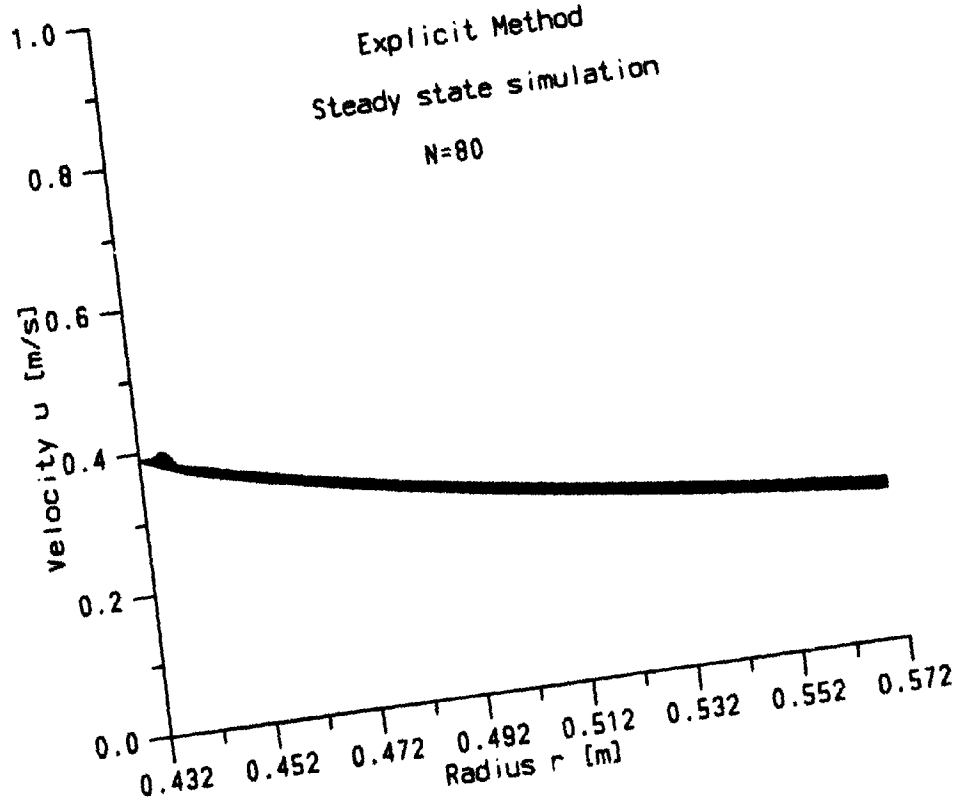

Figure 2.4: Steady state simulation using explicit numerical scheme with total number of time steps $N = 80$.

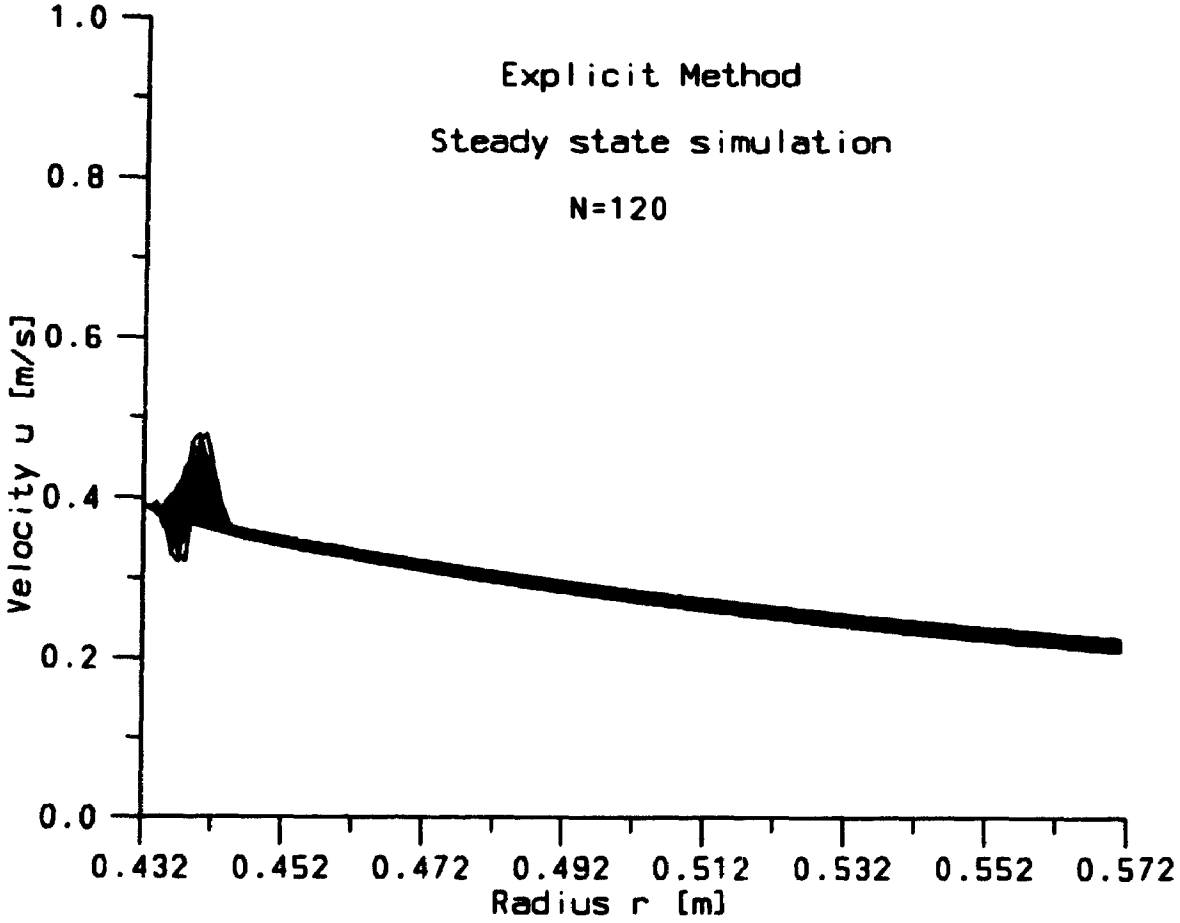

Figure 2.5: Steady state simulation using explicit numerical scheme with total number of time steps $N = 120$.

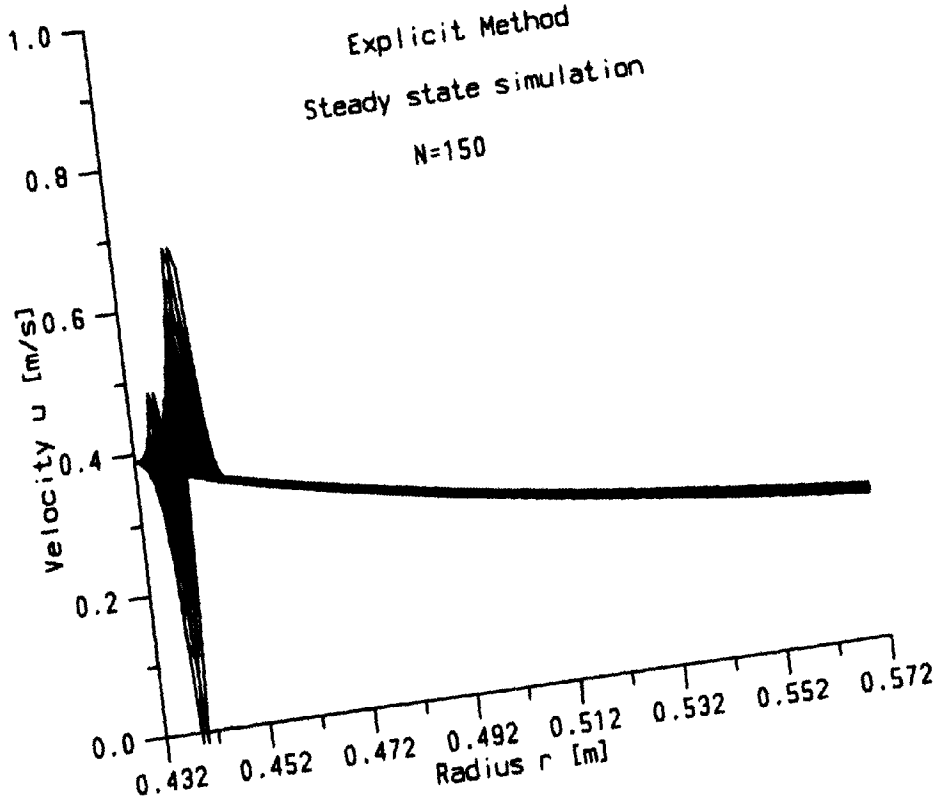

Figure 2.6: Steady state simulation using explicit numerical scheme with total number of time steps $N = 150$.

the situation for the feed rate change. In order to make the change consistent, we also make a corresponding change for ρ_1 to ρ_{1new} according to Equation (2.11) where $\partial u/\partial t$ at r_1 will be approximated by the ways that u_1 is changed to u_{1new} specified.

1). Changing u_1 to u_{1new} in one time step

We change u_1 to u_{1new} in one time step Δt, and $\partial u/\partial t$ at r_1 can be approximated by the following difference equation in the numerical scheme:

$$\left.\frac{\partial u}{\partial t}\right|_{r=r_1} = \frac{u_{1new} - u_1}{\Delta t} . \tag{2.26}$$

Figures 2.7 and 2.8 show that u_{1new} is about ± 0.03 m/s away from the steady state solution $u_1 = 0.39$ m/s. These are the largest changes for u_{1new} that we can give to u_1, since otherwise the oscillations will be simply out of the scale of u in the graphs. We can manage to give u_{1new} a slightly higher value of $u_{1new} = 0.50$ m/s for the case $N = 60$ (Figure 2.9). Here, only the profiles of u with respect to r are shown, because the profiles of ρ follow very similar trends, as can be seen in Appendix A.

2). Changing u_1 to u_{1new} linearly in time steps

The procedure is the same as in 1) except that the boundary condition u_1 is changed linearly over the entire time steps N to u_{1new}. In other words, an increment of Δu_1 is given for each time step so that u_{1new} is equal to $(\Delta u_1 \times N)$. Obviously, $\partial u/\partial t$ at $r = r_1$ can be approximated by $\Delta u_1/\Delta t$. Figures 2.10 to 2.13 show the effects of changing u_1 linearly to u_{1new}. The increment of Δu_1 is from -0.002 to +0.003. Again, the profiles of ρ with respect to r are illustrated in Appendix A.

3). Changing ρ_1 to ρ_{1new}

Similar trends are observed for changing ρ_1 to ρ_{1new}, when compared with the cases of changing u_1 to u_{1new}. But in order to keep the work focused, we put these results into Appendix A.

2.9 Observations

A disturbance is only confined to a small segment of r no matter how large it is (in a range of $r_1 = 0.432$ m to $r = 0.440$ m). Even in the steady state simulations, some unstable deviations occur at time about $T = 2 \times 10^{-3}$ s, and later change to

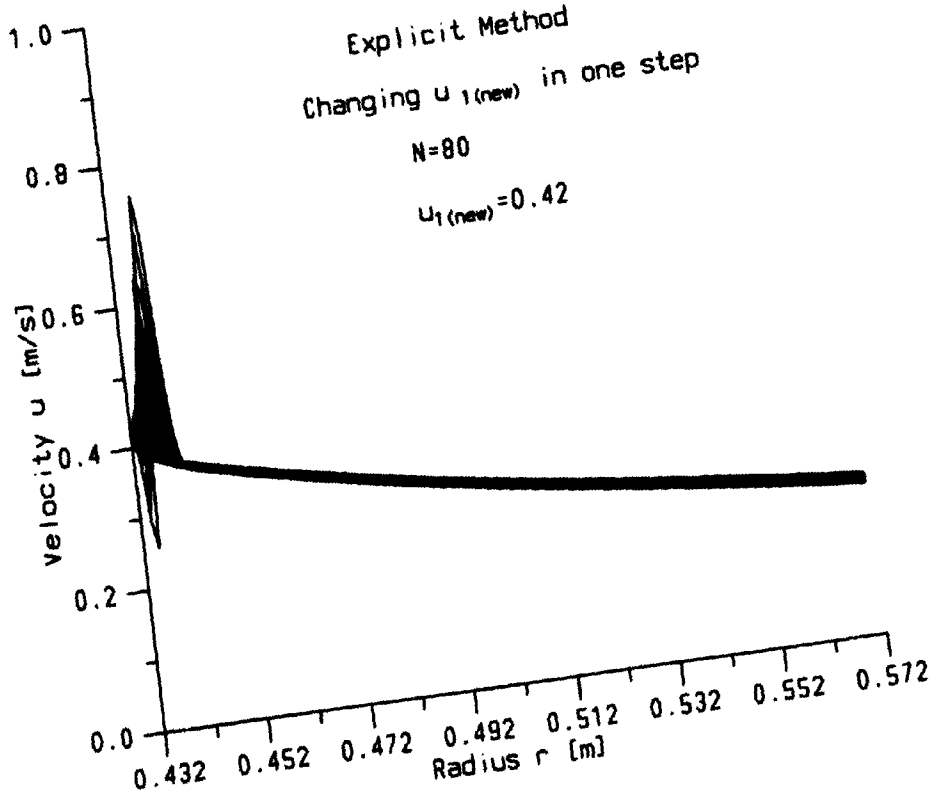

Figure 2.7: Dynamic state simulation using explicit numerical scheme with $u_1 = 0.39$ changed to $u_{1new} = 0.42$ in one step.

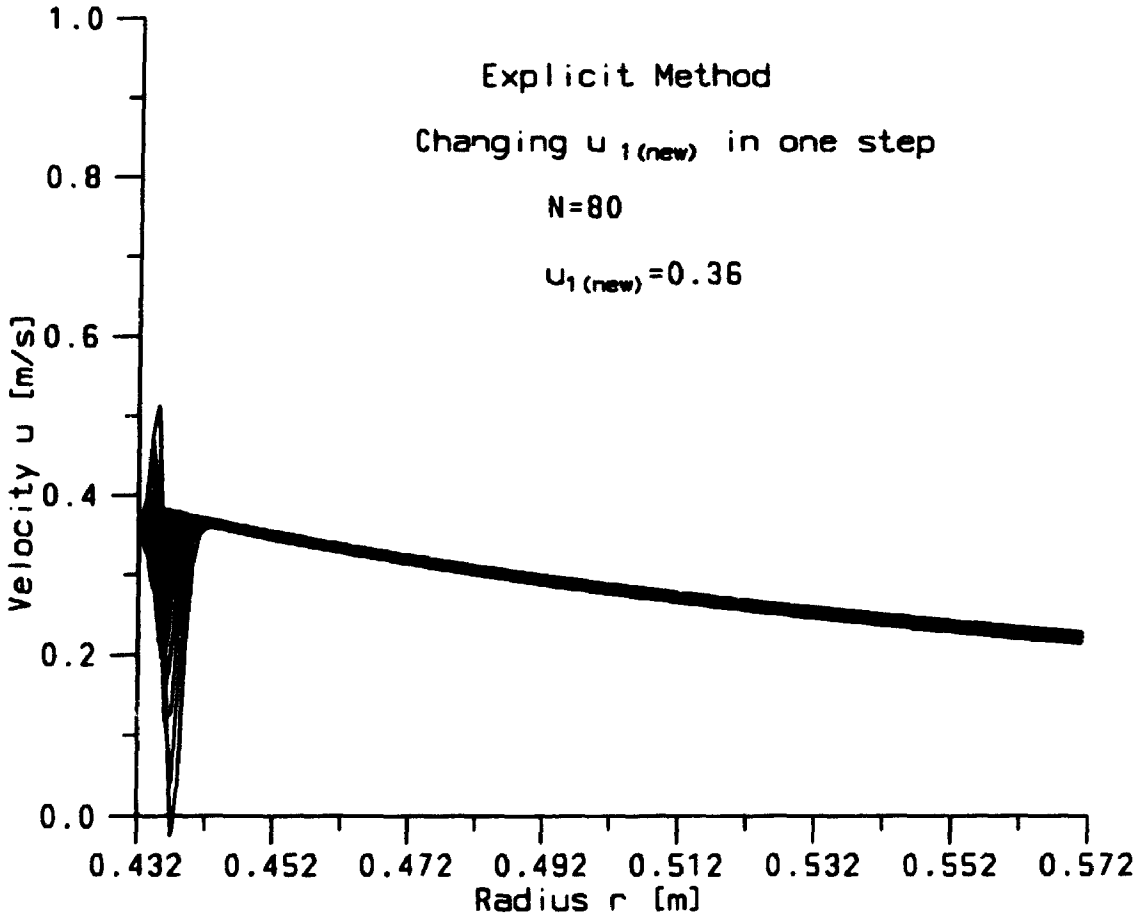

Figure 2.8: Dynamic state simulation using explicit numerical scheme with $u_1 = 0.39$ changed to $u_{1new} = 0.36$ in one step.

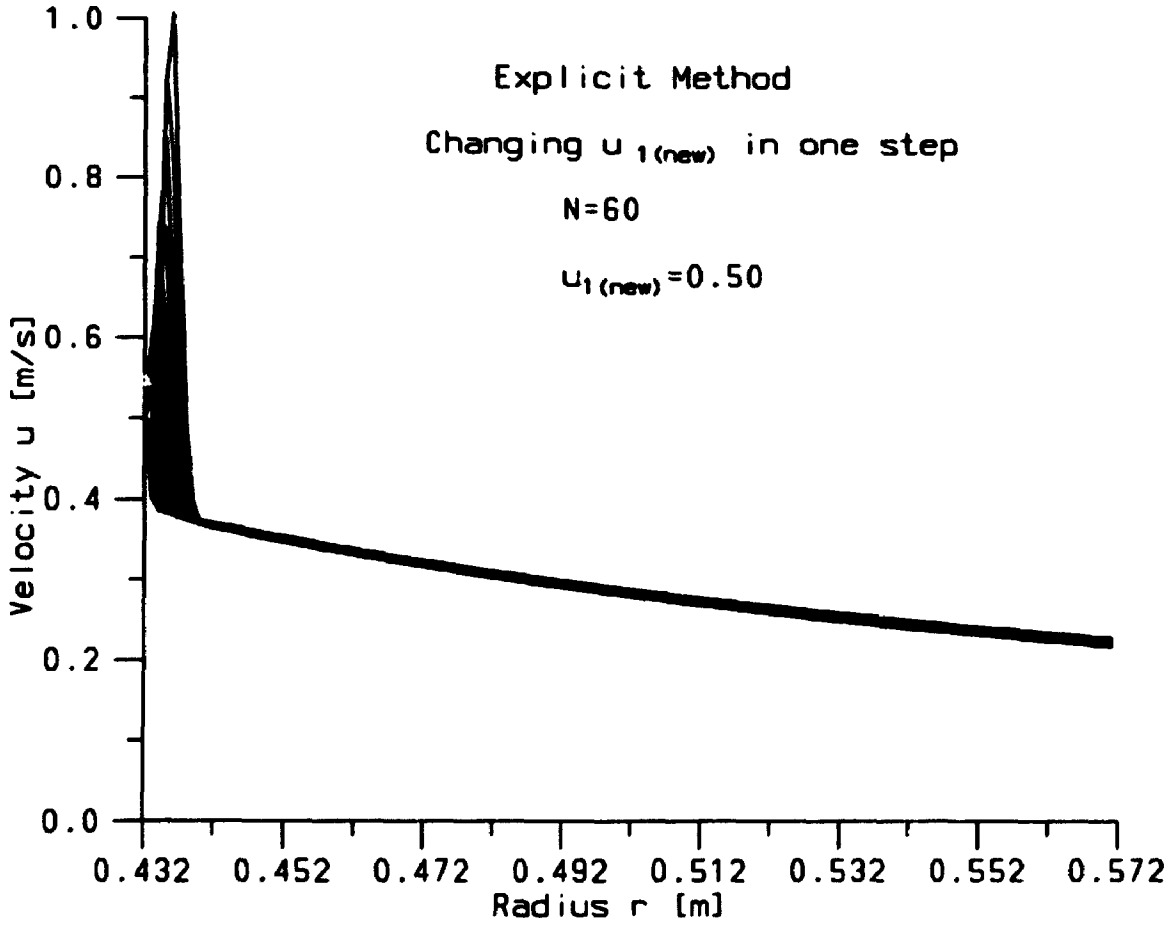

Figure 2.9: Dynamic state simulation using explicit numerical scheme with $u_1 = 0.39$ changed to $u_{1new} = 0.50$ in one step, and $N = 60$.

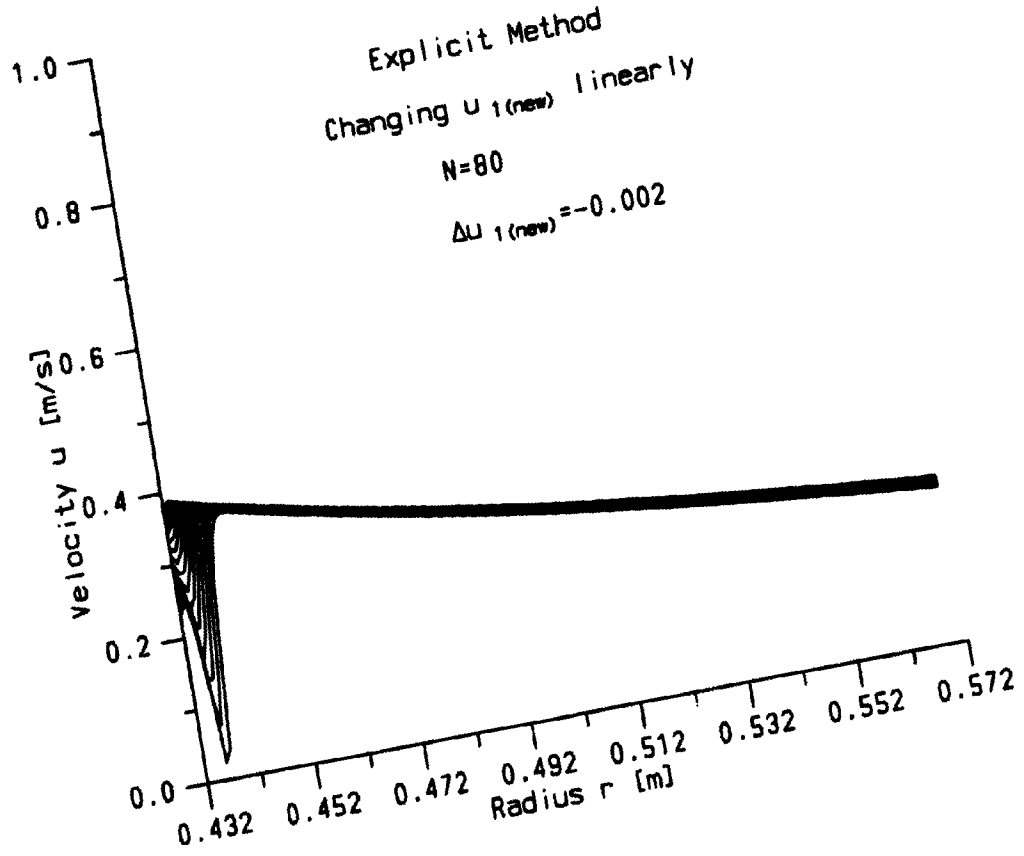

Figure 2.10: Dynamic state simulation using explicit numerical scheme with $u_1 = 0.39$ changed to $u_{1new} = 0.23$ linearly.

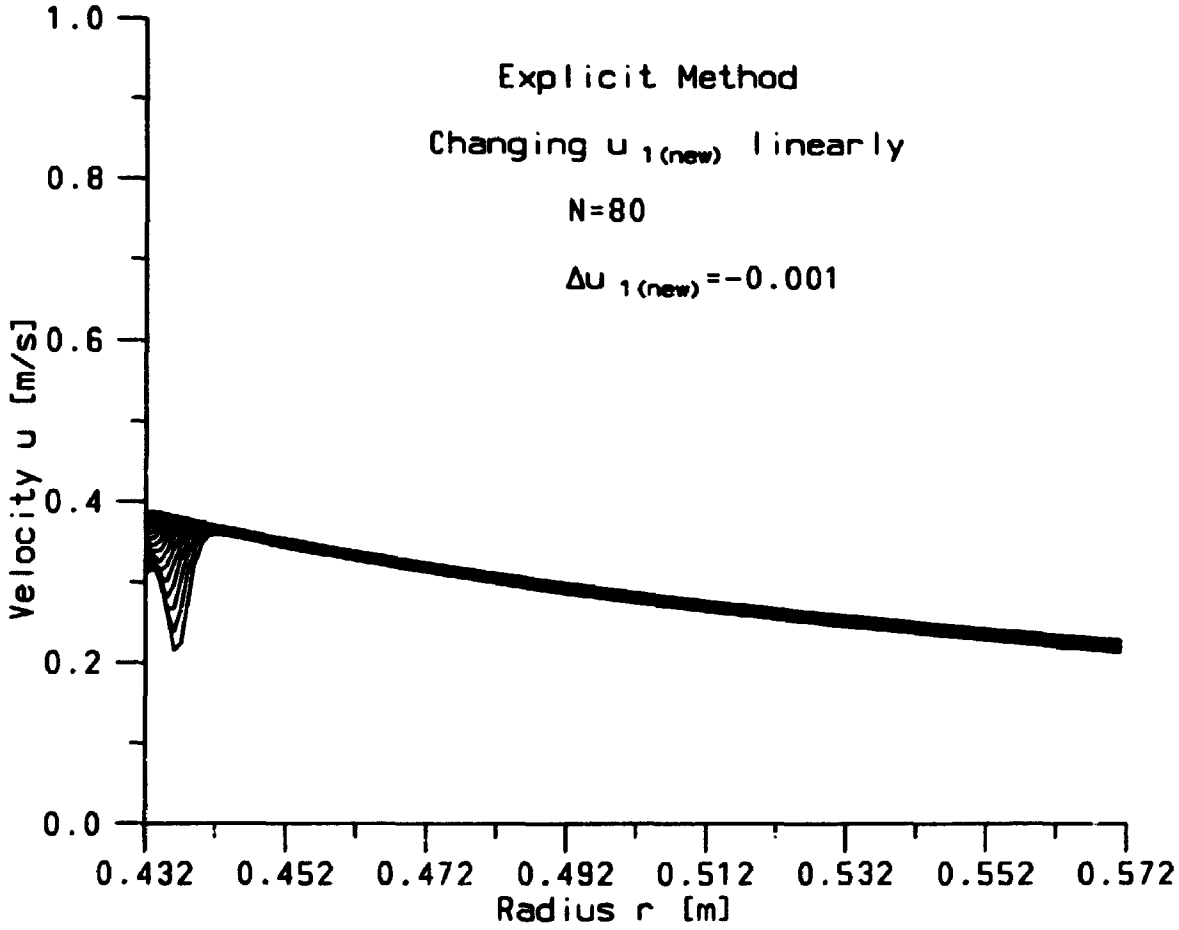

Figure 2.11: Dynamic state simulation using explicit numerical scheme with $u_1 = 0.39$ changed to $u_{1new} = 0.31$ linearly.

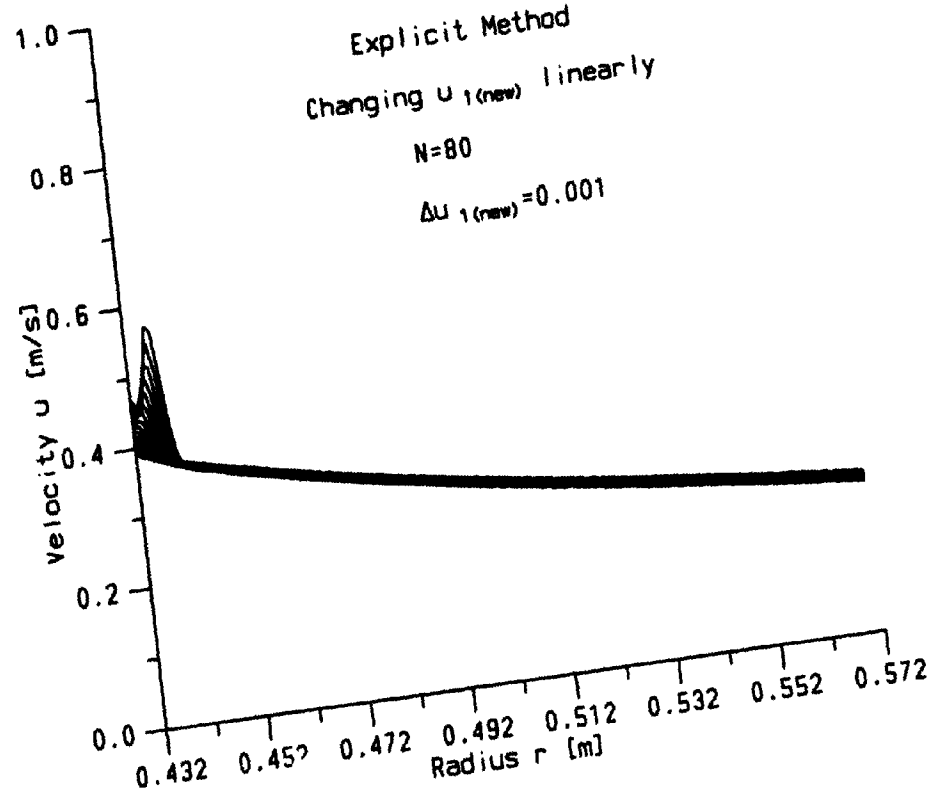

Figure 2.12: Dynamic state simulation using explicit numerical scheme with $u_1 = 0.39$ changed to $u_{1new} = 0.47$ linearly.

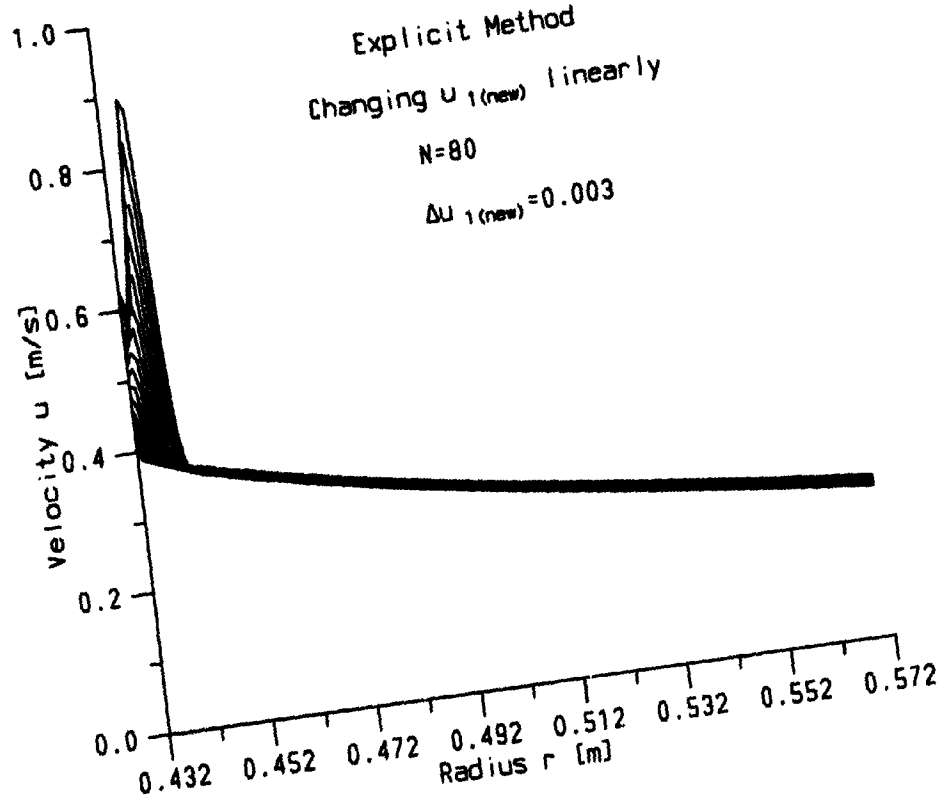

Figure 2.13: Dynamic state simulation using explicit numerical scheme with $u_1 = 0.39$ changed to $u_{1new} = 0.63$ linearly.

oscillations as time advances. The disturbances in the boundary cannot travel along radius r for too far.

The magnitude of u_{1new} is always amplified whether using one step change to u_{1new} or linear change to u_{1new}. But we see that using one step change to u_{1new} causes much more severe oscillations than using linear change to u_{1new}, i.e., linear change to u_{new} gives less degree of disturbance than one step change to u_{1new}. However, using linear change to u_{1new} still predicts that the peak of the disturbance is about twice of the magnitude given in the boundary condition u_{1new}. This means that the system amplifies any disturbances as time advances.

Another phenomenon is observed that the unstable disturbance in the steady state simulation is stronger above the steady state curves, i.e., the centre of oscillations is above the steady state curves. While in both cases of one step change to u_{1new} and linear change to u_{1new}, the disturbances are always one-sided (either above or below the steady state curve) except for the case of using larger time steps. And in both cases, they display a symmetrical pattern about the steady state curves when u_{1new} is larger or smaller than u_1 for the same amount (e.g., Figure 2.11 where $\Delta u_1 = -0.001$ versus Figure 2.12 where $\Delta u_1 = 0.001$).

2.10 Implicit Method to Test the Stability of the System

The numerical method used before is explicit, i.e., in each calculation we solve u and ρ on time $t + \Delta t$ using values of u and ρ in previous 3 points on time t. The explicit method is easy to implement, but has conditions for stability. On the other hand, the implicit method expresses u and ρ of 3 points on time $t + \Delta t$ in term of values of u and ρ at 1 point on time t, and therefore the unknowns of u and ρ on time $t + \Delta t$ are coupled. This method requires special techniques to solve the unknowns in exchange of more favorable stability conditions. Thus, we employ the implicit method to test the stability of the system.

First of all, we discretize the Equations (2.10) and (2.11) in terms of grid point values at i and j (corresponding to variables r and t), resulting in the following finite

difference equations:

$$u_{i,j+1} - \frac{\Delta t(u_{i,j+1})^2 b_1}{c_i} - \Delta t\omega^2 r_i + \frac{\Delta t \mu P_p \lambda}{\rho_{i,j+1}} = u_{i,j}, \tag{2.27}$$

$$\frac{1}{2}ku_{i,j+1}\rho_{i+1,j+1} + [1 + \frac{1}{2}k(u_{i+1,j+1} - u_{i-1,j+1}) + \frac{\Delta t}{r_i}u_{i,j+1} + \frac{\Delta t}{c_i}b_1 u_{i,j+1}]\rho_{i,j+1} - \frac{1}{2}ku_{i,j+1}\rho_{i-1,j+1} = \rho_{i,j} \tag{2.28}$$

where k is the ratio of $\Delta t/\Delta r$.

Suppose we know all the information about time t (at step j), and want to advance our solution to time $t+\Delta t$ (at step $j+1$). The term $\rho_{i,j+1}$ in Equation (2.27) is coupled with Equation (2.28), and $(u_{i,j+1})^2$ in Equation (2.27) is nonlinear. To get a solution, iteration has to be used, where m indicates the mth iteration. In order to break the nonlinear term, we use Newton-Raphson linearization, i.e.,

$$(u_{i,j+1})^2 = 2u^m_{i,j+1}u^{m+1}_{i,j+1} - u^m_{i,j+1}. \tag{2.29}$$

To uncouple the Equations (2.27) and (2.28), we let $\rho_{i,j+1} = \rho_{i,j}$ for $m = 1$, and $\rho^{m+1}_{i,j+1} = \rho^m_{i,j+1}$ in Equation (2.27) for the iterations. Now we start with Equation (2.27) to generate $u^m_{i,j+1}$, then substitute $u^m_{i,j+1}$ into Equation (2.28) using Thomas Algorithm [40] to produce $\rho^m_{i,j+1}$. And we put this $\rho^m_{i,j+1}$ back to Equation (2.27) to start another round of iteration until certain level of accuracy is achieved. In our case, we take $\partial u/\partial r$ at r_1 as an indication of convergence, i.e., when the difference between the previous and current value of $\partial u/\partial r$ at r_1 is less than a set value (10^{-5}) we stop the iteration. The boundary and initial conditions are exactly the same as those used in the explicit method before.

2.10.1 Steady state simulation

Figures 2.14 to 2.16 show the results produced by using the implicit method. From Figure 2.14, we see that using the implicit method predicts almost the same steady state profiles for u compared with those of using the explicit method. The minor difference here is that there is a small disturbance below the steady state profiles as r

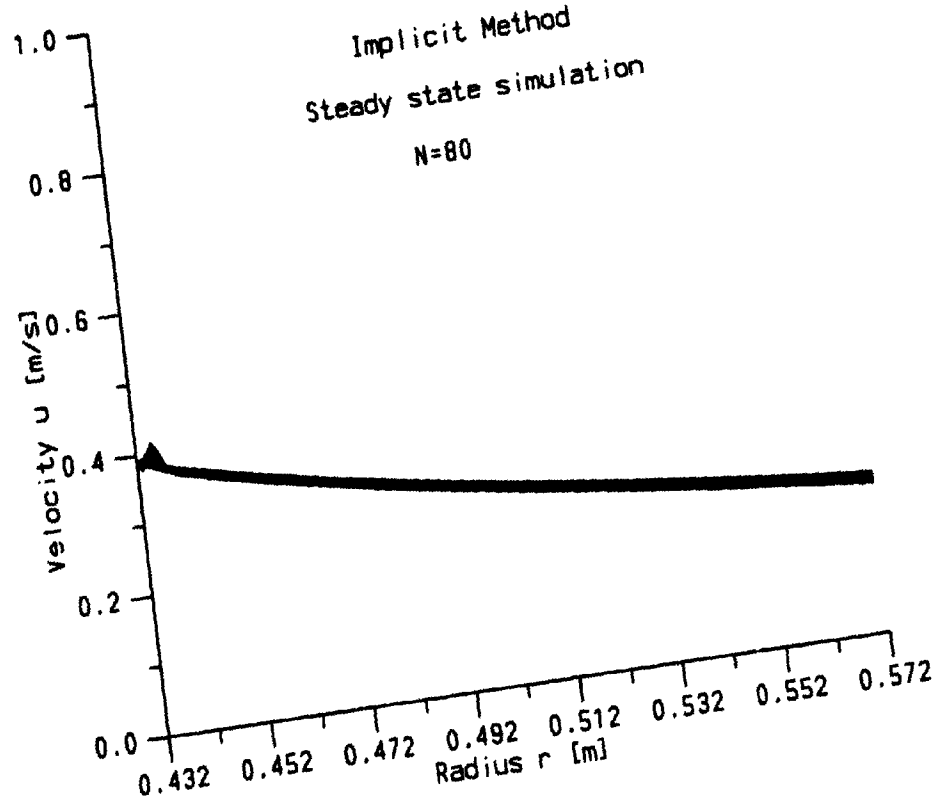

Figure 2.14: Steady state simulation using implicit numerical scheme with total number steps $N = 80$.

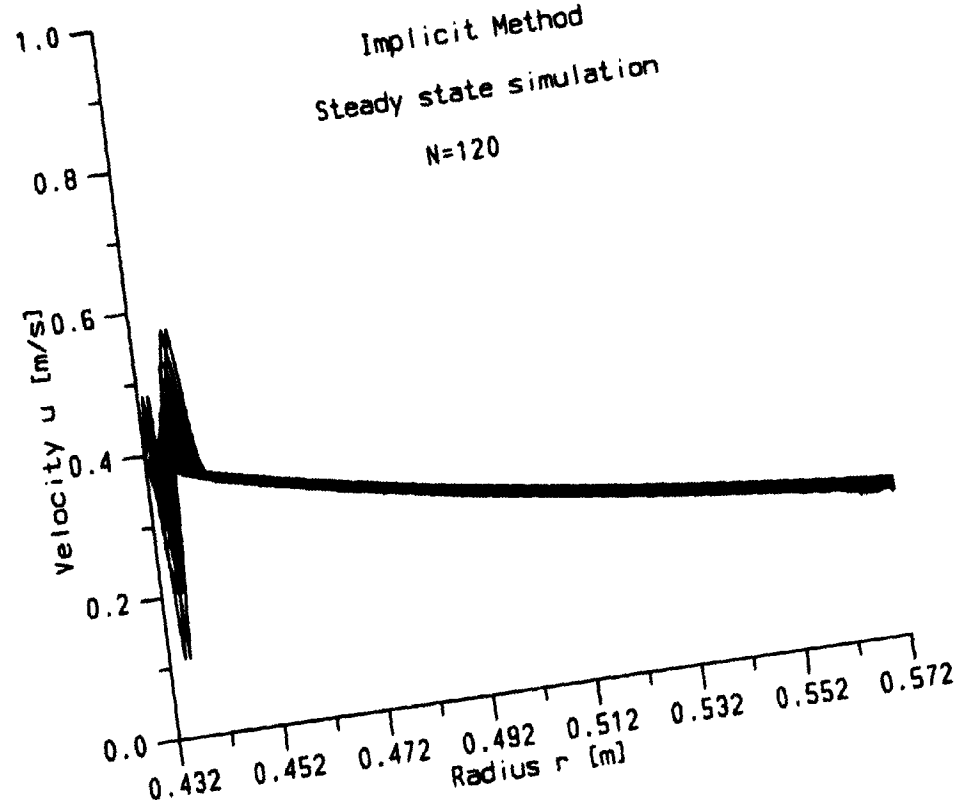

Figure 2.15: Steady state simulation using implicit numerical scheme with total number steps $N = 120$.

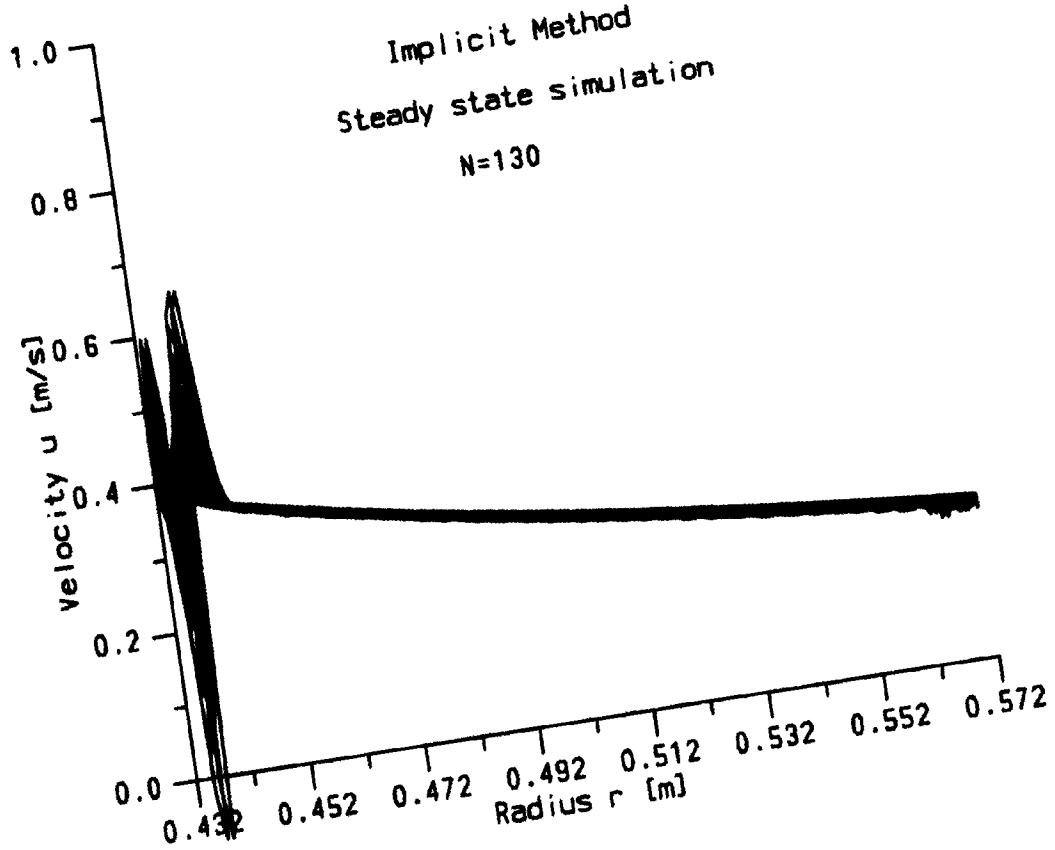

Figure 2.16: Steady state simulation using implicit numerical scheme with total number steps $N = 130$.

is near r_1. We also see that the stability of using this method does not improve over the explicit one in the steady state simulations, which is evidenced in Figure 2.16. The corresponding ρ profiles are shown in Appendix A.

2.10.2 Dynamic state simulation

Figures 2.17 and 2.18 illustrate the results of changing u_1 to u_{1new} in one step and linearly. In both cases, the method is very stable, but the disturbances introduced in the boundary conditions cannot travel along radial direction r at all. The ρ profiles show a similar trend, as illustrated in Appendix A.

An important conclusion can be drawn from using the implicit method that even though we use this more stable method some disturbances will grow in steady state simulation after certain time steps. This kind of behaviour suggests that the equations we try to solve might possess some unstable character.

2.11 Discussions and Further Work

According to the general theories of hyperbolic P.D.E.'s [31], discontinuities may occur within the domain of a solution for a hyperbolic system, even though there is no discontinuities introduced in boundary or initial conditions, resulting in non-unique solutions.

We have tested both the explicit and the implicit methods to solve our system of equations. Both methods generate oscillations when simulating the steady-state of the system, in spite of the fact that the implicit method is so stable that there is no amplification of any disturbances given on the boundary conditions. It appears, therefore, that the instability comes from the equations of the hyperbolic system. To tackle the problem, we have two choices. We can reexamine the terms and assumptions used in deriving the governing equations of the system, especially the effect of steam that we ignored. The ways in which we introduce disturbances on the boundary conditions may also be crucial to the stability of the system. Alternatively we could add an artificial diffusion (or viscosity) term [41] to our numerical scheme. By

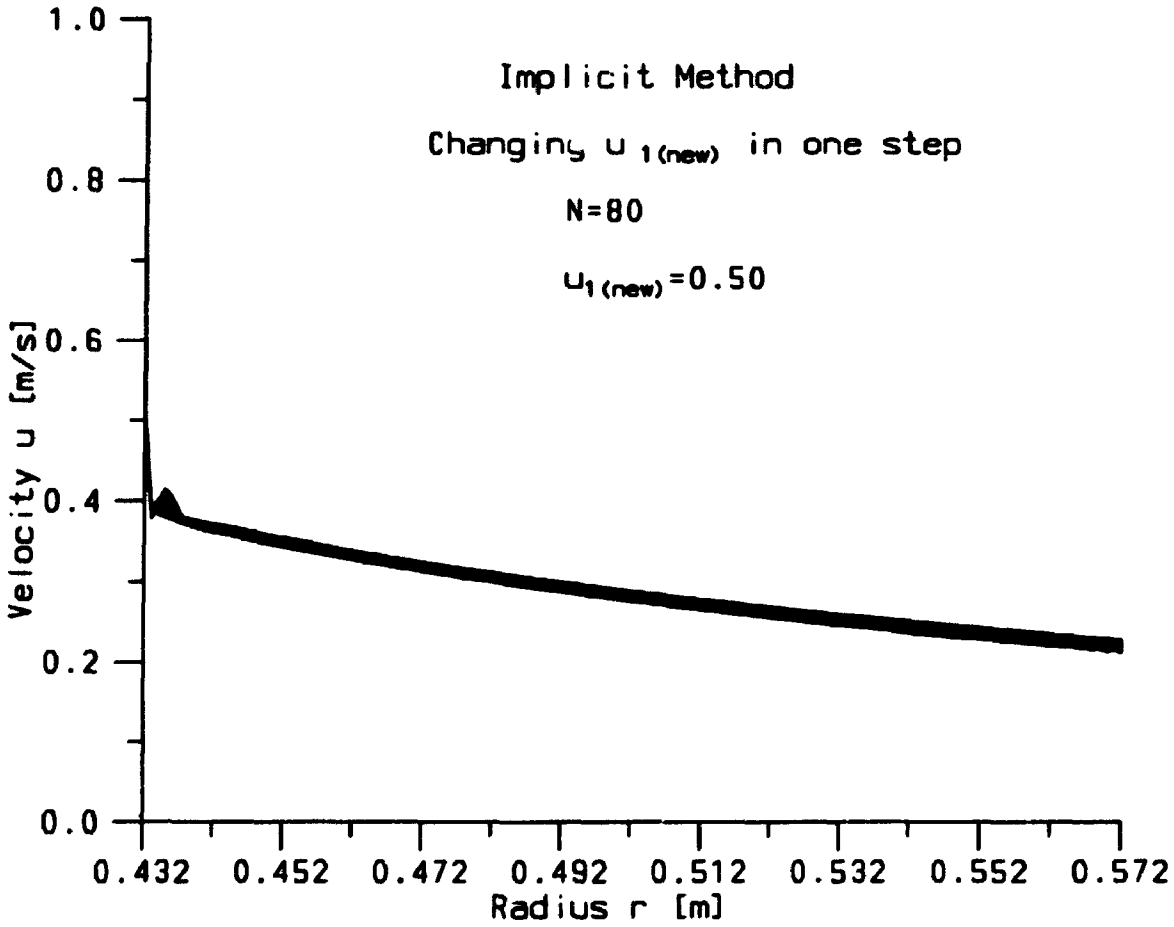

Figure 2.17: Dynamic state simulation using implicit numerical scheme with $u_1 = 0.39$ changed to $u_{1new} = 0.50$ in one step.

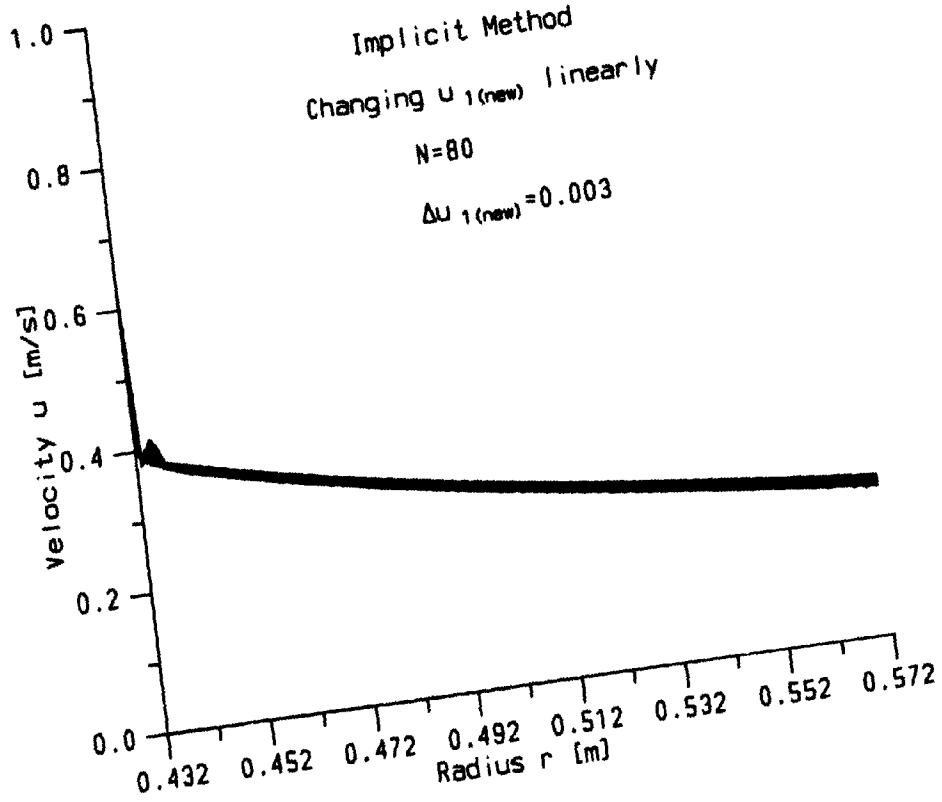

Figure 2.18: Dynamic state simulation using implicit numerical scheme with $u_1 = 0.39$ changed to $u_{1new} = 0.63$ linearly.

adding this term we could improve the stability of the hyperbolic system. An accurate numerical solution could still be achieved by letting the artificial diffusion term be the same order as the truncation error of the numerical scheme. However, as we shall see in the next Chapter, there are many effects of refining that we cannot expect to handle in a continuum model, and so we try instead a discrete model.

Chapter 3

DISCRETE MODEL AND STOCHASTIC MOTION

3.1 Introduction

One of the obvious weaknesses of the theoretical models described so far is the fact that no attempt is made to take into account the fact that bars and grooves are present on the plates of the refiner. In contrast, the widely held view within the pulp and paper industry is that pulp within the grooves behaves differently from the pulp between the bars. For example, the reason given for the placing of dams in the grooves of refiner plates is that they force the pulp out of the grooves into the space between the plates, in order that the pulp can be treated there by the mechanical forces generated from the moving bars. Another aspect that the current models fail to address is that experiment observations emphasize the fact that pulp inside a refiner breaks up into (temporary) flocs (The definition of pulp flocs is given in Appendix B). To develop an improved model, we have to address these fundamental questions first. Our initial focus of development has been the calculation of the residence time of the pulp in a refiner.

The amount of time that pulp spends inside a refiner is a significant factor in both low-consistency and high-consistency refining. For low consistencies, a number of studies have shown that residence time is important both for the quality of the pulp produced and for the operation of the refiner [42, 43, 44, 45]. For high-consistency refining, much less is known about residence time and its effects, because little experimental data are available [46]. In spite of this, concepts related to residence time have been used in models of refining with some success [47]. The theoretical models

of refining already introduced can calculate the residence time of pulp in a wood-chip refiner [25, 24]. The models share the following similarities.

1. The pulp inside a refiner is treated as a continuous medium, flowing from the inlet to the outlet.

2. A single velocity describes the motion of all the pulp at a given radial position. The exact interpretation of this velocity varies between the models. In Reference [25] it is called the velocity in the refiner plate grooves, and in Reference [24] the velocity averaged over the whole surface of the refiner plates.

3. The mathematical equations obtained for the two models are similar.

These mathematical models successfully describe some aspects of refiners, but do not capture all of the ideas used to explain refiner behaviour. For example, Miles *et al.* [48] suggest that fibres stapled to a rotor blade behave differently from fibres stapled to a stator blade. There is no place for such a difference in existing mathematical models. In both models, assumptions (1) and (2) imply that the residence time is simply the integrated reciprocal of the pulp radial velocity, and it thus has a unique value for a given set of conditions. Experimental measurements of residence time, however, show that it takes a range of values [42, 43] and is not unique.

In order to build a mathematical model that incorporates more of the modern experimental evidence and more of the modern theories, we have reexamined the assumptions and incorporated recent experimental observations [49] into a new set of assumptions that more closely describe the conditions inside a refiner. An immediate consequence will be a model of pulp flow which gives a distribution of residence times, but it is also a framework for future expansion.

Starting with assumption (1), we reconsider whether pulp can be treated as a continuous medium. From an examination of high-speed still photographs and ciné films, Atack *et al.* [29, 50] concluded that pulp moves inside a refiner in the form of flocs. These flocs probably do not have a permanent identity, but rather breakup and re-form continuously. More recently, a new technique was used to obtain blur-free

pictures of pulp in motion between refiner plates [49]. The results show that the pulp is not continuously distributed on the bars of the plates, and indeed the concentration of wood fibres in a small segment of refiner radius fluctuates considerably, even on the frame-by-frame time scale of 10^5 frames per second. Figure 3.1 shows typical high-speed photographs taken inside an industrial refiner through a transparent plate, and Figure 3.2 is a close-up picture of the pulp flocs [49]. The white parts in these pictures indicate the pulp coverage on the rotating bars of the refiner plate. We have, therefore, replaced assumption (1) with an assumption that pulp moves inside a refiner in the form of discrete flocs. We shall speak of these flocs as though they are permanent entities, but it is understood that there is no evidence that they are in fact permanent. We are thus treating the flocs in an average sense.

We next examine assumption (2). The idea that pulp flow is not confined only to the gaps between the plates was put forward by Miles and May [51] as part of an extension of their earlier model of pulp flow [24]. A numerical calculation is given in Appendix C to support the idea that the volume between the plates is not large enough to contain all of the pulp that is present inside a refiner under normal operating conditions. Miles and May [51] stated that 'the pulp is assumed to flow along the grooves at the same average velocity as it does along the bars, so that the network remains essentially interconnected'. We go further, however, and assume that the pulp in the grooves behaves differently from the pulp in the gap. Specifically, our new model departs from assumption (2) by dividing the refining zone into three regions: the grooves on the stator plate, the grooves on the rotor plate and the gap between the plates. For convenience, we refer to these regions as the stator, the rotor and the gap. It is generally thought that the bottom part of the grooves is packed with stationary pulp, and that only a mobile layer of pulp lying on top of this packed pulp flows significantly. It is this mobile layer that we refer to when we speak of pulp moving in the grooves of the plates. It is also generally thought that pulp moves from one region to another. For example, dams are placed in grooves to force the pulp out. In a recent experiment carried out in a laboratory single disc refiner. Ouellet *et al.* observed that the stagnant pulp inside the stator grooves could be suddenly pulled

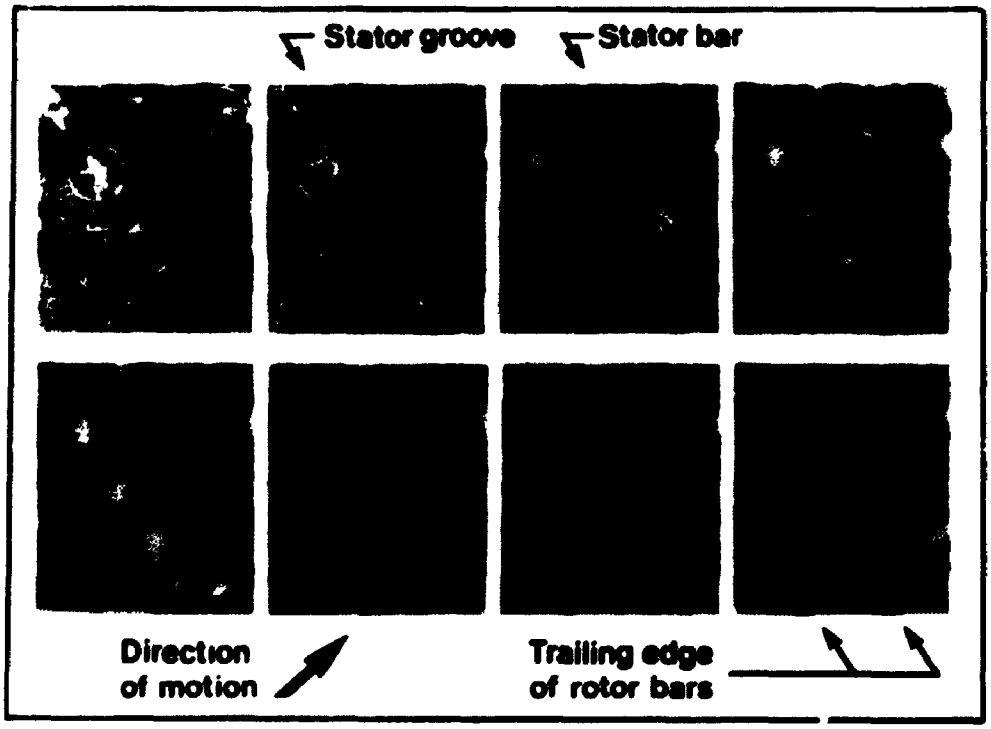

Figure 3.1: IMACON photograph inside refining zone of the transparent plate. The numbers show the sequence of taking the picture. In the time frame that the pictures were taken the leading edge of the rotating bar has moved over one bar of the stator plate. The circles in frame 1, 2 and 3 identify the same fibre floc in the three photographs.

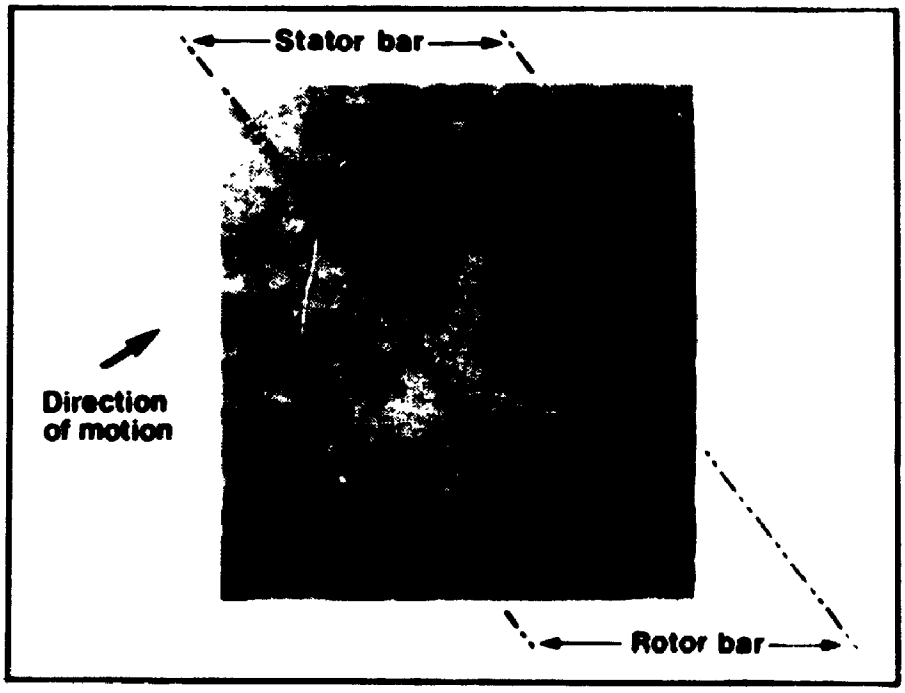

Figure 3.2: A single frame IMACON photograph showing a fibre floc at the leading edge of stator bar; individual fibres can identified within the floc.

out of the grooves [52]. The experiments reported by Miles, Lunan and May [48] were explained by postulating different mechanisms for the pulp moving from one plate to another. There are several mechanisms that can cause this, for example, dams in the grooves, turbulence in the flow, and entanglements between the flocs. The present version of our model does not specify these mechanisms further, but assumes their existence in order to explain the transport of pulp between regions. The transport is then treated as a stochastic process specified by a parameter.

These assumptions form the basis of the new model of pulp movement. In its present form, the model is a kinematic one, in that the forces acting on pulp inside the refiner are not taken explicitly into account, and pulp is simply assigned a constant radial velocity in each of the three regions. The kinematic model alone yields some new results, in particular for the residence time distribution, but in the longer term, it needs to be extended to include dynamic effects. A detailed description of the model and its implementation on a computer are given in the next section.

3.2 Description of the Model

We assume that the refiner is working at a steady production rate and motor load. The pulp flocs are assumed to be discrete individual particles or flocs of the same size, and we further assume that inside the refiner they are in one of three possible regions: inside a stator groove, in the gap between the plates or inside a rotor groove. The pulp flocs are assumed to move radially outwards at different velocities depending on which of these three regions they are lying in. Miles [53] studied the relations between the steam effect and the pulp radial velocity and found that steam flow has little impact on the average pulp radial velocity, although the local pulp radial velocity depends on steam flow. For simplicity, we have assumed that the radial velocity is constant within each region, and in particular we shall denote the radial velocity of pulp in the rotor grooves by u. And we shall point out that u represents the average radial velocity for all the pulp in the rotor grooves. A numerical estimate for u is given in the next section based on a model in which there is a force balance

between centrifugal force driving the pulp outwards and friction resisting the motion. The pulp velocity on the stator is assumed to be zero, the justification being that on the stator there is no centrifugal force, and the only forces that might cause the pulp to move are steam drag forces. Observations have shown that pulp can move radially inwards on the stator grooves [29], presumably because of steam forces. Such an inward velocity could be incorporated into our model, and indeed the possibility of doing so is one of the advantages it offers over previous models. We felt, however, that since the magnitude of this velocity is small compared with that in the rotor grooves or the gap between the plates, it would be better to leave this effect until we add steam flow to the model. Hence we approximate the velocity of the pulp in the stator groove by 0. Between the plates, we assume that a pulp floc is stapled either to the bars of the rotor or to the bars of the stator, and as a consequence has the same tangential velocity as the bar. The extra frictional resistance to motion, which the fibres will experience as a result of being stapled on the bars, will reduce their radial velocity. We therefore suppose the outward velocity in this region is $u/2$, a more accurate estimate of the reduction factor requiring experimental observations.

We suppose that the flocs stay in a single region for a fixed time interval Δt before they have the possibility of shifting to another one. The radial displacement of a pulp floc in a time interval Δt will be $\Delta r = u\Delta t$ in the rotor, $\Delta r = (u/2)\Delta t$ in the gap and $\Delta r = 0$ in the stator. After each time interval, the flocs are allowed to switch to a different region. The change takes place so quickly that the time required is negligible. In other words, the model makes the approximation that all the time that a floc spends in the refining zone is divided between the three regions. This exchange mechanism is therefore instantaneous and is modelled as a stochastic process, as illustrated schematically in Figure 3.3. For example, suppose that a floc is at present in the stator. At the next time step, the floc will either remain in the stator or go to the gap between the plates. For the first possibility we assign a probability P_{ss} and for the second P_{sg}. A floc that is in the gap will have three possible positions to go to at the end of a time step: the stator, the gap or the rotor, the associated probabilities being P_{gs}, P_{gg} and P_{gr} respectively. Similarly the pulp floc in the rotor

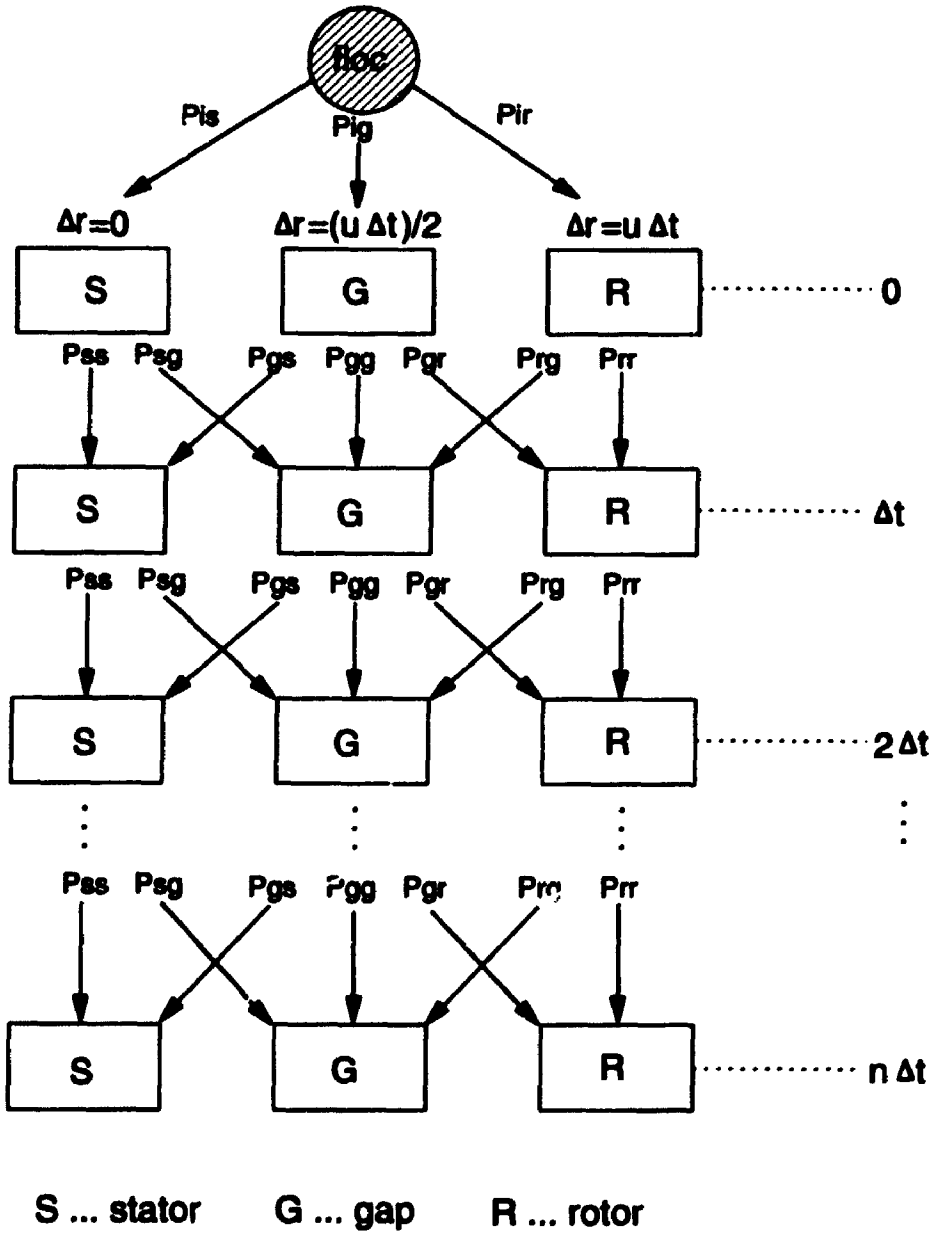

Figure 3.3: Schematic of positions available to the pulp flocs in different time steps.

will have two possible positions to go to, namely to stay in the rotor or to go to the gap, with probabilities P_{rr} and P_{rg} .

In general we denote the probability of a change by P and two alphabetic indices. The first index refers to the present position and the second index refers to the position at the next time step. The characters s, g and r are used to represent the stator, the gap and the rotor. There are seven probability parameters altogether, but the following relations mean that only four are independent:

$$P_{ss} + P_{sg} = 1, \tag{3.1}$$

$$P_{rg} + P_{rr} = 1, \tag{3.2}$$

$$P_{gs} + P_{gg} + P_{gr} = 1. \tag{3.3}$$

We choose P_{gs}, P_{sg}, P_{gr} and P_{rg} as independent probability parameters. We also need to assign probabilities to the way in which a floc enters the refining zone. The probabilities for it entering the stator, the rotor or the gap are P_{is}, P_{ig}, P_{ir}. These probabilities obey

$$P_{is} + P_{ig} + P_{ir} = 1 \tag{3.4}$$

and P_{is} and P_{ir} are chosen to be independent.

The algorithm of the process is illustrated in Figure 3.4. Before a pulp floc enters the refining zone, a random number is drawn to determine the region through which it enters, i.e., the state function is initialized to stator, gap, or rotor according to the random number drawn and to the initial probabilities P_{is}, P_{ig} and P_{ir}. The time is set to $t = 0$, and the radial position to $r = r_1$. An iterative process is then started by drawing a random number that determines the value of the state function to be used during the time step. This decision process depends on the existing value of the state function, since the probabilities of the new state are tied to the old state. The state function is now updated to the value just determined. The increment Δr on the radial position of the floc is calculated using the velocity appropriate to the state. An iteration is completed by incrementing the radial position r and the time counter t. All of the above steps are repeated until r is greater than or equal to r_2, indicating

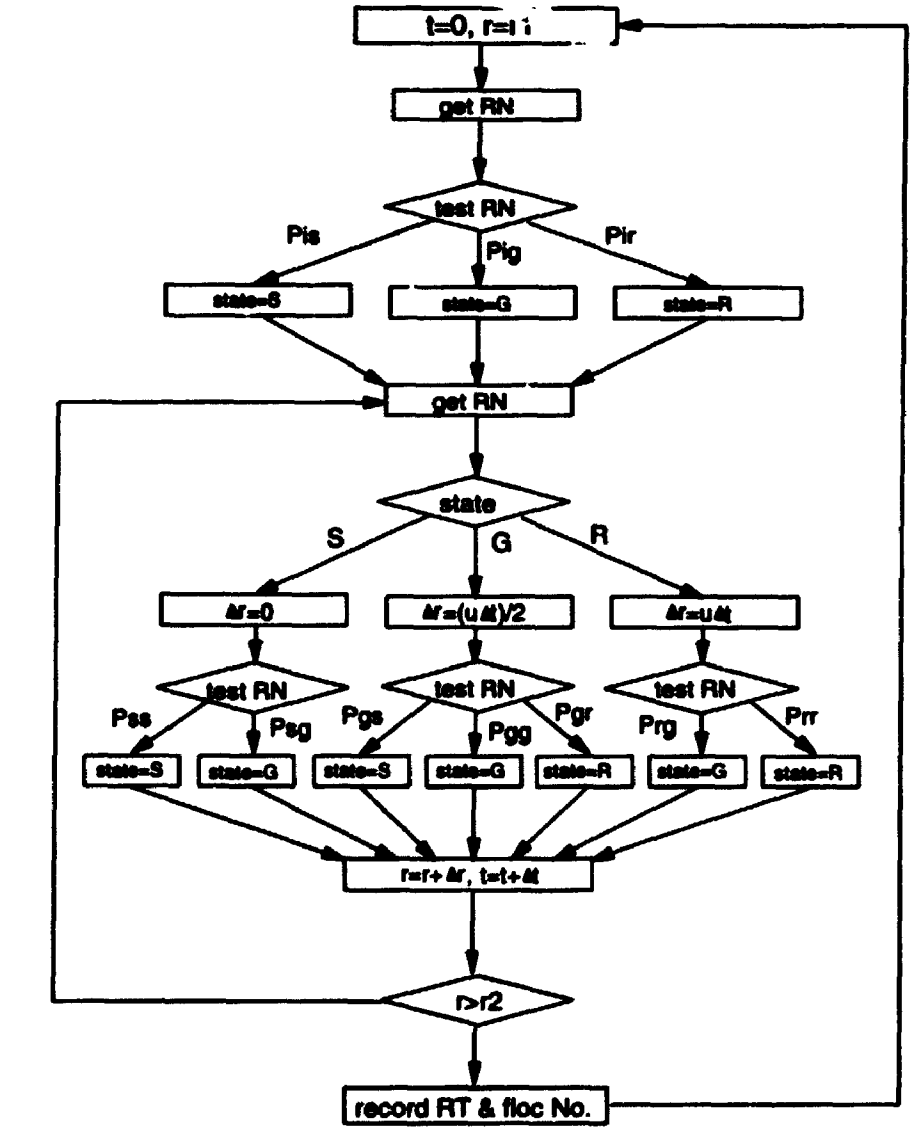

Figure 3.4: Flow chart of the steps to determine the residence time of a single floc.

that the floc has reached the refiner outlet. At that point, the residence time of the floc is recorded and the whole process is repeated for another floc. After enough pulp flocs have passed through the simulation, the residence time distribution of the pulp can be plotted.

3.3 Implementation of the Model

A Fortran program has been written to implement the above algorithm. The four independent probabilities and the two initial probabilities are treated as constants throughout the calculations. The program includes a random number generation subroutine to generate uniformly distributed random numbers between 0 and 1.

The geometrical and operational parameters of the refiner used in the simulations were taken from Reference [25], and the pulp radial velocity u was taken as the average velocity predicted by Reference [25]. This makes comparisons with previously calculated residence times easier. Some parameters cannot be estimated from Reference [25]. Three additional groups of parameters must be specified for the model, namely, the size of the time step Δt, the total number of pulp flocs to run through the simulation, and the independent probabilities.

We assume that there are equal chances for a floc to enter the refining zone through the stator or the rotor, so that $P_{is} = P_{ir}$. Because of the smaller space for the gap, we further assume that the probability of entering through the gap is smaller, i.e., $P_{ig} < P_{is}$. In the simulations we took the values of initial probabilities as $P_{is} = P_{ir} = 0.45$ and $P_{ig} = 0.1$.

A standard set of values for the parameters were selected to calculate a basic case against which others can be compared. The refiner operating parameters taken from Reference [25] were pulp radial velocity $u = 0.3$ m/s, refiner inlet radius $r_1 = 0.432$ m, and refiner outlet radius $r_2 = 0.572$m. The independent probabilities were $P_{sg} = P_{rg} = 0.5$; $P_{gr} = P_{gs} = 0.4$. The above values of the probabilities reflect the assumptions that there is an equal chance for a floc in the stator to stay there or to go to the gap, and similarly for a floc in the rotor. For a floc in the gap, there is an

equal chance to go to either the stator or the rotor, and a slightly smaller chance to stay there.

In order to give a definite value to the time step used in the simulation, Δt, we need to specify a mechanism that causes a floc to change region, for example, the doctoring/stapling mechanism described in Reference [48]. Our knowledge of the operation of this mechanism does not allow us to calculate Δt directly, and we must be content with estimating an upper bound on possible values of Δt. The estimate below is an order-of-magnitude only, and two things must be kept in mind. First, it will be shown below that the standard deviation of the residence time distribution depends significantly on the value of Δt, implying that a good value of Δt will be important for fitting data; second, the values chosen here are only starting points, and comparison with an experiment (residence time directly measured from an industrial refiner) will be necessary before anything definitive can be claimed for the quantity.

The order of magnitude of the time step Δt used in the simulations was chosen according to the observed size of pulp flocs [49] and the average distance between the flocs as determined by the geometry of the bars of the refiner plates. The width of the refiner plate bars for the refiner considered is in the order of $2-3$ mm, which in turn limits the maximum size of the pulp flocs between the plates. If we assume that the diameters of the pulp flocs are approximately equal to the width of the refiner plate bars, and that the maximum distance that a floc is likely to travel before changing region is equal to its diameter, then $\Delta t = 2 \times 10^{-3}/0.15 \approx 10^{-2}$ s. Consequently we chose $\Delta t = 10^{-2}$ s as the maximum size of time step. For most runs we reduced this further and chose $\Delta t = 2$ ms as the time step for the standard set of parameters, but in the end, experiment must decide.

3.4 Results and Discussions

The results shown in Figures 3.5 to Figure 3.13 are the residence time distribution curves calculated with the model. Along the horizontal axis, the residence time is measured in seconds, while on the vertical axis the corresponding frequency of

pulp flocs is expressed as a percentage of the total number of pulp flocs used in the simulation. The model was run for several different time steps Δt, but to allow easy comparisons of different cases, all the results are presented using histograms based on a fixed time width. The time step equals the longest one used in the simulations and is $\Delta t = 10^{-2}$ s. The other time steps were fractions of this basic one. For instance, for time steps equal to $\Delta t/3$, we collect the points from 3 consecutive bins, thus obtaining one bin of width Δt. In the same way, if the time step is $\Delta t/5$, we collect the points from 5 consecutive bins and assign the total to a bin of width Δt. In any event the results are plotted as curves passing through the tops of the histograms, and the bars of the histograms are suppressed.

Some general observations concerning all the curves can be made. First, we notice that there is a minimum residence time. The shortest theoretical residence time corresponds to a floc never leaving the rotor and is approximately equal to the residence time calculated in Reference [25]. The minimum value observed on the curves presented here is significantly higher than that however. This is simply because the probability of this case is too small to be resolved by our numerical calculations. The observed and theoretical minimum residence times become close if the probability parameters take values that force most of the pulp flocs to go to the rotor. Secondly, we notice that the distribution has a finite tail. Although it is possible for flocs to stay on the stator indefinitely, in practice, almost no floc stays there longer than twice the mean. Finally we notice that most distributions are close to being symmetrical about their maximum values, implying that the means and the medians of the distributions are approximately equal. We describe later the circumstances under which the curves become less symmetrical.

In addition to these general observations, some particular aspects of the results can be selected for comment.

1. Total Number of Pulp Flocs

The total number of pulp flocs is chosen according to two criteria. The first is the smoothness of the residence time distribution curve. As can be seen in Figure 3.5, the curves get progressively smoother as we increase the total number of flocs from 5×10^2

to 5×10^5. However, a second criterion is to minimize the computing time used. We found that a simulation using 3×10^5 was a reasonable compromise between these two requirements, and this value was used for the rest of the simulations presented here. With this number of flocs, a computer run on a workstation took about 40 minutes. The equivalent dry mass of wood for this number of pulp flocs is about 0.6 kg, which corresponds to about 1.5 s of production time for the refiner being considered.

2. Time Step Δt

The effect of changing the value of the time step Δt is illustrated in Figure 3.6. The residence time distributions become progressively narrower as Δt is decreased, but their means change very little. When Δt is reduced, the number of times a floc changes regions during its transit of the refining zone increases, making it more likely that different flocs will sample the three different regions a similar number of times.

3. Probabilities

The two independent entrance probabilities, P_{is} and P_{ir}, were found to have very little influence on the predicted residence time, because they only affect the initial step of the simulations. The other probability parameters have a more pronounced influence that is worth exploring.

Figures 3.7 and 3.8 show the effect of changing one particular probability parameter at a time in either the stator or the rotor while keeping the others at their standard value. Figures 3.9 and 3.10 illustrate the effect of the probability parameters in the gap. In Figure 3.9, P_{gs} has a fixed value of 0.1 while P_{gr} is assigned different values, and vice-versa in Figure 3.10. In both cases, P_{gg} varies according to Equation 3.3. It is clear from these figures that changing one probability parameter affects both the height and the position of the peak in the distribution, but has little effect on the skewness of the distribution (the curves remain approximately symmetrical about their mean).

4. Pulp Velocity u

Pulp velocity is a major parameter in determining the residence time distribution curves of a refiner because it directly influences the time the pulp flocs spend inside the refiner. Figure 3.11 shows that changing the value of the pulp radial velocity u

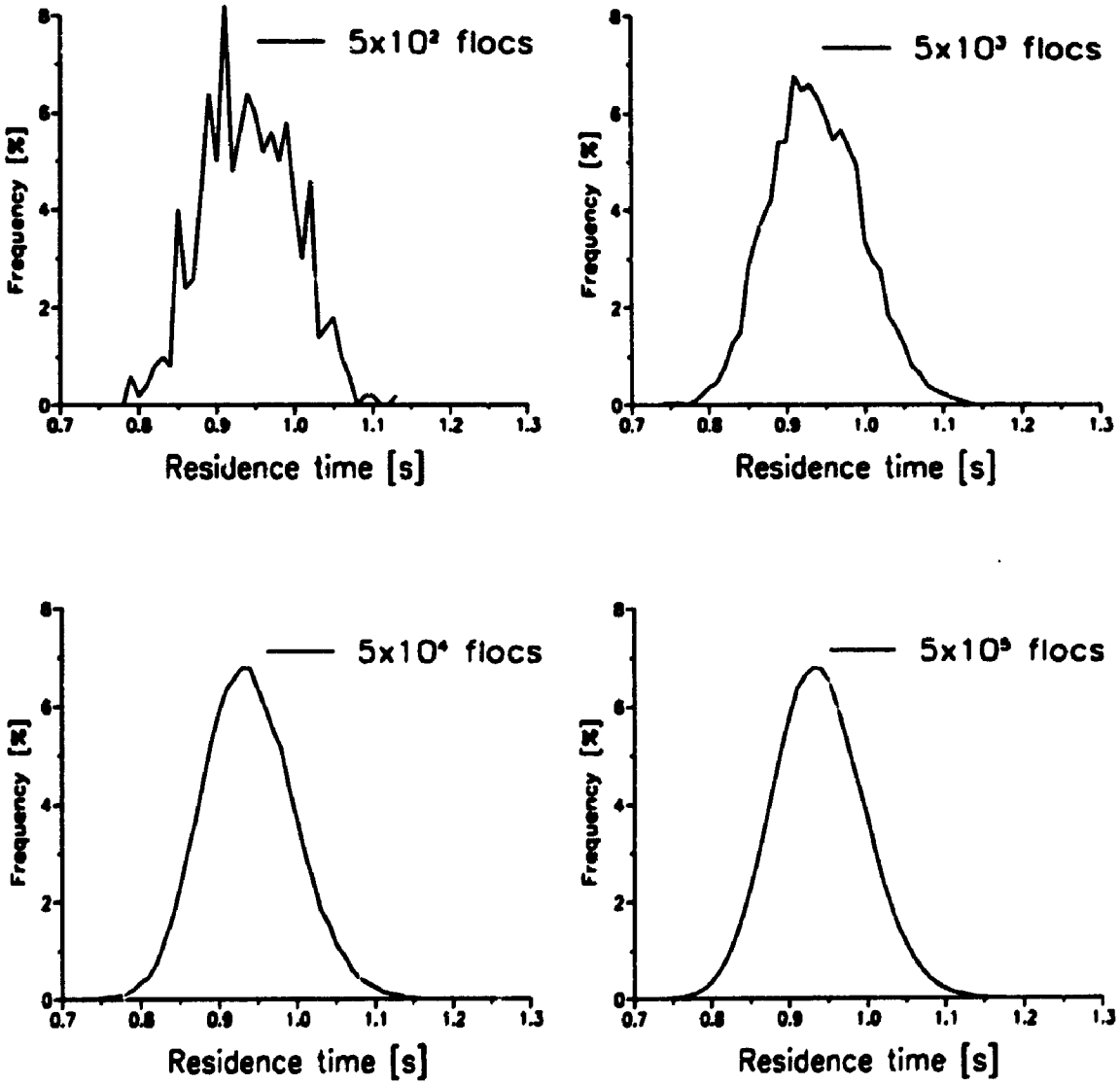

Figure 3.5: Residence time distributions in a refiner using the standard set of parameters with different total numbers of pulp flocs.

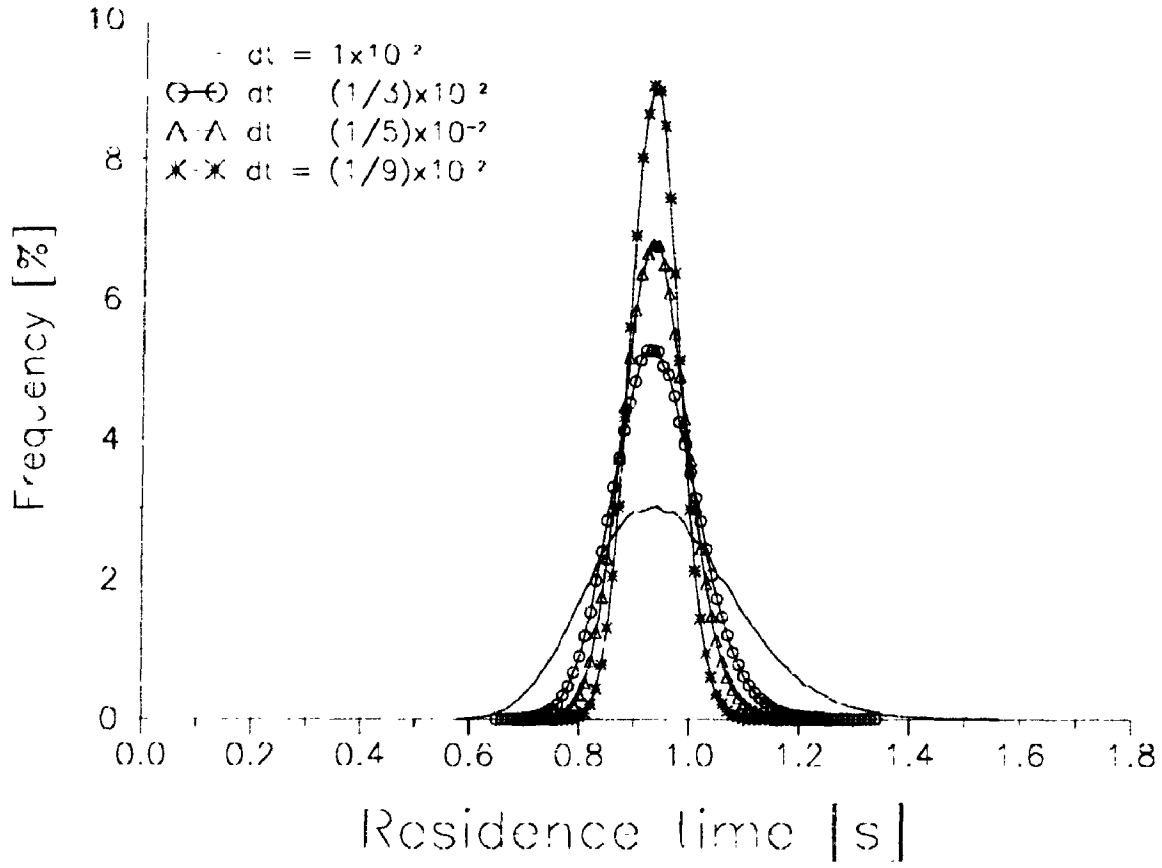

Figure 3.6: Residence time distributions in a refiner using different sizes of time steps.

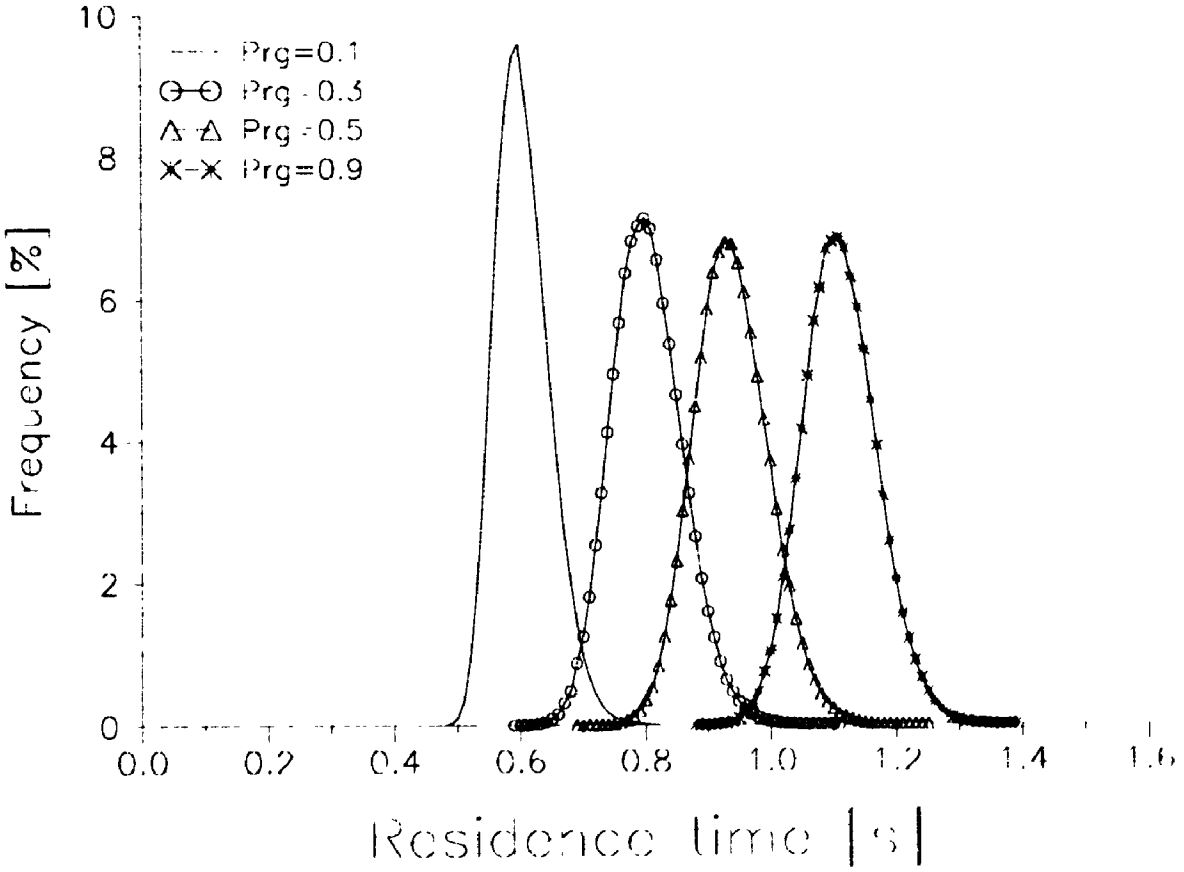

Figure 3.7: Effect of the probability P_{rg} on the residence time distribution, other probability parameters taking the standard set values, i.e., $P_{sg} = 0.5$; $P_{gr} = P_{gs} = 0.4$.

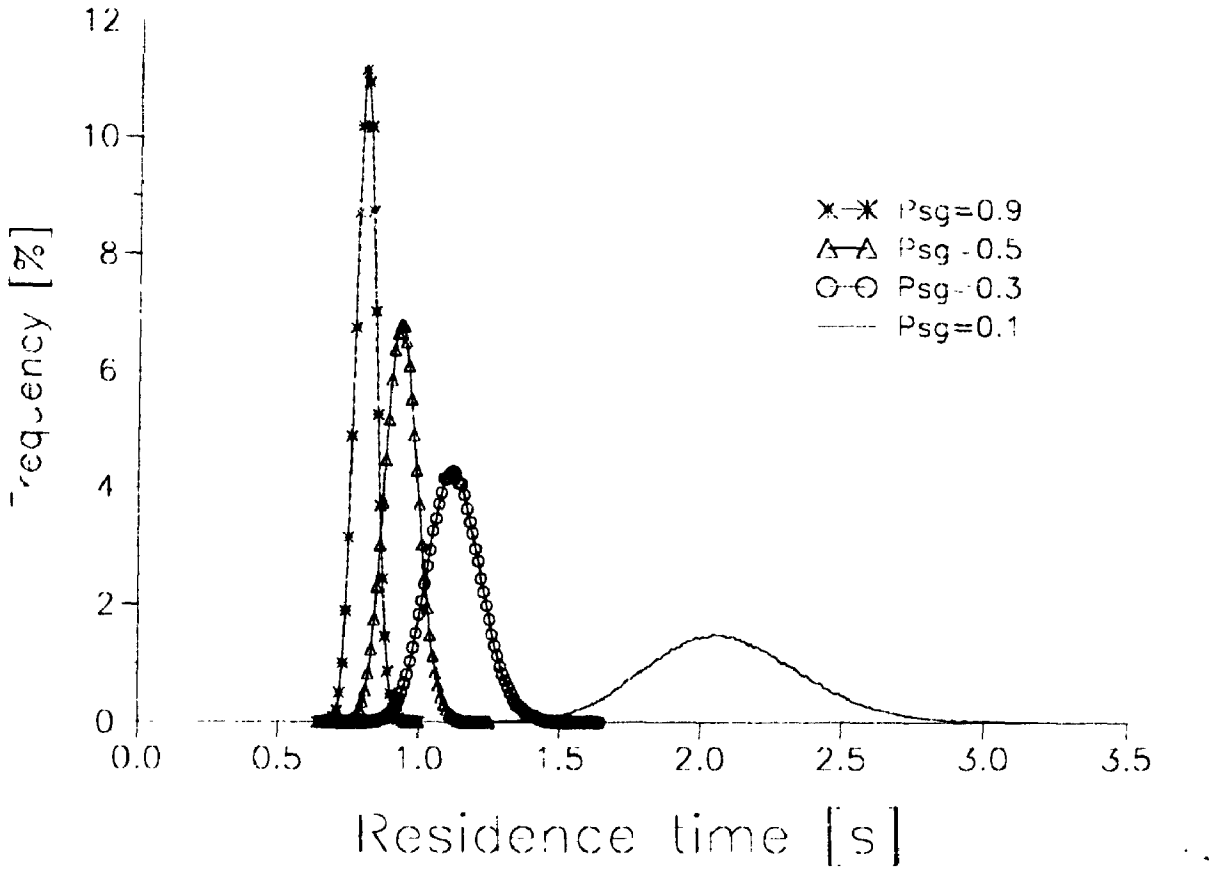

Figure 3.8: Effect of the probability P_{sg} on the residence time distribution, other probability parameters taking the standard set values, i.e., $P_{rg} = 0.5$; $P_{gr} = P_{gs} = 0.4$.

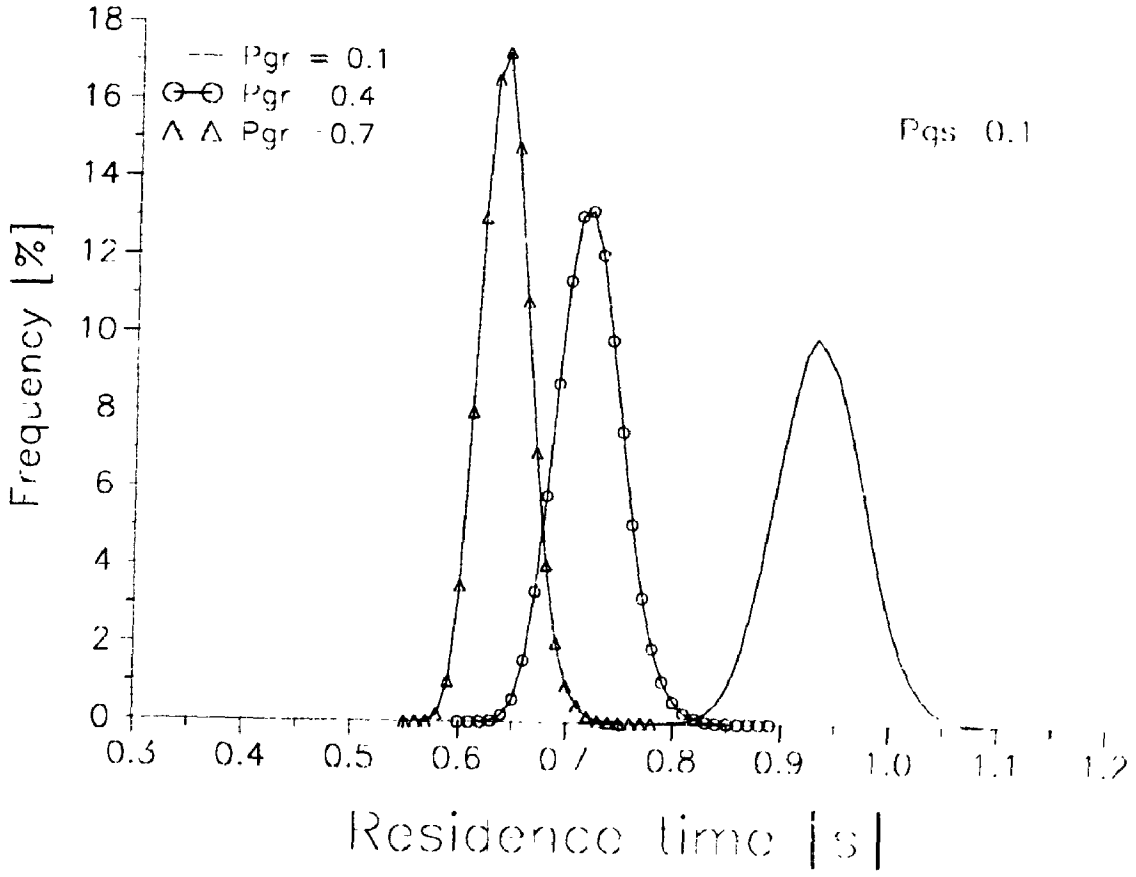

Figure 3.9: Effect of the probability P_{gr} on the residence time distribution when $P_{gs} = 0.1$.

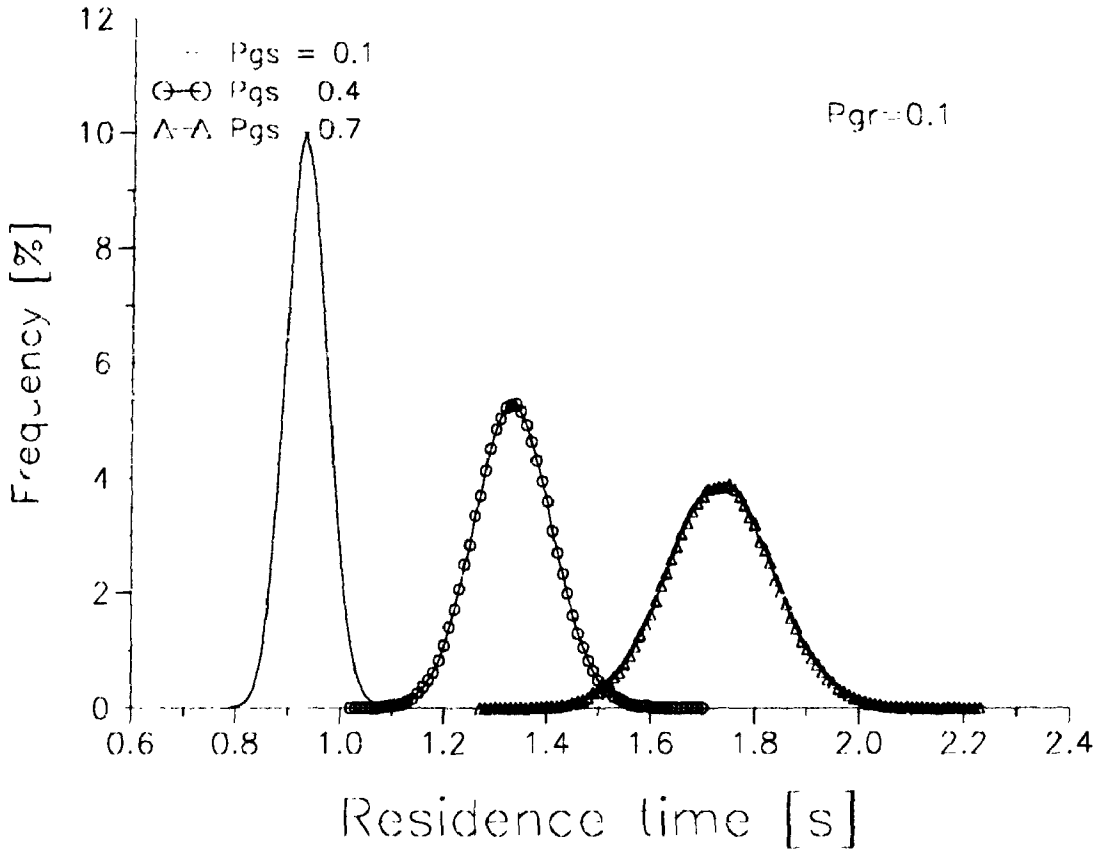

Figure 3.10: Effect of the probability P_{gs} on the residence time distribution when $P_{gr} = 0.1$.

has a significant effect on both the height and the position of the peak of the residence time distribution.

We also tested the sensitivity of the model to pulp velocity profiles using $u = u(r)$, which is the approximation of the result obtained from the previous model [25]. Figure 3.12 shows the distribution curves generated by using $u = u(r) = 0.2u_1/[0.2 + (r - r_1)]$, where u_1 is inlet pulp velocity, compared with the case of using u = constant = 0.3. In order to make the two cases comparable, we define an average pulp velocity as

$$\bar{u} = \frac{\int_{r_1}^{r_2} u(r)dr}{r_2 - r_1}, \tag{3.5}$$

and then we found in particular that the average pulp velocity is $\bar{u} = 0.758u_1$ using the above equation. We compared the two cases with the same average pulp velocity using different velocity profiles. From Figure 3.12, we can clearly see that the effect of using $u(r)$ profile is to shift the distribution to the right a little and the shape of the distribution is very similar to the one using u = constant. Therefore, no further effort is made to explore the effect of different pulp velocity profiles.

5. Skewness of the Distribution Curves

So far, all the results indicate that the residence time distributions obtained by changing the various parameters are approximately symmetrical about their mean values. However, the asymmetry of the residence time distribution can be accentuated by forcing the probability parameters to take extreme values. This effect is shown in Figure 3.13.

The reason behind the asymmetrical distribution is that since P_{sg} and P_{gs} are both small, the pulp flocs in the stator will stay there for a long time before they get a chance to go to the gap and from there to the rotor in order to advance in the radial direction. As a result, a considerable portion of the pulp flocs spends much more time than average in the refiner.

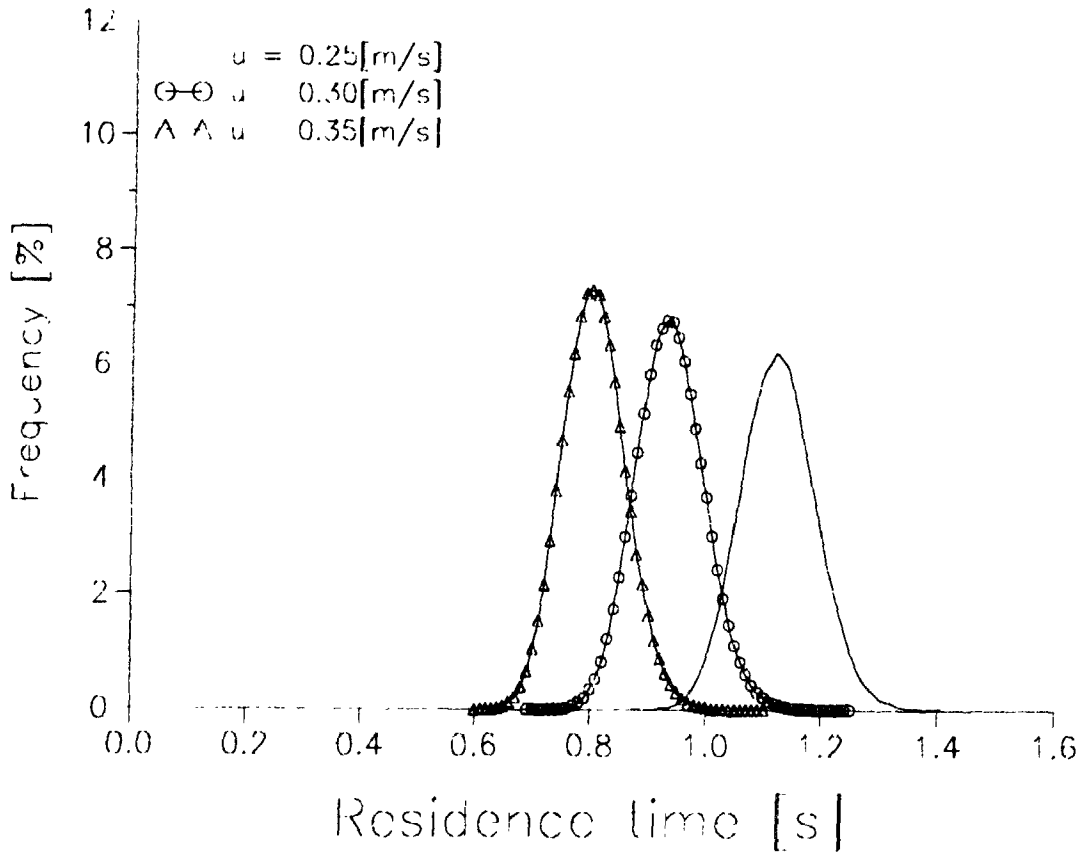

Figure 3.11: Effect of the velocity u on the residence time distribution.

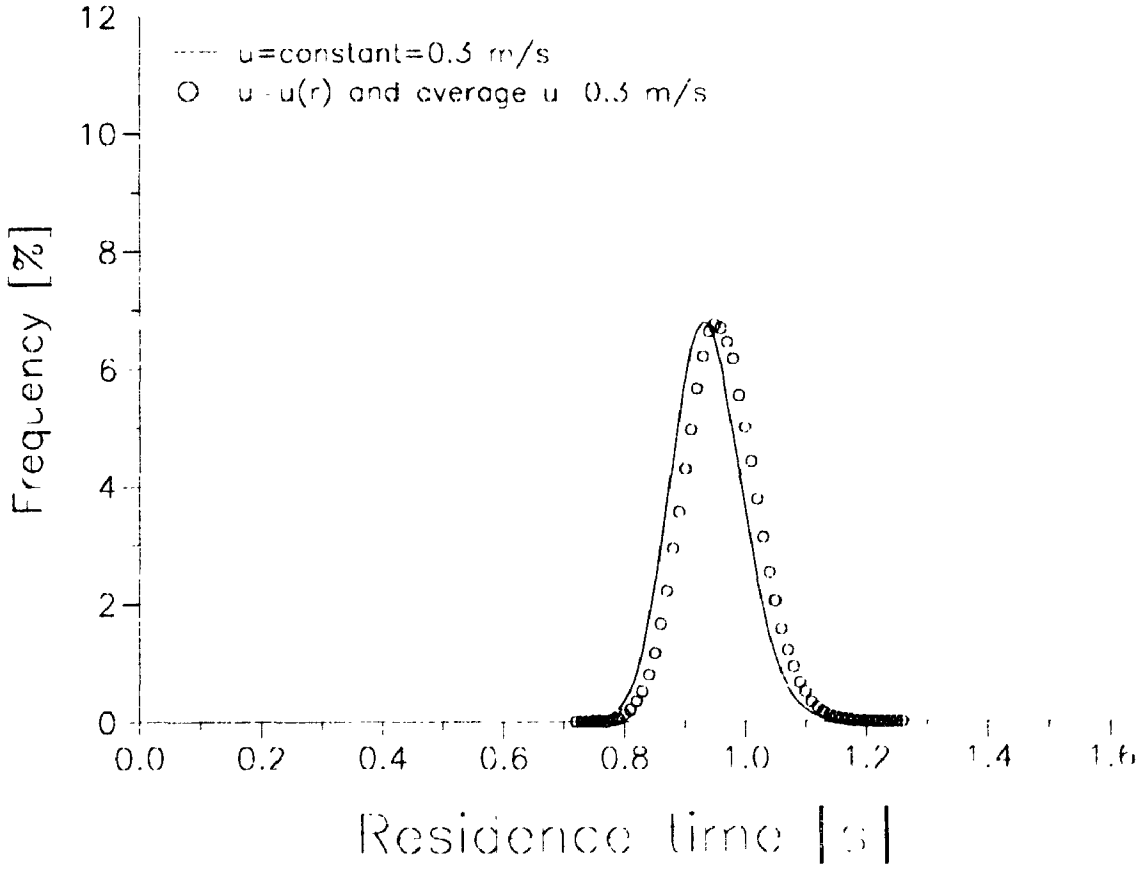

Figure 3.12: Residence time distributions in a refiner using $u = u(r)$ profile compared with that using constant u profile, the rest of the parameters being the values of the standard set.

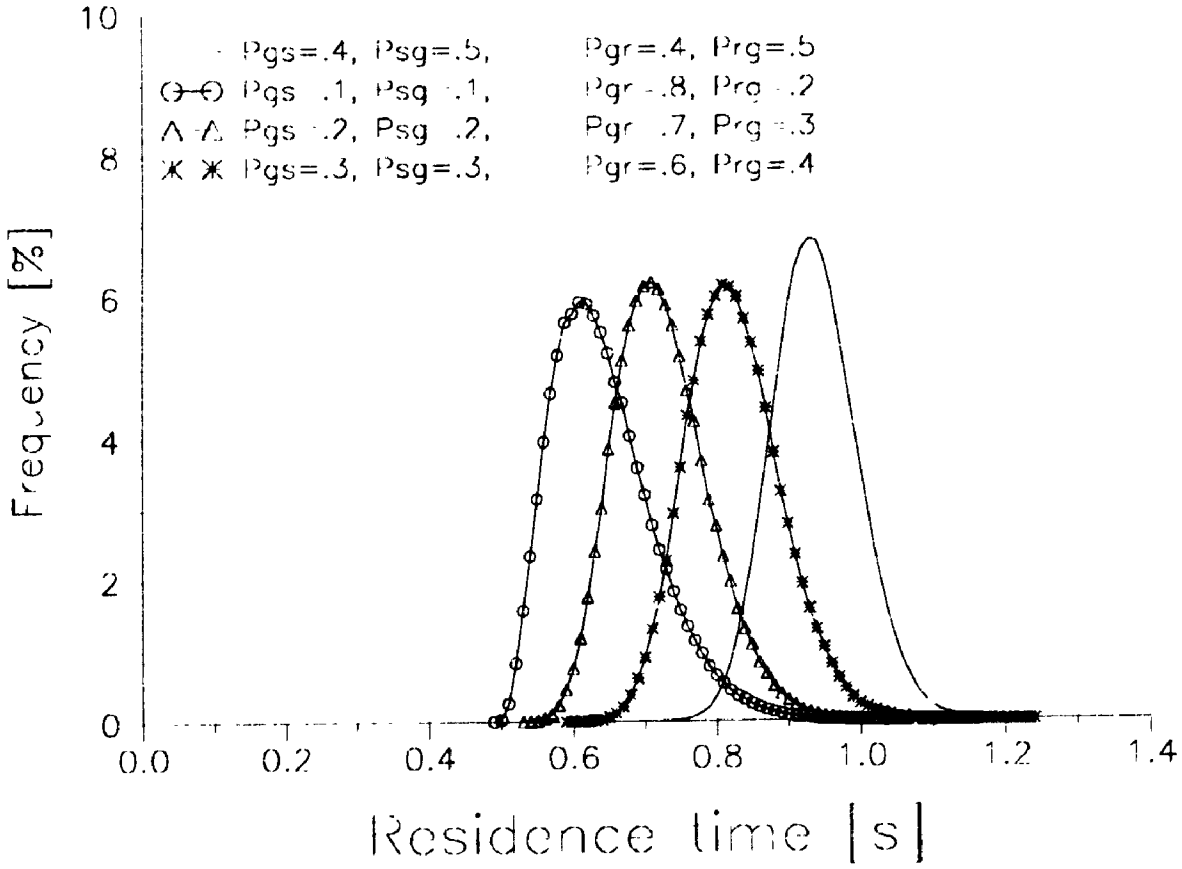

Figure 3.13: Residence time distributions in a refiner when all four probability parameters are assigned extreme values.

3.5 Conclusions

We have presented a first attempt at incorporating recent experimental observations into a model of pulp flow in a refiner. The new model, in the form presented here, improves on some aspects of the existing models, but is weaker than them in other aspects. The improvements lie in the treatment of floc movement, while the main weakness is the approximate treatment of the forces that determine pulp radial velocity. The weaknesses, however, are not inherent in the model, which is intended to be a generalization of existing ones. Therefore the dynamic modelling done in previous models can be added in further work on this model. The benefits of the new model are both qualitative and quantitative. The immediate quantitative benefit has been a more realistic prediction of residence time, but in the longer term, we hope that the model will provide a clearer way of thinking about pulp flow in general.

Through the parameter study made here, we have indicated a range of possibilities which experimental studies can evaluate. Such experimental studies will help us improve our model. In particular, the following conclusions have been drawn from the model:

1. The time step Δt used in the model is the minimum time a pulp floc stays in a groove or the gap between the plates, and it has a strong influence on the standard deviation of the residence time distribution. The smaller Δt is, the sharper the curves are.

2. The tendency of pulp flocs to leave the grooves or the gap between the plates is described by probability parameters. These parameters give nearly symmetrical distributions, except when they take extreme values.

3. The computer simulation treats each floc passing through the refiner separately, and in order to obtain predictions that are reasonably smooth and not affected by statistical fluctuations, one must run the program for about 10^5 flocs.

4. Changing the probability parameters will change both the height and the position of the peak of the residence time distribution.

5. The pulp velocity in each region has a strong effect on the residence time distribution, both on the values of the mean and the standard deviation. The magnitude of the effect is similar to that of the probability parameters. Using different pulp velocity profiles along r does not seem to affect the residence time distribution significantly.

Many aspects of the model can be improved. For example, the motion of pulp flocs could be predicted from a force balance rather than being simply prescribed. Mechanisms to determine the probabilities of transition between the three regions could also be included and tested. Furthermore, the mathematical treatment of the model could be refined to extract new statistics that the present treatment cannot calculate, for example the fluctuations in the bar area covered. Finally, the time for pulp flocs to spend between the plates has its own importance because this is the time believed to be the indication of amount of treatment that the pulp receives during refining.

Chapter 4

NON-MONOTONIC TREATMENT TIME

4.1 Treatment Time Calculation

The first thing that we consider, after the residence time, using the stochastic model is the treatment time. As we mentioned in the end of the previous Chapter, this is a significant improvement over other models in that we can actually distinguish pulp in different regions during refining. We define treatment time as the time that pulp flocs spend in the space between the plates only, because according to the current theories of refining, this is the place where pulp is refined. On the same principle, we can calculate the times spent by pulp flocs in the other two regions, i.e., in the stator and in the rotor. The three individual times add up to the residence time for pulp in a refiner. After implementing the stochastic model numerically, we can easily obtain all of the distributions of times that the pulp spends in the different regions so that we can study the behaviour of the treatment time.

Figure 4.1 shows the three distributions of the individual times compared with the residence time distribution, using the standard set of parameters. We can see in general that the treatment time is a small portion of the residence time, and usually has a much narrower distribution than the residence time. As we expect, the distribution of the time in the rotor is the sharpest and that in the stator the most flat among the three distribution curves, because of the obvious velocity differences in the three regions assumed. However, after examining the treatment time distribution closely, we found an interesting phenomenon that the treatment time distribution curves are always not as smooth as all the other distribution curves, which prompted

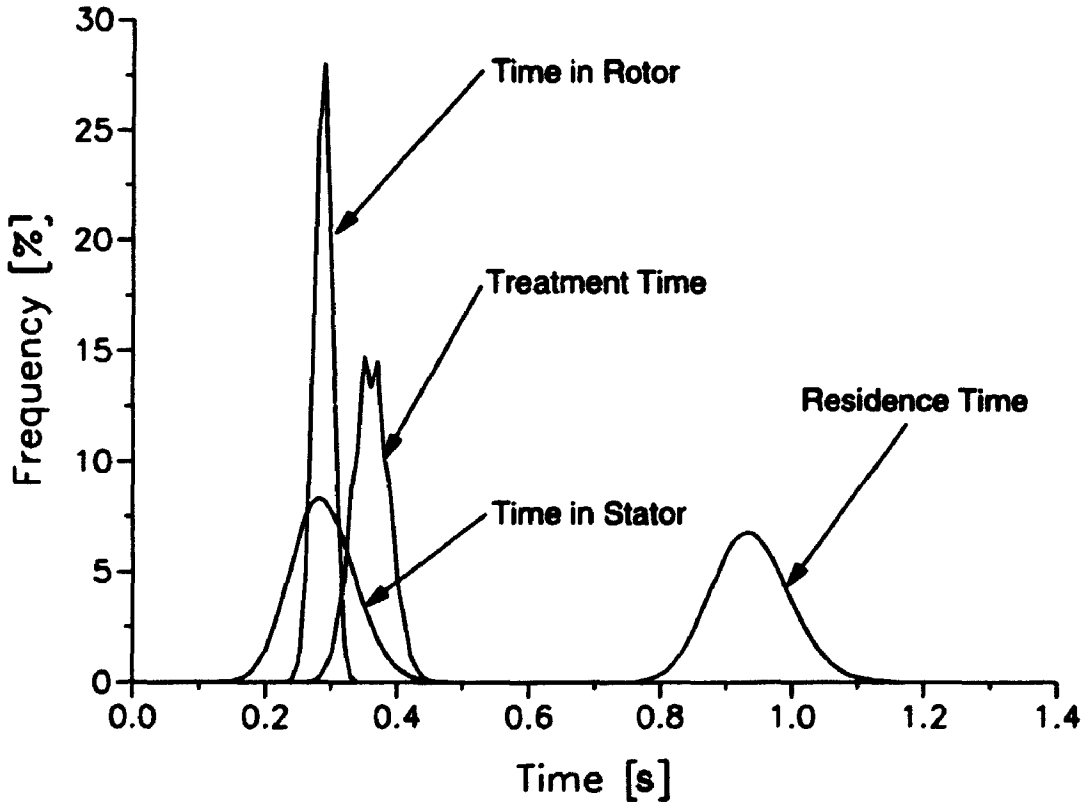

Figure 4.1: Time distributions for pulp in the individual regions compared with the total residence time using the standard set of parameters.

us to investigate the nature of this behaviour.

4.2 Simulation Accuracy or Probabilistic Character

First, we investigated whether there is a connection between this phenomenon and the total number of flocs N used to calculate the distribution curves, and found that the situation does not improve with increasing N. After we changed the plotting method using every data point in the time step, i.e., no average is used to plot the original data, the phenomenon can be seen more clearly (Figure 4.2). Secondly, we tested the sensitivity of this phenomenon to changing different probability parameters, and there seems no correlation between them. Thirdly, we found that changing the velocity ratio between the gap and the rotor significantly changes the patterns of these seemingly regular wiggles. Thus, it is important to establish whether this phenomenon is an artefact of the numerical simulation, for example because of the random number generator used, or whether it is inherent in the stochastic model. After comparing the numerical results of the treatment time with the ones obtained using several different random number generators (Mcleod [56], Mcleod [57] and Wichmann *et al.* [58]), we concluded that the phenomenon has nothing to do with the random routines employed in the program. In what follows, we demonstrate that the two-level behaviour shown in Figure 4.2 is indeed due to the stochastic properties of he model. Therefore, we conclude that our computation of the treatment time is accurate.

4.3 Preparation of a Simplified Case

Let us build up a simplified model so that we can study the behaviour of the treatment time effectively. Based on the experience of testing the sensitivity of different parameters to the patterns of this non-monotonic behaviour of the treatment time distribution, we thus chose to simplify the model in such a way that it shall be the simplest form, but its character remains. Since the pulp is assumed to be stationary in the stator in the current version of the model, we simplified the model to a 2-channel system (consisting of the rotor groove and the gap between the plates),

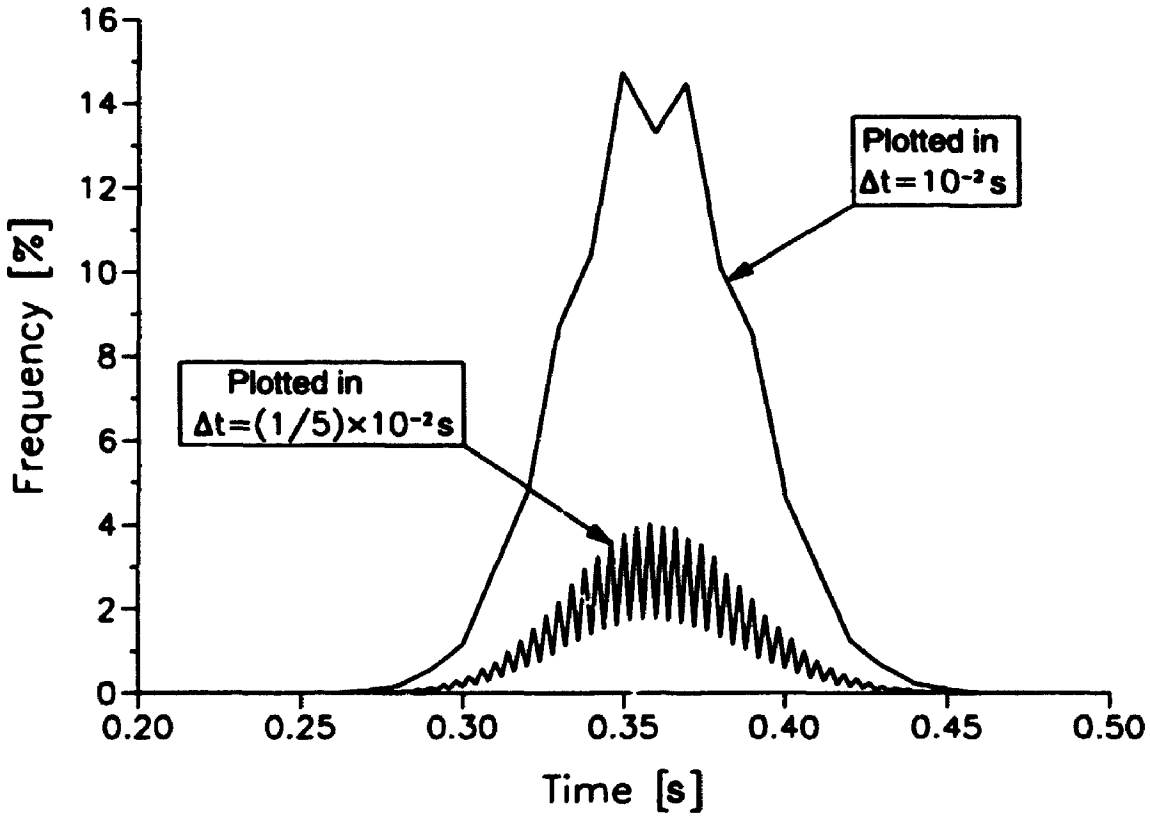

Figure 4.2: Treatment time distribution for pulp with different methods of plotting: one that has wiggles is the one using data in every time step, i.e., using time step as it is $\Delta t = (1/5) \times 10^{-2} s$; the other is the one to collect the 5 neighbouring bins, average to one bin, and plot using the basic time step $\Delta t = 10^{-2} s$ (this method of plotting has been used throughout the previous Chapter for residence time plotting to make easy comparison).

which nonetheless has a non-monotonic behaviour that is similar to that of the industrial model. The above statement has been confirmed by letting the probability for flocs to stay in the stator be zero in the industrial model. Also, since changing the probability parameters does not significantly affect the pattern of this behaviour in a wide range, we took equal probabilities for the flocs to leave or stay in the 2-channel system.

Now this simplified model resembles some general problems found in the field of probabilistic process. For example, we consider a queuing system consisting of 2 queues, with one fast queue and one slow queue. Suppose the probabilities for a customer to go from one queue to the other are equal. We are interested in the probability of the time spent in the slow queue. Another similar example is that if we have two equal length conveyor belts with one fast and the other slow moving, and a particle being transported can randomly jump from one to the other with equal opportunities. We want to study the behavior of the time a particle spends in the slow moving belt. From now on, let us call it the two-channel model, and concentrate on the principle that governs the probability distribution of times.

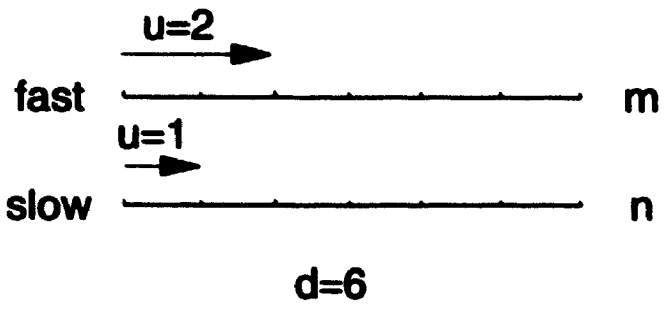

Figure 4.3: Schematic of the 2-1 speed model.

4.4 Preliminary for the Probabilities

1. Let the two queues be labelled 1 and 2;

2. Let queue 1 move with speed 1 and queue 2 with speed 2;

3. Let the total distance to travel be d.

First we consider a case for $d = 6$ and enumerate the probabilities. The schematic of the details of this 2-1 model is shown in Figure 4.3. Suppose at time $t = 0$, and distance $r = 0$, we start with a particle. At the end of $t = 1$, the probability for a particle to travel in the fast lane is $P_f = 1/2$, so is the probability to travel in the slow lane $P_s = 1/2$. Now the particle moves corresponding distance $r = 2$ or $r = 1$ depending on which lane it travels. The distance it travelled is less than $d = 6$, so we continue with another time step.

At the end of time $t = 2$, there are 4 possible cases. We define the probabilities for each case by the ordered combinations of letters f and s in the subscript. For example, P_{fs} stands for the probability of a particle to enter via the fast lane first and then switch to the slow lane. Thus for a particle to follow the path of ff (in short for fast-fast), the probability is $P_{ff} = 1/4$, and the distance travelled is $r = 4$; similarly, for a particle to follow the path of fs, $P_{fs} = 1/4$ and $r = 3$; using the same principle, $P_{sf} = 1/4$ and $r = 3$; and finally $P_{ss} = 1/4$ and $r = 2$. Since none of the above distance travelled has reached $d = 6$ yet, we process with another time step.

Table 4.1: All probabilities for time $t = 3$.

Prob.=1/8	P_{fff}	P_{ffs}	P_{fsf}	P_{fss}	P_{sff}	P_{sfs}	P_{ssf}	P_{sss}
Distance	6	5	5	4	5	4	4	3

Table 4.2: All probabilities for time $t = 4$.

Prob.=1/16	P_{ffsf}	P_{ffss}	P_{fsff}	P_{fsfs}	P_{fssf}	P_{fsss}	P_{sfff}
Distance	7	6	7	6	6	5	7
Prob.=1/16	P_{sffs}	P_{sfsf}	P_{sfss}	P_{ssff}	P_{ssfs}	P_{sssf}	P_{ssss}
Distance	6	6	5	6	5	5	4

We repeat the process for time $t = 3$. The probabilities and distance travelled are listed in Table 4.1. Since a particle via the path fff has already travelled the distance $r = 6$, we remove it and continue for the next time step.

For time $t = 4$, we have only 14 probabilities to consider since P_{ffff} and P_{fffs} are no longer present, and they are listed in Table 4.2. This time we remove the cases of both $r = 6$ and $r = 7$, i.e., the cases of $ffss$, $fsfs$, $fssf$, $sffs$, $sfsf$ and $ssff$ for $r = 6$, and $ffsf$, $fsff$ and $sfff$ for $r = 7$.

For the next time $t = 5$, there are 10 cases to consider and they are listed in Table 4.3. Again we remove the cases of both $r = 6$ and $r = 7$, i.e., $fssss$, $sfsss$, $ssfss$, $sssfs$ and $ssssf$ for $r = 6$, and $fsssf$, $sfssf$, $ssfsf$ and $sssff$ for $r = 7$.

Finally for the last time step $t = 6$, we have only two cases to consider, i.e., $P_{sssssf} = 1/64, r = 7$ and $P_{ssssss} = 1/64$ and $r = 6$. Now we rearrange and add up the probabilities for the cases of $r \geq d$ in the order of time spent in the slow lane. The

Table 4.3: All probabilities for time $t = 5$.

Prob.=1/32	P_{fsssf}	P_{fssss}	P_{sfssf}	P_{sfsss}	P_{ssfsf}
Distance	7	6	7	6	6
Prob.=1/32	P_{ssfss}	P_{sssff}	P_{sssfs}	P_{ssssf}	P_{sssss}
Distance	6	6	5	6	5

Table 4.4: All probabilities for time spent in the slow lane.

t in slow lane	r in slow lane	t in fast lane	r in fast lane	Probability
0	0	3	6	1/8
1	1	3	6	3/16
2	2	2	4	6/16
3	3	2	4	4/32
4	4	1	2	5/32
5	5	1	2	1/64
6	6	0	0	1/64

results are shown in Table 4.4. We see from Table 4.4 that an interesting pattern has emerged. For example, for time spent in the slow lane $t = 2$, the probability is much higher than the values in the neighbouring time steps. Certainly we need more time steps to unveil the nature of this phenomenon.

4.5 Analysis of Two-channel Model

We consider two channels of length d units, and assume that a particle in the fast channel moves at twice the speed of one in the slow channel. We further assume that the motion of the particle can be divided into equally spaced time intervals. For the duration of one interval, the particle stays in one channel and moves with the appropriate velocity. The time interval is chosen so that a particle moves one distance unit in the slow channel, or two distance units in the fast channel (we call it the 2-1 speed model). At the end of each time interval, a particle either remains in the current channel, or jumps to the other channel, both possibilities having probability 1/2. Let n and m denote the number of steps spent in the slow and the fast channel respectively and assume that d is even. Similar results would be obtained if d is odd.

If n is even, then any arrangement of fast and slow steps is permissible, and the total distance travelled is $d = n + 2m$. Thus $m = (d - n)/2$, and if we define

$$P[n \text{ (even) slow steps, } m \text{ fast steps}] = P(n),$$

we get

$$P(n) = \binom{n+m}{n} \left(\frac{1}{2}\right)^{n+m} = \frac{\left(\frac{d+n}{2}\right)!}{n!\left(\frac{d-n}{2}\right)!} \left(\frac{1}{2}\right)^{\frac{d+n}{2}} . \tag{4.1}$$

In contrast, if n is odd, then the distance travelled after $(n+m)$ steps will be $n+2m = (d+1)$ units, and the last step *must necessarily be fast.* This is the key to the analysis. Therefore, if we define again

$$P[n \text{ (odd) slow steps, } m \text{ fast steps}]=P(n),$$

we obtain

$$P(n) = \binom{n+m-1}{n} \left(\frac{1}{2}\right)^{n+m} = \frac{\left(\frac{d+n-1}{2}\right)!}{n!\left(\frac{d-n-1}{2}\right)!} \left(\frac{1}{2}\right)^{\frac{d+n+1}{2}} . \tag{4.2}$$

Let N denote an even positive integer. Comparison of these equations leads to the following relationships:

$$P(N-1) = P(N)\left(\frac{2N}{d+N}\right) \leq P(N); \qquad N = 0, 2, ..., d \tag{4.3}$$

so that odd probability is less than the next even one. And

$$P(N+1) = P(N)\left(\frac{d-N}{4(N+1)}\right) . \qquad N = 0, 2, ..., d \tag{4.4}$$

Furthermore $P(N+1) \leq P(N)$ for $5N \geq d-4$. In the context of Figure 4.4 where $d = 100$, we can see that $P(18) < P(19)$, but that indeed $P(21) < P(20)$ as the theory suggests. From this point onwards, all of the odd probabilities are less than the adjacent even ones, below and above.

The same line of reasoning can be used to show that when a particle moves in the fast channel at thrice the speed of the slow one (the 3-1 speed model), the probability distribution $P(n)$ for the number of slow steps is usually larger when n is a multiple of 3 than when it is not. In this case, we assume that d is divisible by 3.

If n is also a multiple of 3, then $n + 3m = d$, so that

$$P(n) = \frac{\left(\frac{d+2n}{3}\right)!}{n!\left(\frac{d-n}{3}\right)!} \left(\frac{1}{2}\right)^{\frac{d+2n}{3}} . \tag{4.5}$$

If n exceeds a multiple of three by one, then $n + 3m = d + 1$, and

$$P(n) = \frac{\left(\frac{d+2n-2}{3}\right)!}{n!\left(\frac{d-n-2}{3}\right)!}\left(\frac{1}{2}\right)^{\frac{d+2n+1}{3}} , \tag{4.6}$$

whereas if $n + 3m = d + 2$, we get

$$P(n) = \frac{\left(\frac{d+2n-1}{3}\right)!}{n!\left(\frac{d-n-1}{3}\right)!}\left(\frac{1}{2}\right)^{\frac{d+2n+2}{3}} . \tag{4.7}$$

In both of the previous two cases, *the last step is necessarily fast.* Letting N now be a multiple of 3 and using Equations (4.7) and (4.6) respectively, we find

$$\begin{aligned} P(N-1) &= \frac{\left(\frac{d+2N}{3}-1\right)!}{(N-1)!\left(\frac{d-N}{3}\right)!}\left(\frac{1}{2}\right)^{\frac{d+2N}{3}} \\ &= P(N)\frac{3N}{(d+2N)} \leq P(N) . \qquad N = 0, 3, ..., d; \end{aligned} \tag{4.8}$$

$$\begin{aligned} P(N-2) &= \frac{\left(\frac{d+2N}{3}-2\right)!}{(N-2)!\left(\frac{d-N}{3}\right)!}\left(\frac{1}{2}\right)^{\left(\frac{d+2N}{3}-1\right)} \\ &= P(N-1)\frac{6(N-1)}{(d+2N-3)} \\ &= P(N)\frac{18(N-1)N}{(d+2N)(d+2N-3)} . \end{aligned} \tag{4.9}$$

For example, if $d = 99$, $P(N-2) \leq P(N-1)$ up to $N = 24$ and $P(N-2) \leq P(N)$ up to $N = 42$. Similarly using Equation (4.6), we get

$$\begin{aligned} P(N+1) &= \frac{\left(\frac{d+2N}{3}\right)!}{(N+1)!\left(\frac{d-N}{3}-1\right)!}\left(\frac{1}{2}\right)^{\left(\frac{d+2N}{3}+1\right)} \\ &= P(N)\frac{d-N}{6(N+1)} . \end{aligned} \tag{4.10}$$

Thus $P(N+1) \leq P(N)$, if $7N \geq d - 6$ (in our example, if $N \geq 15$ since N is a multiple of 3). Lastly using Equation (4.7), we have

$$\begin{aligned} P(N+2) &= \frac{\left(\frac{d+2N}{3}+1\right)!}{(N+2)!\left(\frac{d-N}{3}-1\right)!}\left(\frac{1}{2}\right)^{\left(\frac{d+2N}{3}+2\right)} \\ &= P(N)\frac{(d-N)(d+2N+3)}{36(N+1)(N+2)} . \end{aligned} \tag{4.11}$$

4.6 Numerical Simulation

In order to test the numerical implementation of the full refiner model, we have applied the same approach to a numerical treatment of the 2-channel model just analyzed. We represent the random process by using a pseudo-random number generation routine to produce uniformly distributed random numbers between 0 and 1. First, a random number X is drawn to determine the initial position of a particle before it enters the 2-channel system, if $X \leq 1/2$ the particle starts in the slow channel, otherwise it starts in the fast channel. Then at each time step, another random number X is generated. For the particle in the slow channel, if $X \leq 1/2$, the particle travels in the slow channel, otherwise it jumps to the fast channel at the end of the time step. For the particle in the fast channel, if $X \leq 1/2$, the particle remains in the fast channel, otherwise it switches to the slow channel. While the particle is in the slow channel during time Δt, it moves a distance $\Delta r = 1$, or else (in the fast channel) $\Delta r = 2$ (in the 2-1 speed model) or $\Delta r = 3$ (in the 3-1 speed model) during time step $\Delta t = 1$. Then, the distance that this particle travelled r ($r = 0$, when $t = 0$) is updated by an iteration $r = r + \Delta r$. We repeat the process until $r \geq d$, then we record the time spent in the slow channel for one particle. When a large number of particles has been accumulated through the loop, the probability for the time n spent in the slow channel can be approximated by the number of particles spending time n divided by the total number of particles used in the simulation.

Figure 4.4 shows a typical comparison between the theoretical prediction and the numerical simulation using the above algorithm for the 2-1 speed model, while Figure 4.5 illustrates a similar comparison for the 3-1 speed model. In the graphs, the theoretical probabilities are plotted joined by lines. The results of the numerical simulation are represented by asterisks. Owing to the large factorials required, for example in Equation (4.1), the theoretical calculations were carried out using the symbolic package Maple V. For Figure 4.4, the total distance was $d = 100$, and for Figure 4.5, $d = 99$. The total number of particles used in the numerical simulations was 300,000.

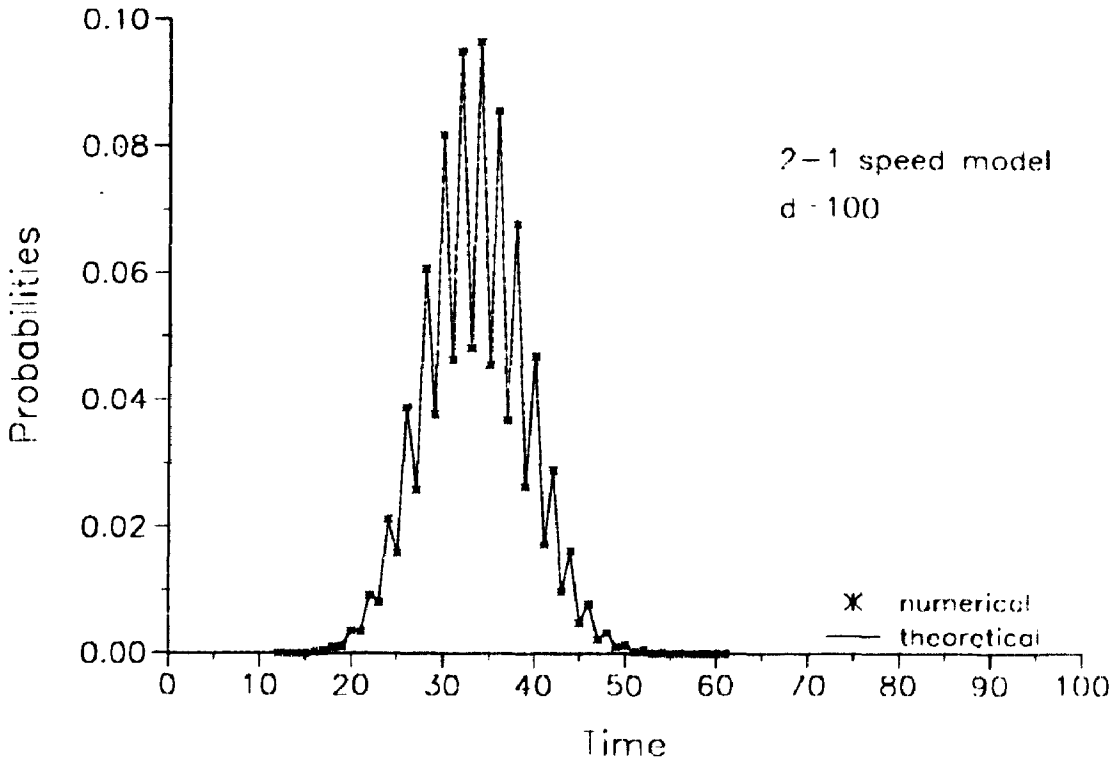

Figure 4.4: Probability distributions for the time spent in the slow channel for the 2-1 speed model.

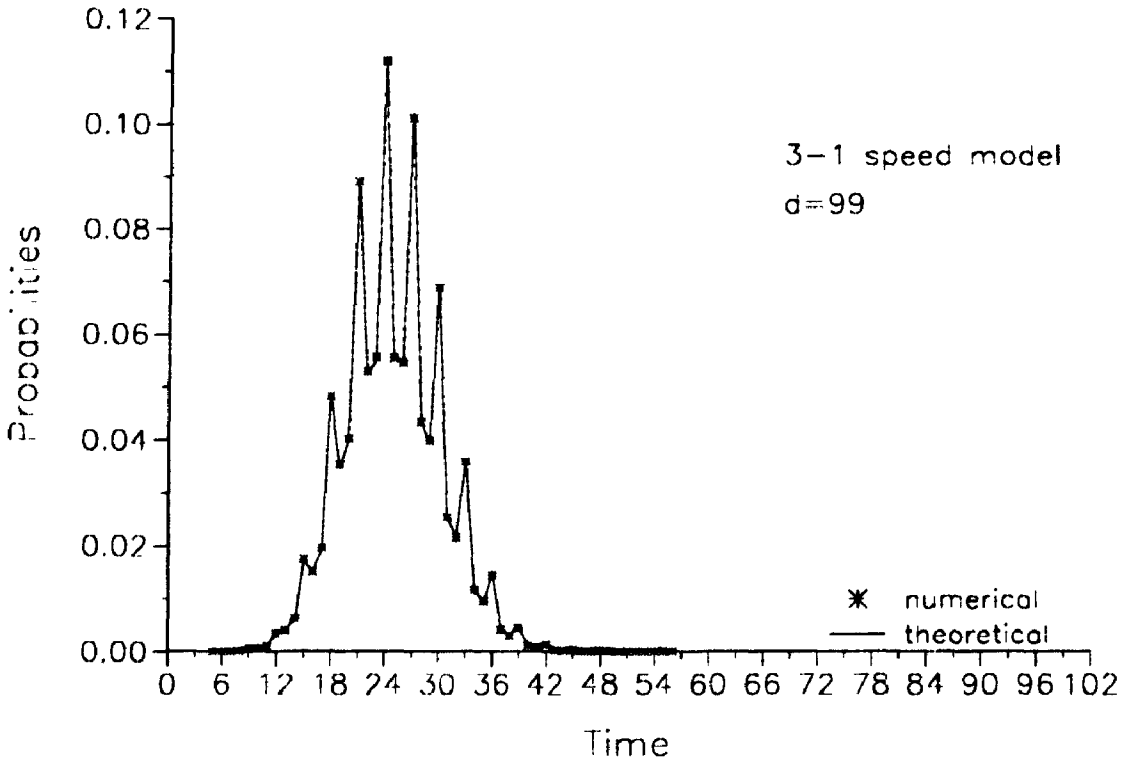

Figure 4.5: Probability distributions for the time spent in the slow channel for the 3-1 speed model.

4.7 Discussion

We see that there is generally very good agreement between the theoretical probabilities and numerical simulations. The oscillating behavior between neighbouring points is well described by the probability distribution for the time spent in the slow channel. The oscillation phenomenon, however, will not be present if we plot the time spent in the fast channel or the total time spent in both channels. In these situations, for example in the case of the 2-1 speed model, we have to merge the paired neighbouring probabilities (one large and one small) for a particular time. As a result, the oscillation is smeared out for the probability distribution for the time other than spent in the slow channel. In addition, we conclude that the lower values of probabilities correspond to the cases in which *the last step has to be in the fast channel.* This can be clearly seen in Figure 4.5, in which the probabilities between any times N and $N+3$ (N is multiple of 3) are generally much smaller than those on times N and $N+3$. For higher speed differences than 2-1 and 3-1, the situation becomes more complicated, owing to increased combinatorial complexity.

From an industrial perspective, the numerical implementation of stochastic modelling has been vindicated. Clearly in a real refiner, flocs of pulp will not always stay in a groove for the same fixed unit of time, and consequently, the real treatment time will likely be smoothed by this extra stochastic element. To implement such a model numerically would increase the computational burden greatly, and weaken the attractiveness of the model to industry. Now that the source of the unexpected non-monotonic behaviour has been identified, it can be taken into account when deducing the overall trends in behaviour. Thus from now on, we can collect paired neighbouring data points for the treatment time calculation, average these points over each pair, then obtain a reasonably smooth treatment time distribution, which will be seen in the next Chapter when we study the effect of the different parameters on the treatment time.

Chapter 5

TIME-DEPENDENT STOCHASTIC MODEL

5.1 Introduction

The time-dependent behaviour of pulp flow in a refiner is an important aspect of refining, because it directly influences the dynamic control of the refining operation. The flow of pulp within a refiner will vary with time because of several causes. First, during steady operation, there are fluctuations in the chip feed rate, because of variations in chip density and moisture [59]; Next, any deliberate change in operating conditions will lead to time-dependent flow, while the refiner adjusts to the new steady state. Finally, the motion of pulp inside the refining zone has a stochastic aspect, and this leads to internal fluctuations. Besides the attempt to study the dynamic aspect of refining described in Chapter 2, we can only find another theoretical study of time-dependent flow in a refiner in the literature to date [23], but this was concerned with steam flow, rather than pulp flow. There are, however, some experimental observations of flow fluctuations.

Experimental studies have looked at pulp on refiner bars during refiner operations; and the bar coverage has been studied in order to understand the nature of pulp flow in refiners [49]. The observations show that bar coverage fluctuates rapidly in time over a wide range along the refining zone. In addition, a connection between feed rate and bar coverage is evident and expected. We have extended the steady state stochastic model described in Chapter 3 [60] into a time-dependent model to study the fluctuations in the amount of pulp in different regions inside a refiner.

The time-dependent model shares several assumptions with the previous version:

1. Pulp is in the form of discontinuous flocs.

2. Flocs move in three regions: the stator, the gap and the rotor.

3. The exchange mechanism between the regions is modelled by a stochastic process governed by parameters.

4. The pulp velocities in the three regions are different.

The time-dependent model, however, differs from the previous one in keeping track of all pulp flocs present in a refiner simultaneously. In the previous version, we followed only one floc at a time, and accumulated averages. Now we can look at fluctuations within a steady state, and also study how changes occur when the steady-state parameters are shifted.

Another quantity that describes the refining action is treatment time, which is defined as the time pulp spends in the gap between the plates through a refiner. This quantity is extremely important for the quality of pulp produced because it directly measures the amount of energy pulp receives during refining. Treatment time arises naturally from the model, in which we treat pulp differently in three regions. The idea of using time spent for pulp between the refiner plates to quantify refining action has already been put into formulas such as 'C-factor' [61], and 'refining intensity' [62]. But it is impossible to predict treatment time by using the approach similar to the early 'one-passage' pulp flow models [24, 25], hence residence time has been used in general for these formulas instead. The current model can calculate the treatment time in addition to the residence time described in the previous model for steady state.

The purpose of this study is to predict the locally averaged density fluctuations of pulp, a phenomenon reflected in the experiment [49], and to see the influence of different parameters on the locally averaged densities especially the feed rate. We also want to study the correlations between the locally averaged densities and the residence time or the treatment time. In its present form, the model is still a kinematic one, in that the forces acting on pulp inside the refiner are not taken explicitly into

account, and pulp is simply assigned a constant radial velocity in each of the three regions. The probabilities of pulp floc exchange and the gap between the plates are also treated as constants in the current model. The kinematic model alone yields some new results, in particular to predict the locally averaged density fluctuations, and to relate the densities to feed rate in different set points of steady states. But in the longer term, it needs to be extended to include the force balance in pulp flocs. A detailed description of the model and its implementation on a computer are given in the subsequent sections.

5.2 Description of the Model

The principle of the current model is the same as in the previous version of the model for steady state. We summarize the positions available to the flocs in Figure 5.1. And the algorithm of the process is expl. ned in detail in Chapter 3 [60].

But in this version of the model we treat each floc simultaneously and individually, so that we can study the time-dependent effect of refining. Each floc is assigned an integer label while it is in the refiner, a different integer for each floc. This label is then used to store the state of the floc in three arrays. We assign the three arrays to describe a floc in the refiner:

1. state(label)= 'stator', 'gap', 'rotor' or 'no floc';
2. time(label)= 0 to the longest time;
3. distance(label)= r_1 to r_2.

When a floc leaves the refiner, its label is returned to a pool for reuse by an incoming floc; this saves computer memory. Thus for each floc (represented by a label), we know at each moment where it is inside the refiner and how long it has been in the refiner. During a time step Δt, flocs that leave the refiner will be added to the labels with state(label)= 'no floc'. In other words, for those labels with distance array greater than or equal to r_2, we will remove the flocs from the refiner and return the labels for the new flocs. While for the labels with state array not equal to 'no floc',

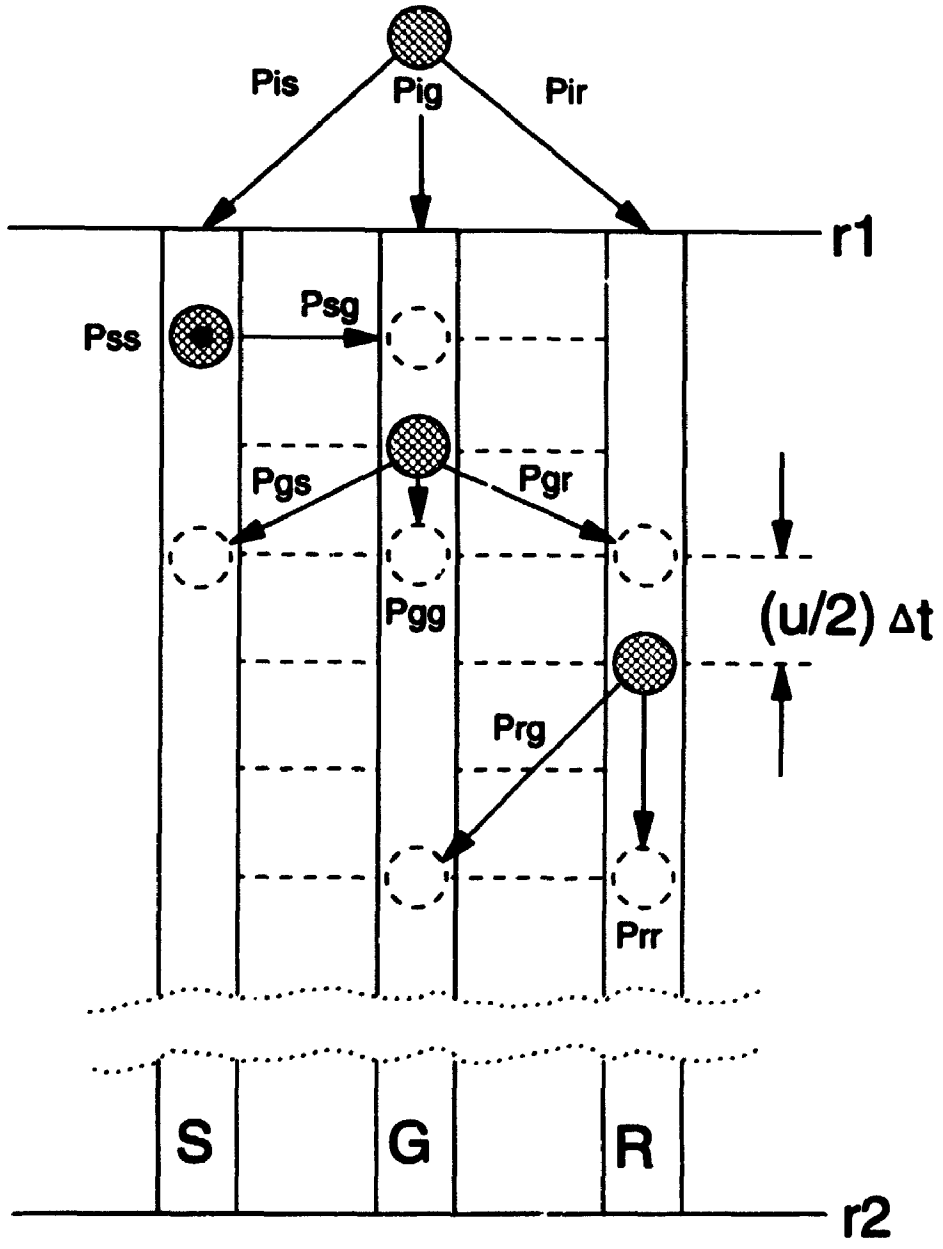

Figure 5.1: Schematic of positions available to the pulp flocs in different radial positions of the refining zone.

we will update the flocs by giving distance array advances according to the schemes described in Figure 3.4 of Chapter 3. The number of labels in use during Δt depends on the number of flocs entering the refining zone in Δt.

We approximate the refining zone by parallel bars and grooves with equal width for simplicity. In addition, we assume that the feed rate is evenly divided by the total number of grooves in the rotor and stator, and the total space between the plates. This will give an average feed rate for the three regions in the refining zone represented by one groove in the stator, one groove in the rotor and $1/n$ of the total space between the plates, where n is the total number of grooves (or bars, since we assume that there is equal number of bars and grooves in a plate). Now we divide the refining zone into a number of segments of equal width δr. Knowing the radial position and the state function of each floc, we can evaluate the locally averaged density in the rotor, gap and stator over δr at any radius r as follows:

$$\beta_r(r) = \frac{N_r(r)m}{A_r(r)\delta r}, \tag{5.1}$$

$$\beta_g(r) = \frac{N_g(r)m}{A_g(r)\delta r}, \tag{5.2}$$

$$\beta_s(r) = \frac{N_s(r)m}{A_s(r)\delta r}, \tag{5.3}$$

where $N_i(r)$ represent the number of flocs in δr, and A_i denote the cross-sectional area in different states with state i ($i = s, r$, or g). Then we can calculate the locally averaged densities of pulp in a refiner if we know the number of flocs appearing in different regions in the simulations, because the rest of the parameters involved in the above equations are all constants as assumed in the current model.

We add the treatment time calculation in that we record the time a floc spends in the gap region only, and use the same method to obtain the treatment time distribution as described in getting the residence time distribution.

In order to relate the locally averaged densities of pulp to the feed rate of the refiner, we have to assume the number of flocs entering refining zone in Δt, because there is no relevant experiment data available about this information. Despite the fact that pulp floc sizes are far from uniform as evidenced in the experiment [49], we

treat all pulp floc in one size in an average sense. Thus for a given level of feed rate F, we will have a corresponding mass m of the averaged individual flocs for different total number of flocs N entering refining zone in Δt assumed.

5.3 Implementation of the Model

A Fortran program has been written to implement the above algorithm. The four independent probabilities and the two initial probabilities are treated as constants throughout the calculations. Most of the parameters used for the simulations in Chapter 3 [60] were adopted for the simulations using the new time-dependent model. In addition, some groups of parameters must be specified for the model, namely, the size of the time step Δt, the total number of pulp flocs to run through the simulation, and the independent probabilities.

From a study of the previous model in Chapter 3 [60], we found that the value of time step Δt is very important for fitting data. However, we also found that Δt only affects the standard deviation, not the mean of the residence time distribution. The size of the time step will have similar effect on the locally averaged density, because the smaller Δt reduces the number of flocs contained in the sample area. Therefore, Δt will affect the magnitude of the locally averaged density fluctuations, but not the mean of this property. Here we chose to use the maximum $\Delta t = 10^{-2}$ s adopted in the simulations using the previous model, but in the end, experiment must decide.

The total number of flocs used to produce the residence time and the treatment time will vary with the number of flocs into the refining zone in Δt. But in most cases, it was well short of 10^5 used to give a reasonably smooth residence time distribution found in Chapter 3 [60]. As a result, the residence time distribution and the treatment time distribution in general are not as smooth as seen before.

As explained in Chapter 3 [60], the values of initial probabilities were taken as $P_{is} = P_{ir} = 0.45$ and $P_{ig} = 0.1$. And the independent probabilities for the standard set of parameters were chosen to be $P_{gs} = 0.4$, $P_{sg} = 0.5$, $P_{gr} = 0.4$ and $P_{rg} = 0.5$, which are denoted by P_0 in the graphs. Then three groups of probabilities were

selected to see the influence of probabilities on the model. In particular, they are $P_{gs} = 0.3$, $P_{sg} = 0.3$, $P_{gr} = 0.6$ and $P_{rg} = 0.4$; $P_{gs} = 0.2$, $P_{sg} = 0.2$, $P_{gr} = 0.7$ and $P_{rg} = 0.3$; $P_{gs} = 0.1$, $P_{sg} = 0.1$, $P_{gr} = 0.8$ and $P_{rg} = 0.2$. And in the same sequence, they are indicated by P_1, P_2 and P_3 in the graphs. The selection of above values of the probabilities was based on the experience gathered on simulations using the previous model. They reflect the assumptions that there is a smaller chance for a floc in the gap to go to the stator, and once a floc is in the stator it tends to stay there due to the feature of the stator. For a floc in the gap, there is a greater chance to go to the rotor because flocs moves faster there. Hence the chance for a floc in the rotor to come back to the gap is also smaller.

In addition to the values for the parameters selected above, some operational parameters for refining were chosen in line with Reference [22] for the standard set of the parameters used in the simulations. They include: the width and the height of a bar (or the width and the depth of a groove) 3 mm; the plate gap $g = 0.3$ mm; and the feed rate of the refiner $F = 0.416$ kg/s. The length of δr for calculating the locally averaged densities was chosen to be a multiple of Δr in the gap, a distance that a floc may travel in time Δt, to reflect the average distance travelled for a floc in three regions in Δt. From the experience of the simulations, we chose to use $\delta r = 4\Delta r$ in the gap to produce a reasonable degree of fluctuations in the locally averaged densities for the range of N adopted in the simulations. We assigned N the total number of flocs entering r_1 in Δt to be from 10 to 120 for the three regions, with the corresponding mass of a single floc being from 4.60×10^{-7} kg to 3.83×10^{-8} kg. For the standard set of parameters, we chose $N = 40$, with mass of a single floc being 1.15×10^{-7} kg.

We used two criteria to define a steady state: All random quantities have reached constant average properties; and all deterministic quantities have constant values. In particular, we declared a steady state,

1. when the averaged density in the gap (averaged over r in one Δt) averaged again in 10 Δt's is less than 0.01 of its previous value;

2. and also when the total number of flocs out of the refiner averaged in 10 Δt's

is equal to the total number of flocs into the refiner, within a tolerance of 0.02 times the total number of flocs into the refiner.

The settings of the above criteria were the results of trial-and-error in dealing with most of the cases in the simulations. We chose to use the averaged density in the gap to represent the state mainly because it is the most significant property for refining. In general the second criterion is larger, because the number of flocs out has been averaged only once instead of twice as in the first criterion except in some extreme cases. If no time average is used, the fluctuations would be too high to define a steady state.

5.4 Results and Discussions

We assume that the refiner is working from empty to a steady production rate and motor load. Then from this steady state, we give a variation to feed rate until the refiner reaches another steady state. We are more interested in what happens in this period of time, because it is relevant to the situation in refining operation.

First of all, we presented a general trend of the locally averaged density fluctuations for the gap region β_g against both time t and radius r in Figure 5.2. It was then followed by figures that show the locally averaged densities in all three regions against time and radius, and the number of flocs out of refiner against time, as well as the residence time and the treatment time predicted by using the standard set of parameters. The rest of results obtained from the simulations were basically divided into two series: one that shows the effect from start of the refiner to the first steady state; the other that shows the effect mainly from the first steady state to the second steady state after a variation to the feed rate is given. Within each series, we plotted the averaged densities and the number of flocs out of the refiner against time, as well as the treatment time distribution and the residence time distribution.

Some general comments can be made from the simulations. From the limited results, the fluctuations in the locally averaged densities are well observed for all the cases, even after they are averaged over radius r. There seems to be a direct relation

between the feed rate and the locally averaged densities. Changing probabilities seems to change the magnitude of the locally averaged densities only, but has little effect on the fluctuations in the locally averaged densities. There are very little influence on the residence time distribution and the treatment time distribution for different number of flocs into the refiner, except for the smoothness of the distributions. Changing the number of flocs into the refiner also has little effect on the average values of the locally averaged densities.

In addition, we can look at some aspects of the results in detail. Particularly, we have the following observations and comments.

1). Observations using standard set of parameters for up to the first steady state

From Figure 5.2, we see that a gradual build-up of the locally averaged density β_g in both r and t directions. In general the values of β_g are higher near the entrance r_1, even when the steady state is reached.

We observe from Figure 5.3 (a) that for using the group of probabilities P_0 the averaged density β_g is much higher than β_s or β_r, due to the smaller cross sectional area of the gap region compared with the other two regions, and the fluctuations in β_g are also much higher.

Figure 5.3 (b) shows the locally averaged density profiles with respect to r. We see that there is a certain degree of fluctuations even through we used $\delta r = 4\Delta r$ in the gap to reduce the fluctuations. The regression of the curves indicates the downward trend of density profiles with respect to r especially for β_g.

There is roughly about half the time for the number of flocs out to reach a steady state from 0 than the averaged density β_g, and it also has a greater degree of relative fluctuations than β_g as well. These effects can be seen from Figure 5.3 (c).

Figure 5.3 (d) illustrates both the residence time and the treatment time distributions. We can clearly see that the treatment time is a small portion of residence time, and it has much narrower distribution than the residence time. We can also see that there is a regular oscillation in a much higher magnitude than the random wiggles seen in the residence time distribution, as explained in Chapter 4 [63]. In other words, if we increase the total number of flocs used to produce the treatment

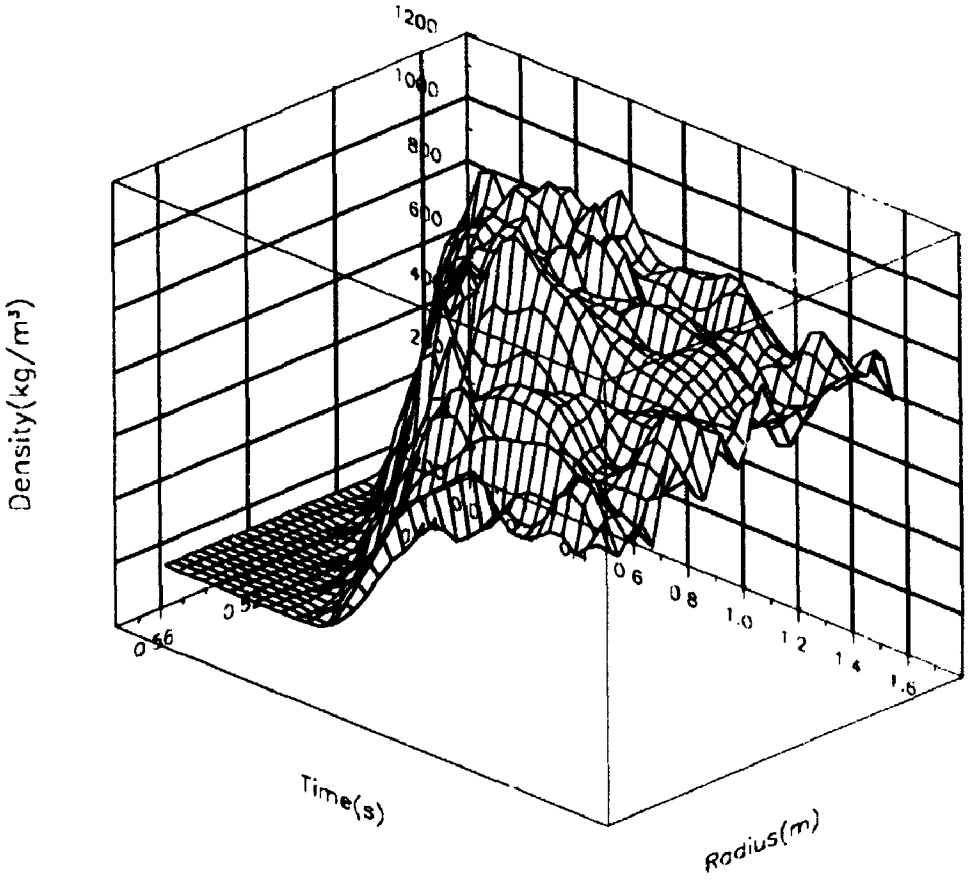

Figure 5.2: The locally averaged density of the gap region β_g against both time t and radius r using standard set of parameters in the case of from start of the refiner to the first steady state.

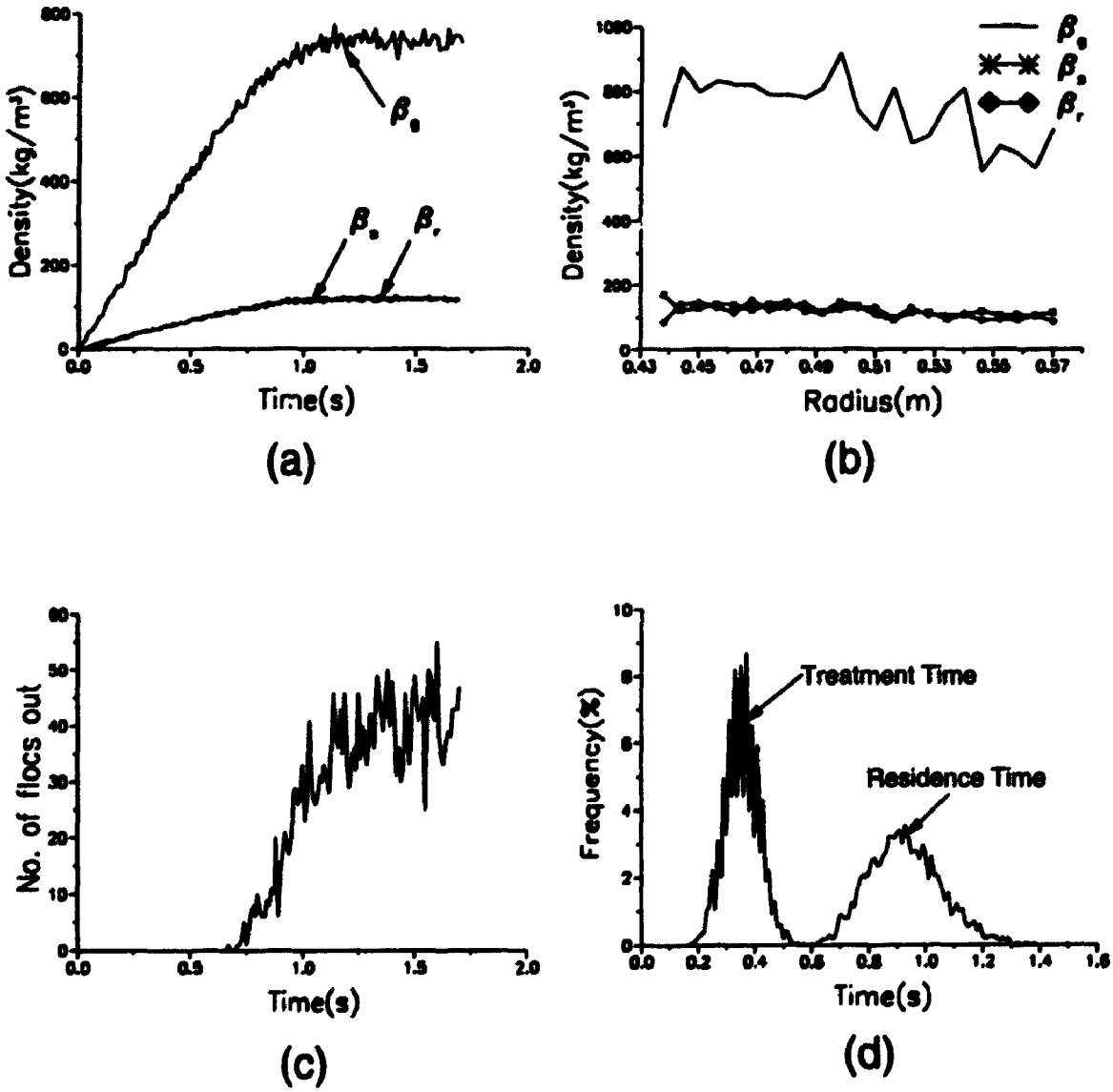

Figure 5.3: The local properties inside the refiner and the residence time and treatment time distributions using the standard set of parameters for up to the first steady state.

time distribution curve, the curve will not get smoother as expected in the case of the residence time distribution. As suggested at the end of the previous Chapter, we averaged the paired neighbouring points in the original data to smear out these regular oscillations in the subsequent calculations for the treatment time.

2). Changing probabilities for up to the first steady state

Figure 5.4 shows the averaged density in the gap using different groups of the probabilities. The averaged density β_g gets progressively lower as the groups of the probabilities change from P_0 to P_3, while the extent of the fluctuations seems to vary little. The next three graphs (Figure 5.5 - Figure 5.7) give the detailed the locally averaged densities for all three regions with respect to r at the end of the first steady state. We can see that as the probabilities vary, the locally averaged densities in all three regions change, but the extent of the fluctuations seems to be more or less the same. Furthermore, although β_g is the lowest in Figure 5.7 among using different groups of the probabilities, the downward trend of the β_g profile with respect to r appears to be evident.

In Figure 5.8, a comparison is given for the number of flocs out using different groups of the probabilities. The only effect observed in this series of graphs on the number of flocs out seems to be the time for the first floc to reach r_2 from r_1, which is progressively shorter as from the case P_0 to P_3. This is probably because in the case of P_3, for example, the probability for a floc to go to the rotor region P_{gr} is the highest among using other groups of the probabilities, therefore, considerable more portion of the flocs spend less time inside the refiner.

Figure 5.9 and Figure 5.10 show the residence time and the treatment time distributions using different groups of the probabilities. It seems that the lower averaged density β_g predicted using P_3 supports sharper distribution and higher mean frequencies of both the residence time and the treatment time, because the flocs get more chances to travel in the rotor region. It also suggests that probability is one of the major control parameters affecting the locally averaged densities, as well as the treatment time or the residence time.

3). Observation for changing set points of steady states

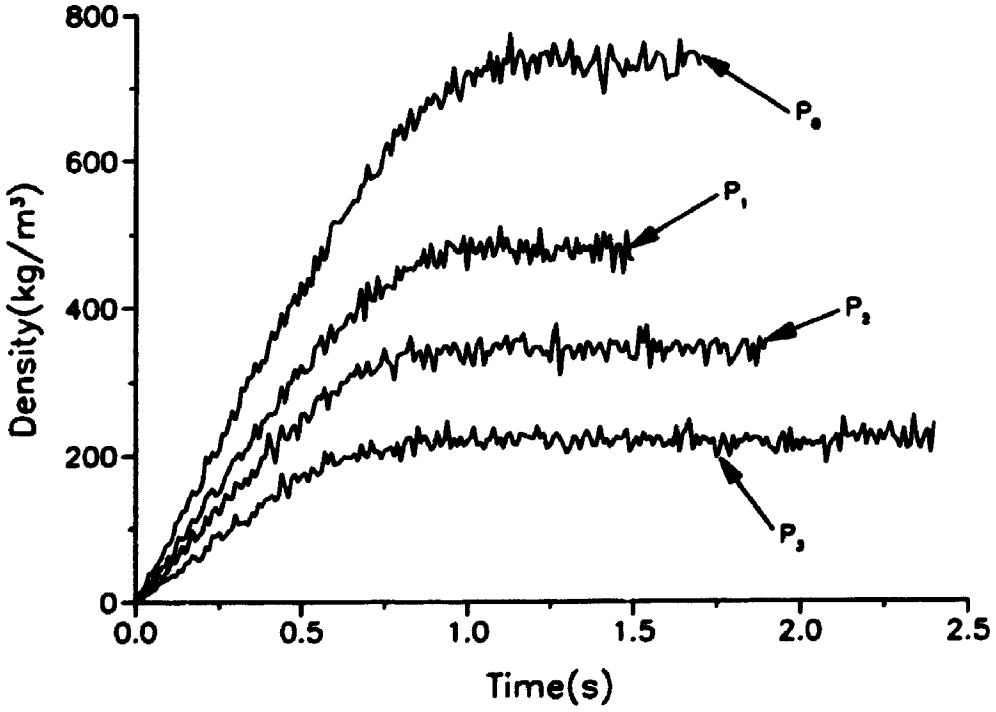

Figure 5.4: The averaged densities β_g versus time t using different groups of the probabilities.

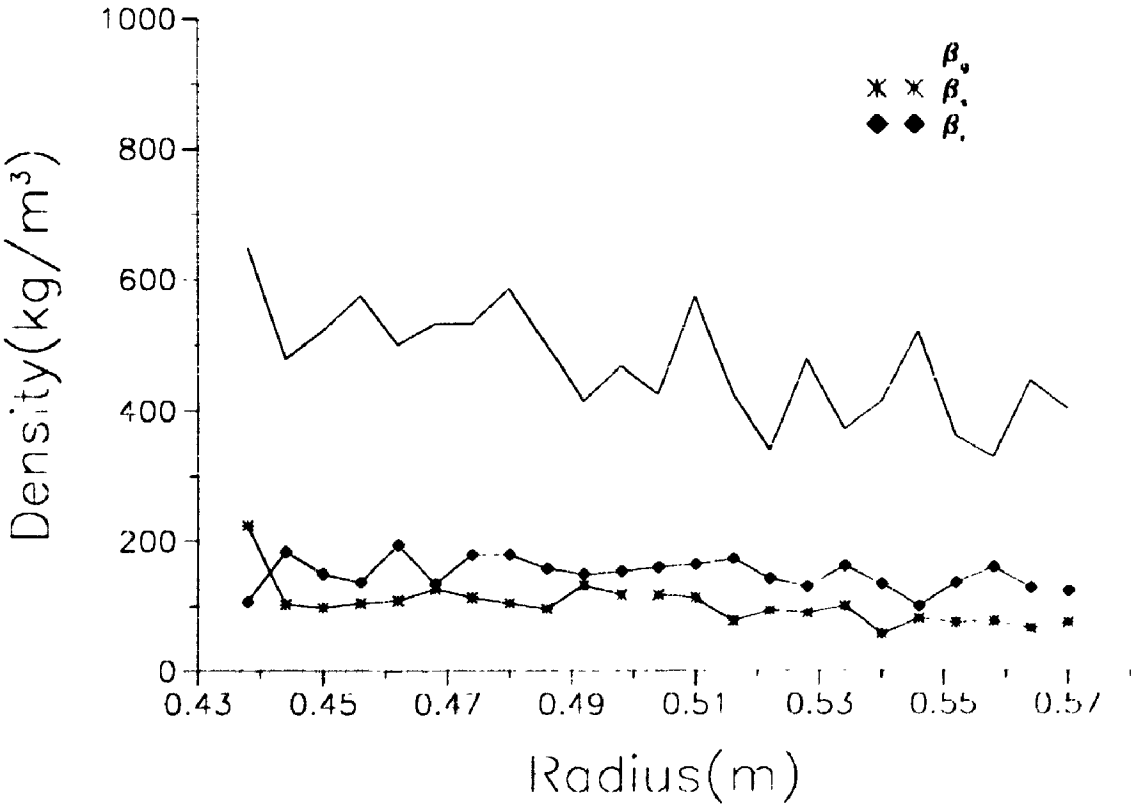

Figure 5.5: Effect of the group P_1 probabilities on the locally averaged densities in all three regions versus r at the end of the first steady state.

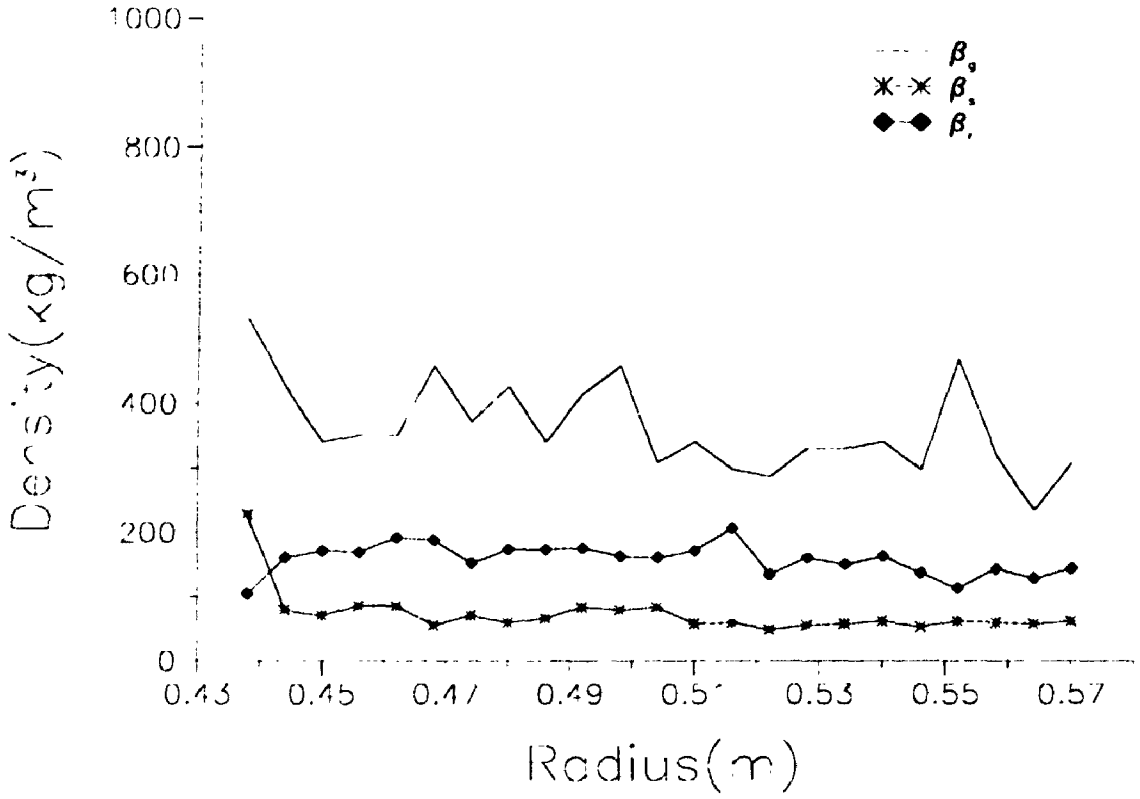

Figure 5.6: Effect of the group P_2 probabilities on the locally averaged densities in all three regions versus r at the end of the first steady state.

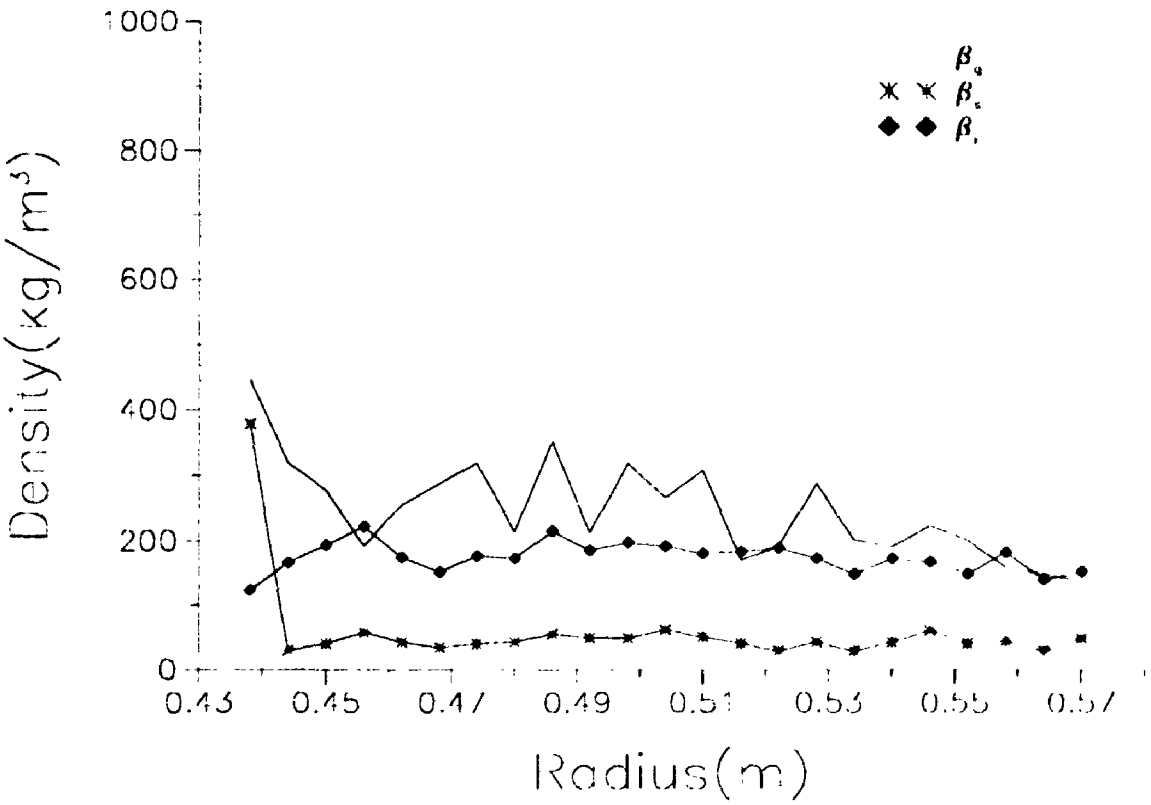

Figure 5.7: Effect of the group P_3 probabilities on the locally averaged densities in all three regions versus r at the end of the first steady state.

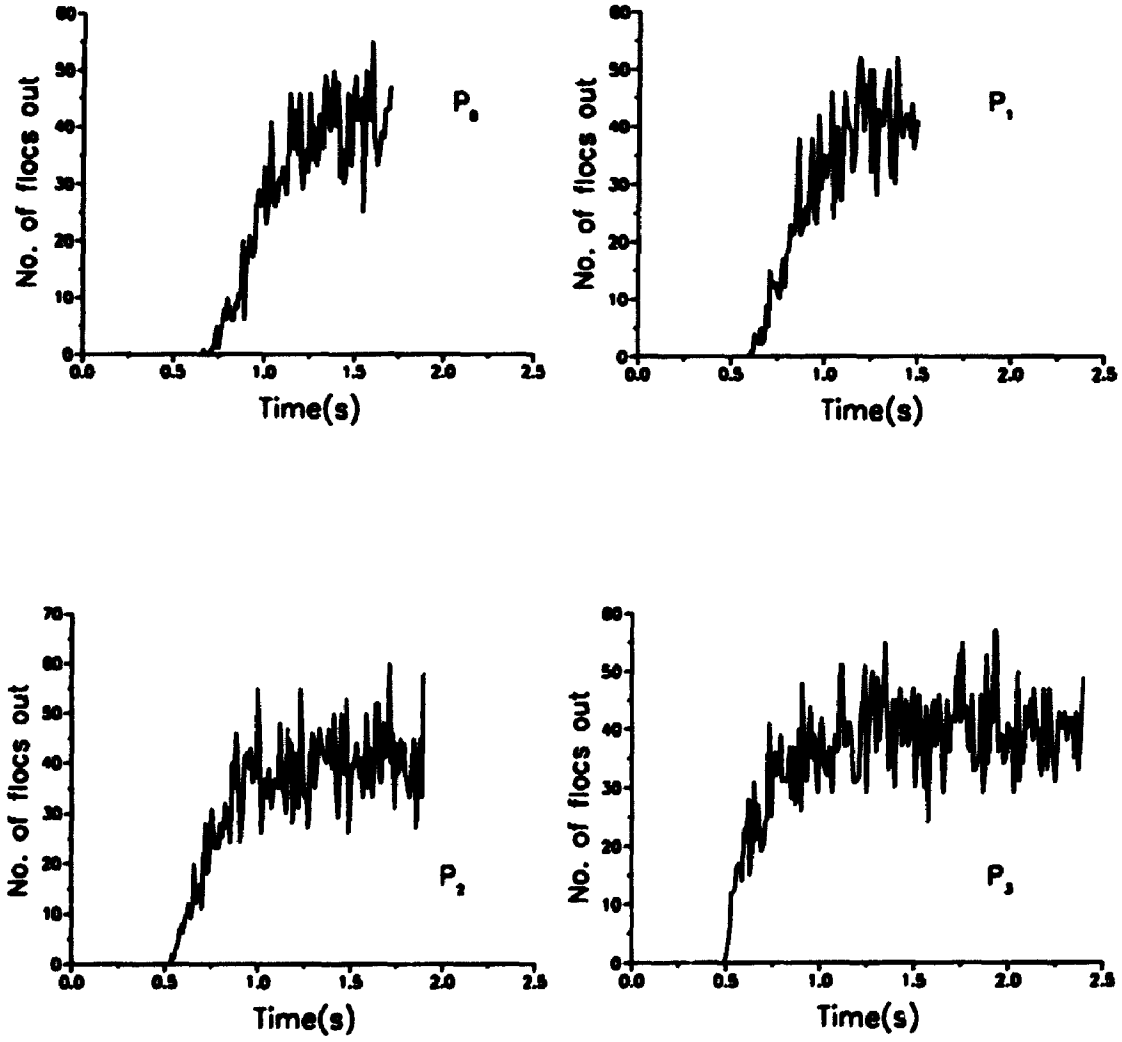

Figure 5.8: Effect of different groups of the probabilities on the number of flocs out of the refiner for up to the first steady state.

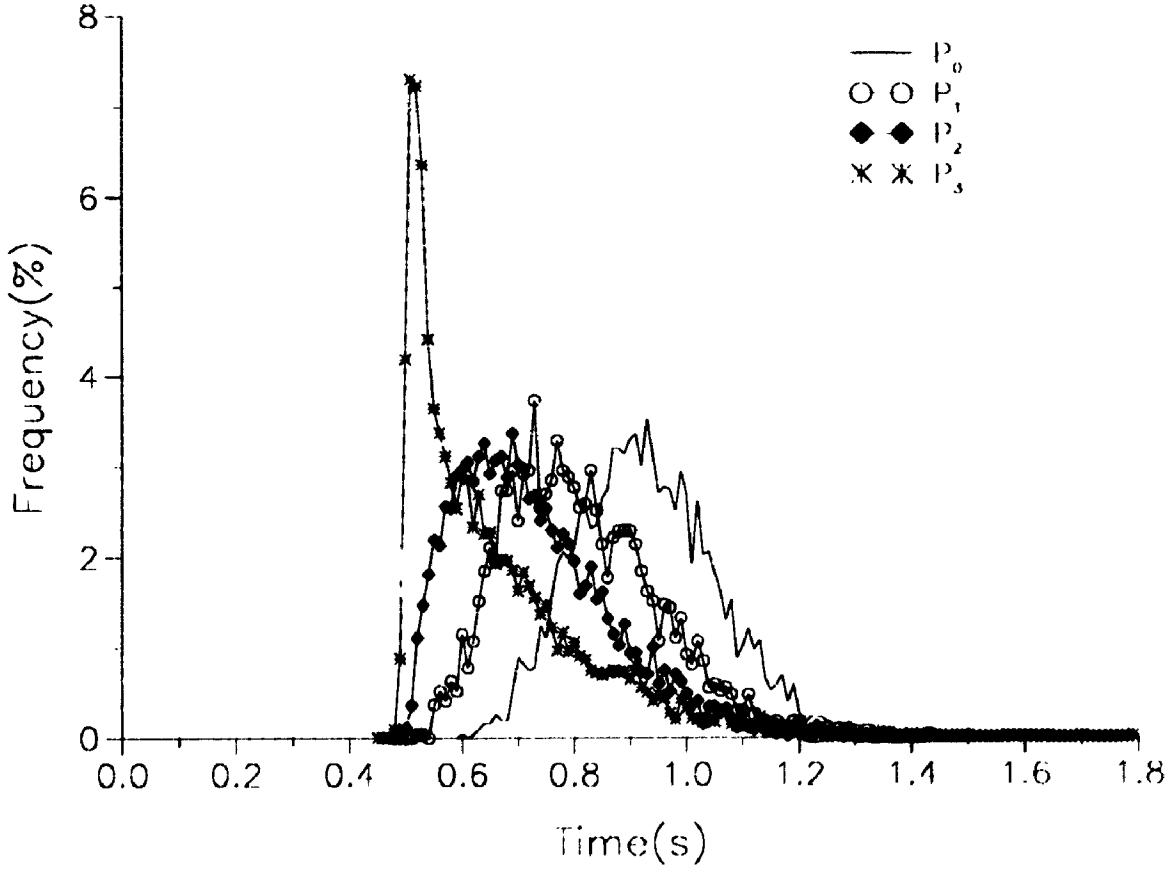

Figure 5.9: Residence time distribution using different groups of the probabilities for up to the first steady state.

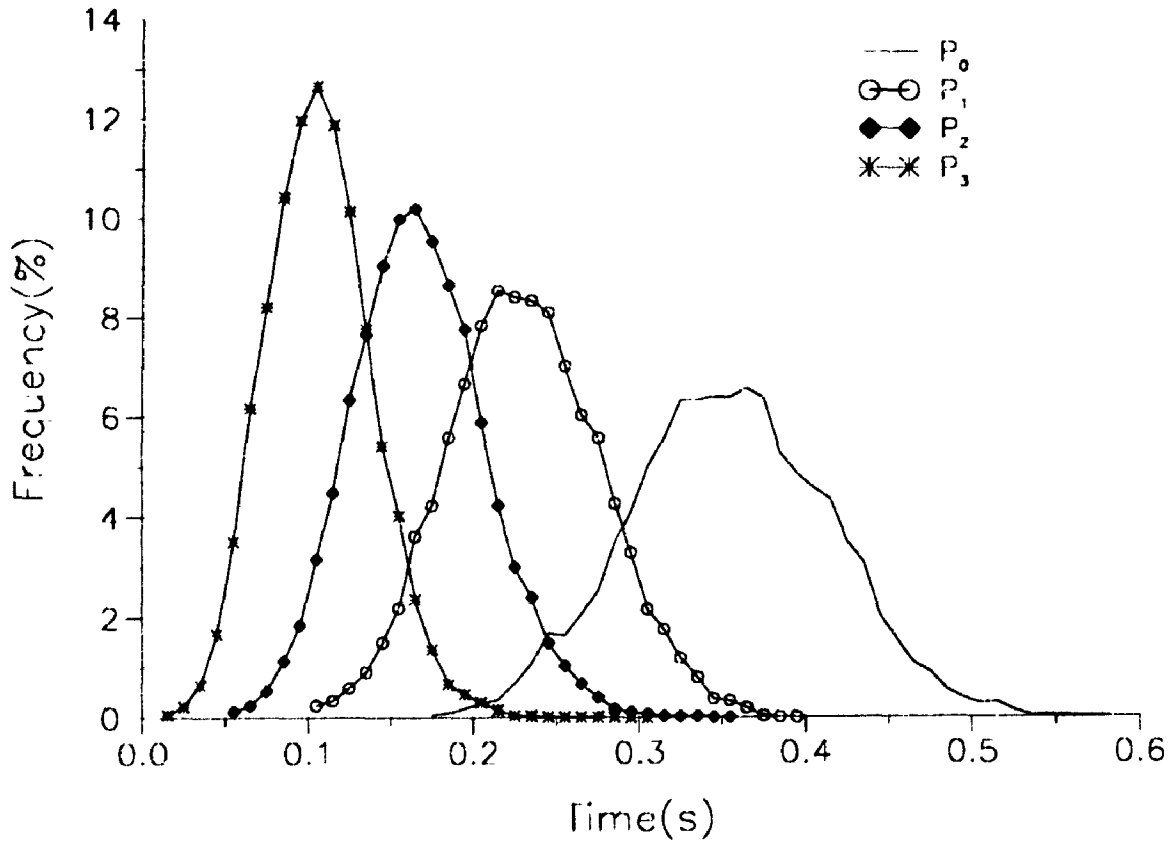

Figure 5.10: Treatment time distribution using different groups of the probabilities for up to the first steady state.

After the first steady state is reached, we give a small variation to the feed rate represented by increasing the number of flocs into the refiner in time Δt. The results are shown in Figure 5.11, in which β_g and the number of flocs out are plotted against t for $N = 40+4$ (10% increase) and $N = 40+8$ (20% increase). If all other parameters are kept the same, the changes in the averaged densities seems to be proportional to the changes in feed rate brought about by the changes in N. Another observation is that the time period for refining to reach new steady state from the previous one is approximately in the same order as from 0 to the first steady state.

4). Changing the number of flocs into r_1 for up to the second steady state

Figure 5.12 shows that using different number of flocs into r_1 has little effect on the mean values of the averaged density β_g, because it does not change the mass of the feed rate. We found, however, that the extent of the fluctuations is greater, say, for the case $N = 10$ compared with that $N = 120$, in which cases the second criterion for defining a steady state has to be altered accordingly to 0.03 and 0.01 respectively to ensure the convergence to a steady state in a consistent way. Or, the extent of the fluctuations in β_g tends to be inversely proportional to the number of flocs into r_1 used in the simulations. On the other hand, as shown in Figure 5.13, the influence of different number of flocs in on the number of flocs out is not obvious. At first sight, there seems to be a greater extent of the fluctuations in the number of the flocs out for the larger N used, but if we look at the results closely, we can find, on the contrary, that the extent of the fluctuations is greater for smaller N in a relative scale (extent of the fluctuations divided by N), because N is different for the different curves shown in Figure 5.13.

The above results can be explained by the following. The lower number of flocs into the refiner will certainly decrease the number of flocs contained in the sample section of δr, thus, will result in excessive fluctuations in β_g and the number of flocs out. The opposite situation is also true for the large number of flocs into r_1, so that the fluctuations are reduced. These results indicate that although N is a very important parameter for the model, it only affects the ways to define a steady state, but not the average properties such as the mean values of the locally averaged densities inside the

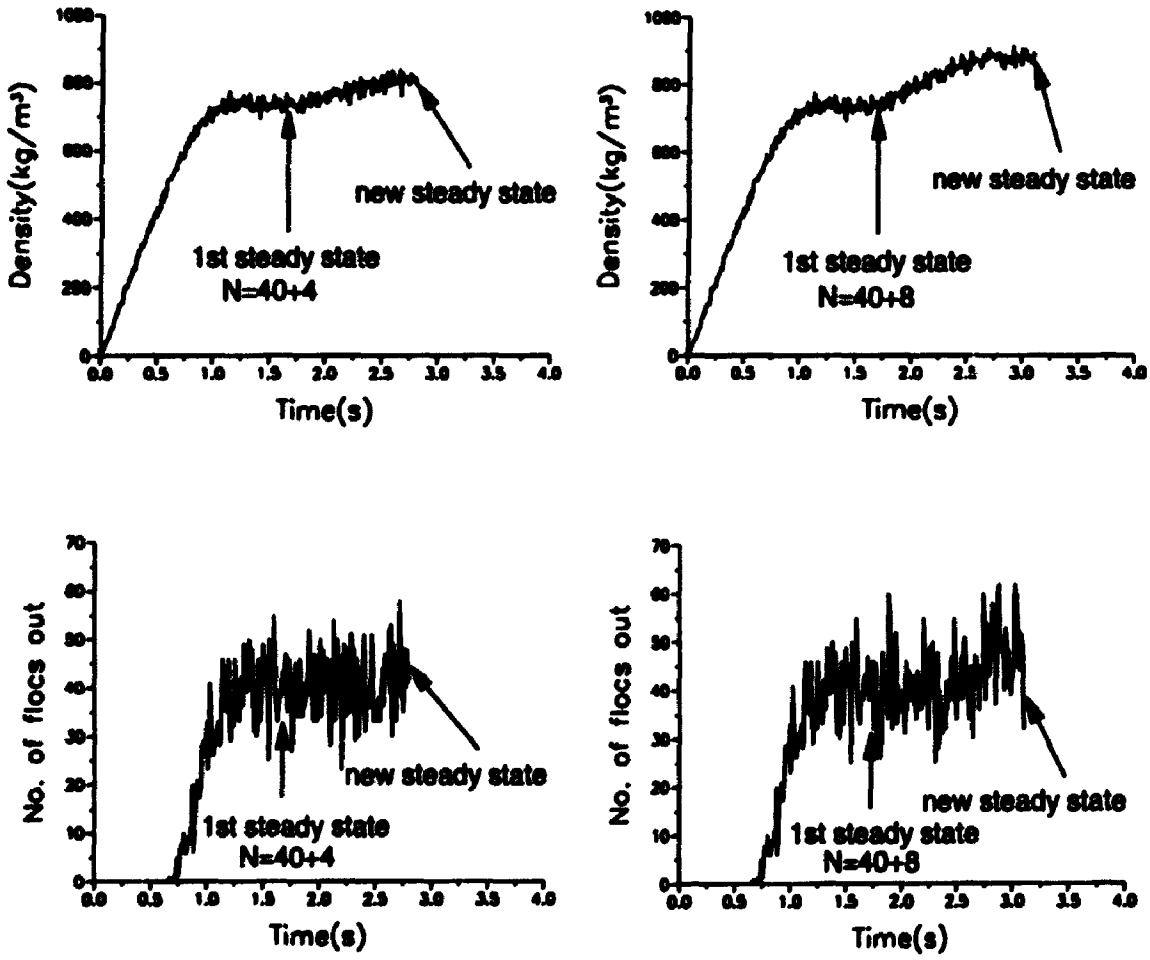

Figure 5.11: The averaged density β_g and the number of flocs out of the refiner versus time t using the standard set of parameters. The simulations are from 0 state to the first steady state, and then a 10% or 20% increase is given to the feed rate until the second steady state is reached.

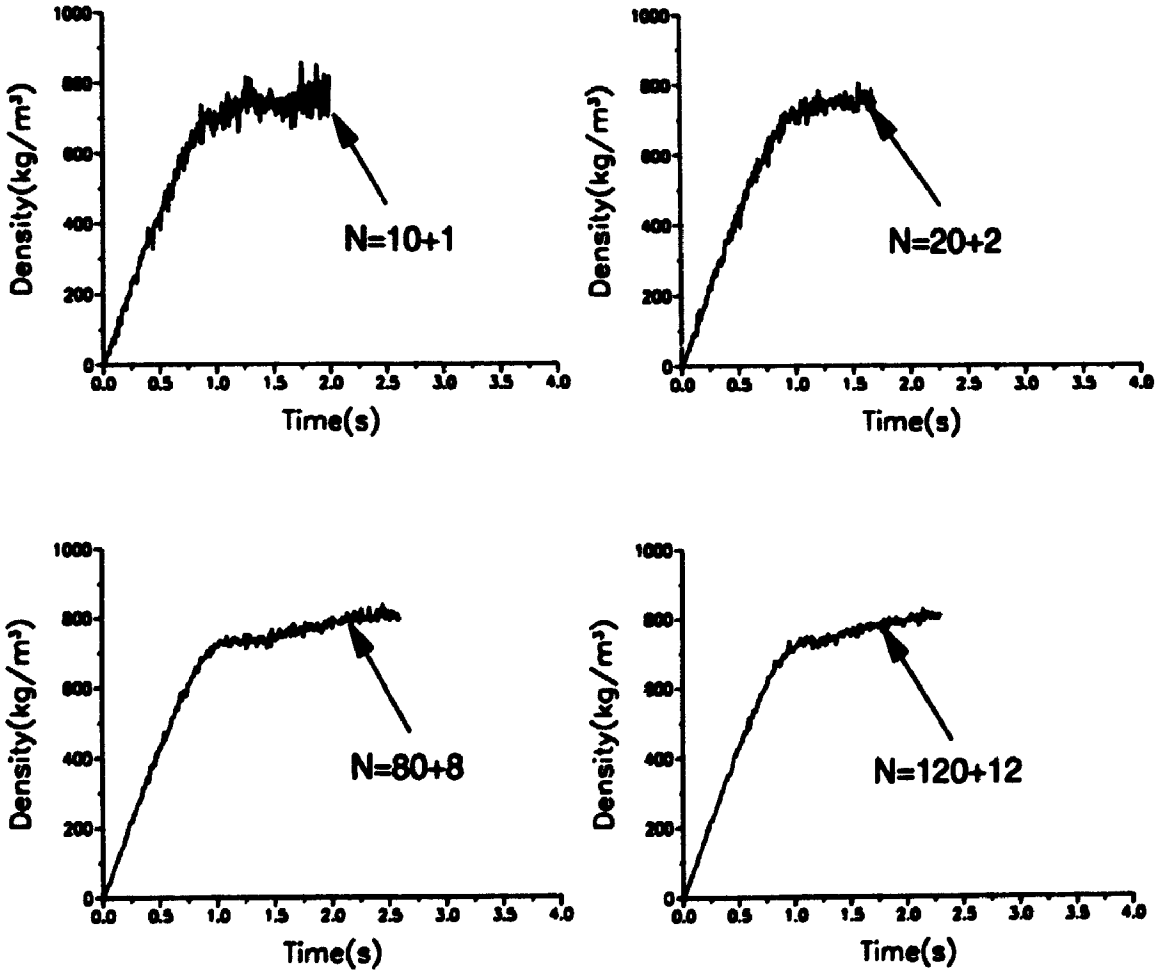

Figure 5.12: The averaged density β_g versus time t using different number of flocs into r_1 with a 10% increase in the feed rate until the second steady state is reached.

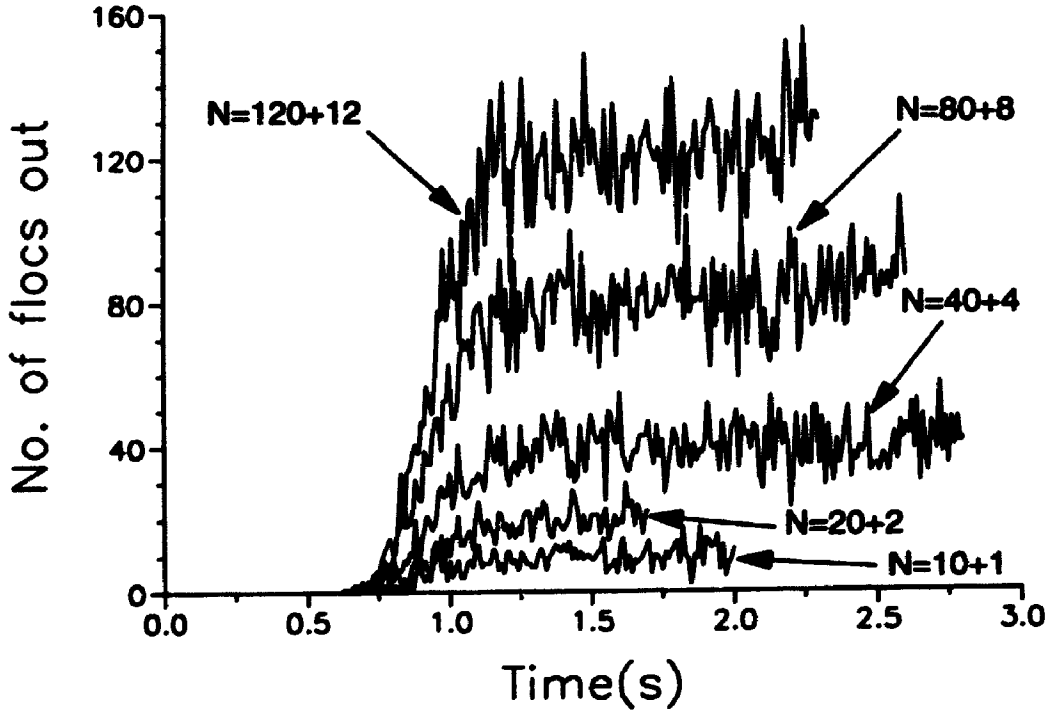

Figure 5.13: Effect of different number of flocs into the refiner on the number of flocs out of the refiner versus time t for a 10% increase of the feed rate until the second steady state is reached.

refiner. If the number of flocs into the refiner is large enough to retain the fluctuations in the local properties to some range, the exact number of flocs into r_1 (or mass of a single flocs assumed) may not be crucial to the model at this stage.

The next four graphs (Figure 5.14 - Figure 5.17) illustrate the growing trend of all three locally averaged densities with respect to r at different time steps between the first steady state and the second steady state for a 20% increase of the feed rate.

The growing of β_g is obvious for different time steps, whereas the growing of β_r and β_s is barely noticeable. The growing of β_g happens in an ordered way along r in succession of the time steps.

There are very little changes using different number of flocs into r_1 for the residence time and the treatment time distributions except for smoothness of the curves, since it directly changes the total number of flocs used to calculate the residence time and the treatment time.

5.5 Concluding Remarks

We have developed a time-dependent stochastic model to predict some important local properties inside a refiner. The model improves from the previous one that it connects the feed rate to the local properties of a refiner, which leads an important step towards to applying the stochastic model to the refining operation. It can also be used to study the property changes on different set points of steady states. In addition, using the model we have tested the correlations between the locally averaged densities and the treatment time and the residence time distributions.

The following conclusions may be summed up from the simulations using the model.

1. The locally averaged densities are predicted to fluctuate in both radius r and time t directions especially for β_g.

2. The mean values of the locally averaged densities are directly proportional to the feed rate of the refiner.

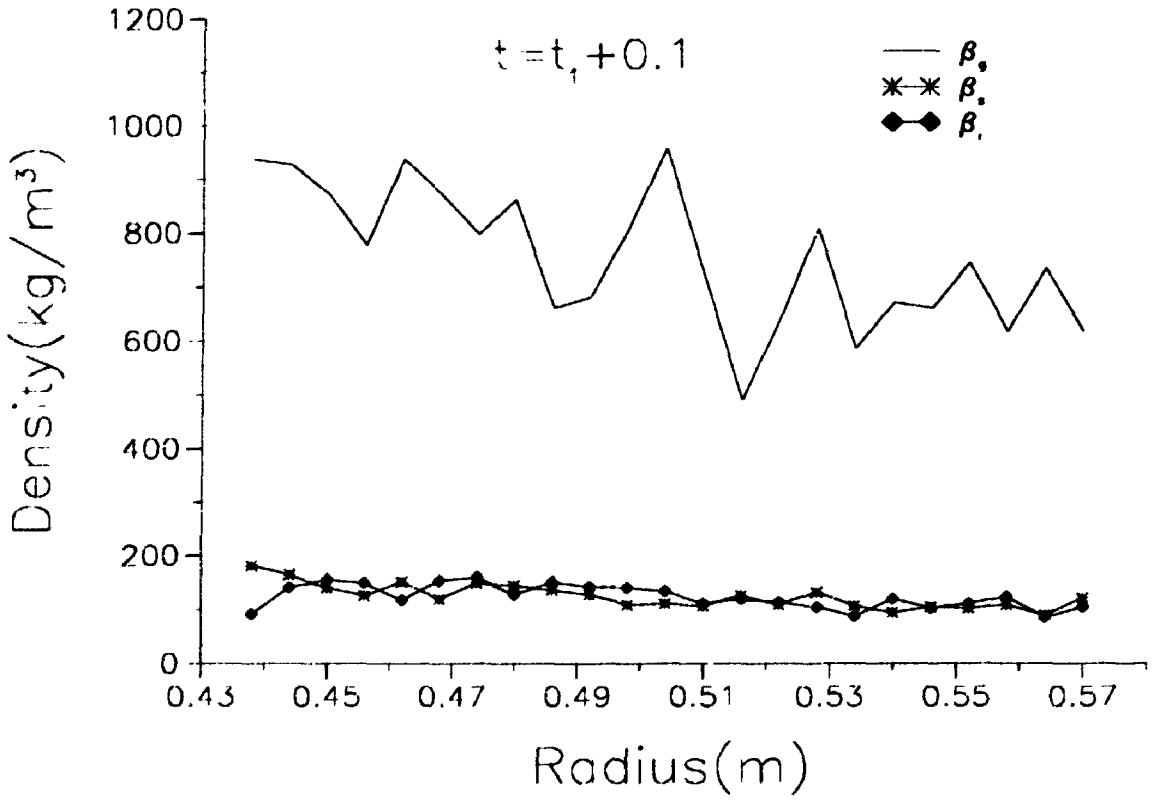

Figure 5.14: All three locally averaged densities versus radius r at the time immediately after a 20% increase of the feed rate is given when the first steady state is reached at $t_1 = 1.8$ s.

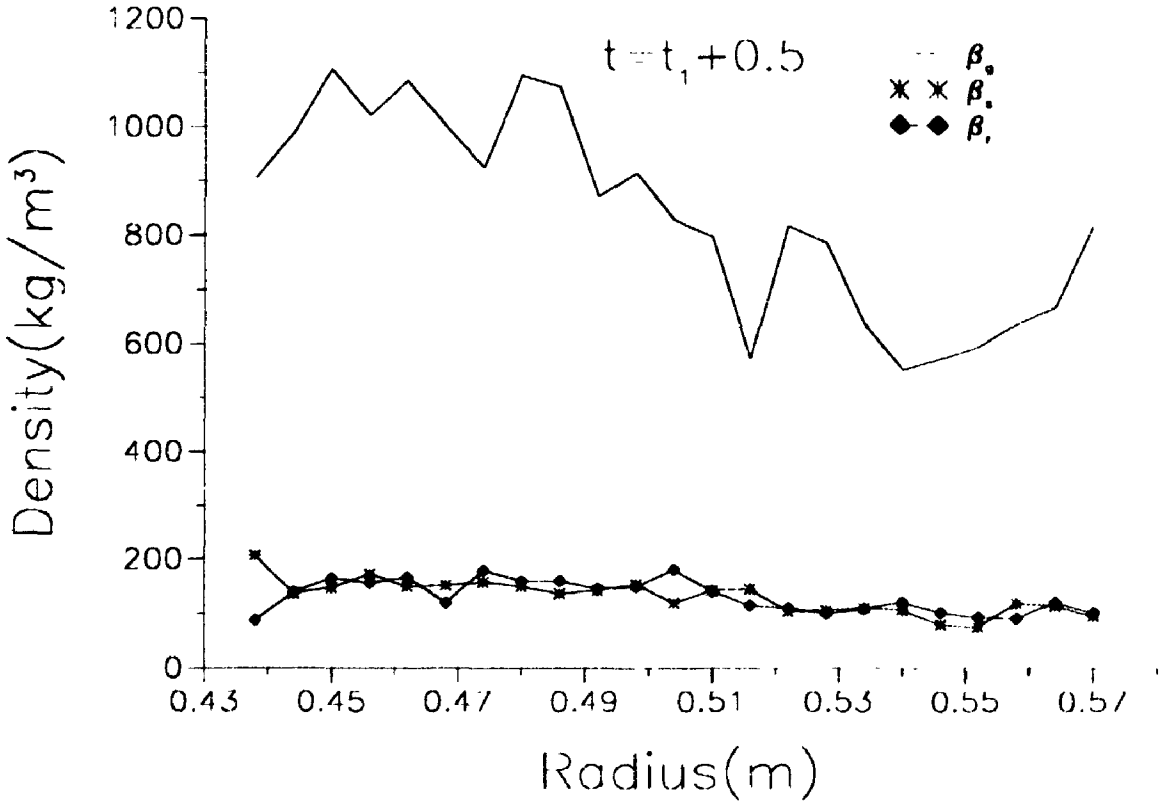

Figure 5.15: **All three locally averaged densities versus radius r at the time 0.5 s after a 20% increase of the feed rate is given when the first steady state is reached at $t_1 = 1.8$ s.**

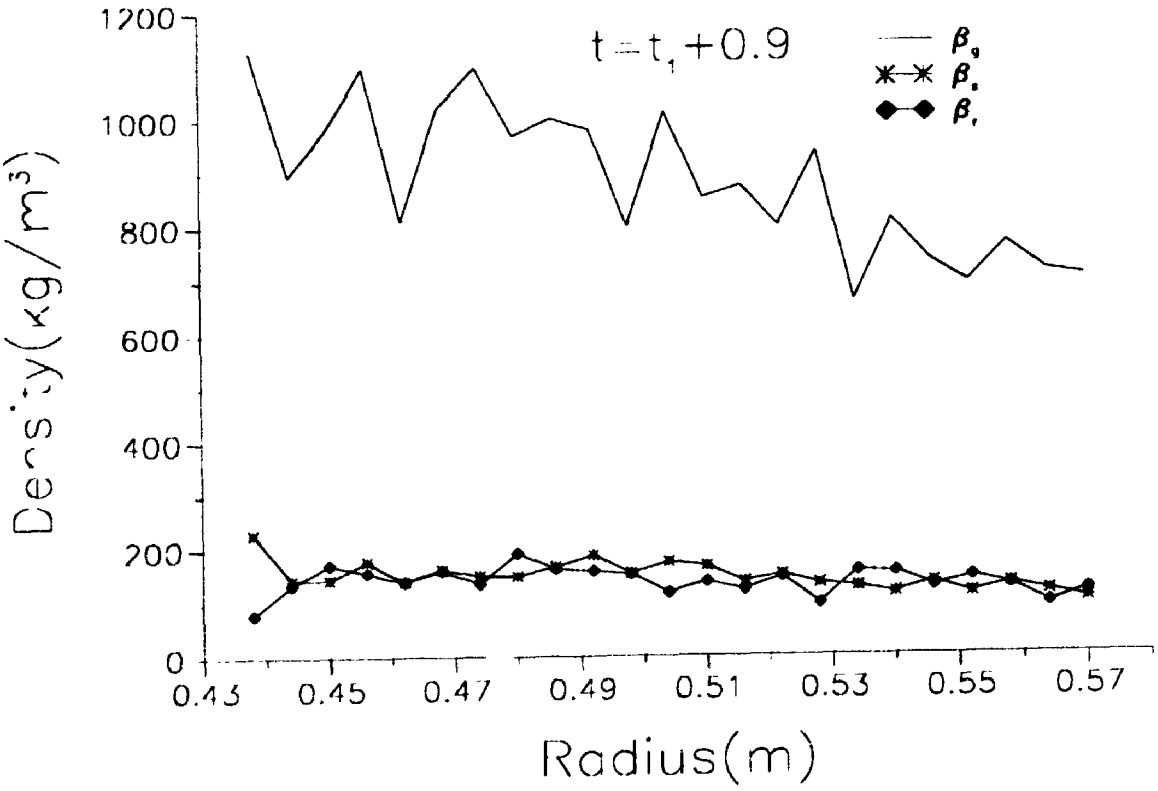

Figure 5.16: All three locally averaged densities versus radius r at the time 0.9 s after a 20% increase of the feed rate is given when the first steady state is reached at t_1.

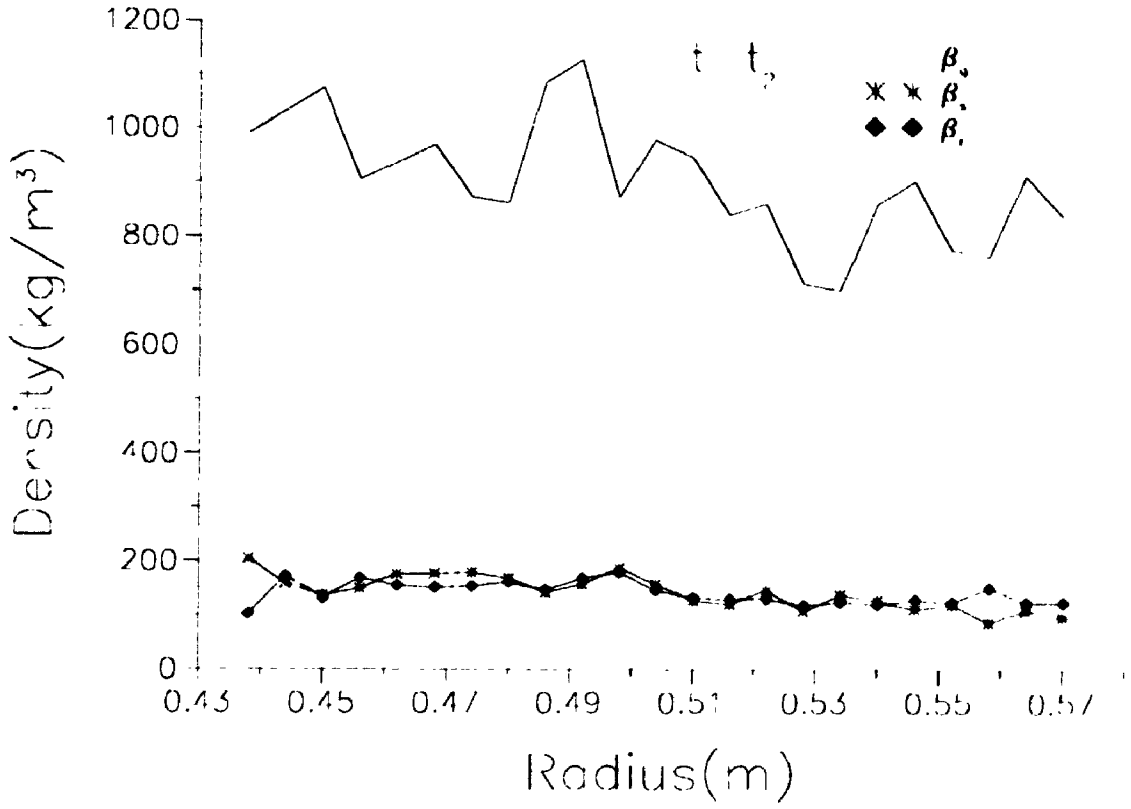

Figure 5.17: All three locally averaged densities versus radius r at the time of the second steady state $t_2 = 3.1$ s after a 20% increase of the feed rate is given when the first steady state is reached at $t_1 = 1.8$ s.

3. The probabilities are a very important parameter for the locally averaged densities, but they affect little on the degree of the fluctuations in these properties.

4. The number of flocs into the refiner (or mass of a single floc) influences the extent of the fluctuations in the local properties, but not the average values of these properties.

5. There is no significant change for the residence time and the treatment time distributions when the locally averaged densities change as a result of the feed rate increase, whereas the locally averaged densities are controlled by the probability, in a similar way as the residence time and the treatment time distributions are.

Through the parameter study, we have accumulated first hand experiences which will be needed for further advance of the stochastic model. The current model can be improved by developing a mechanism to relate the probabilities to the locally averaged pulp densities so that the probabilities will be calculated instead of being assigned constants at the present. Finally, the relation between the dynamic gap width and the local properties must be worked out before the model can be used to predict the dynamic behaviour of refining.

Chapter 6

PROBABILITIES FOR FLOC EXCHANGES

6.1 Factors to Control Floc Exchanges

In the models described in the previous Chapters, the probability parameters were simply taken as constants, and the simulations were done using a range of the probability parameters. Now we want to study the factors that influence the probability exchanges among the three regions, so that we can more precisely predict the floc movement inside refiners. There are many factors that can influence the pulp floc exchanges inside a refiner, but we believe that at least two categories are very important to the model. In order to study these effects efficiently, we try to identify the factors belonging to each category, and study them separately.

The first category are stochastic factors, such as turbulent flow in different regions, forces caused by passing bar edges, as well as the doctoring/stapling mechanism speculated by Miles *et al.* [48]. These factors are hard to put into quantitative form, so we simply assign a constant portion to the probability expressions. But their effect should be represented one way or another in the probability expressions.

The second category is represented by the density difference among the three regions. The basic concept we use to specify the probability parameters as functions of the locally averaged densities (defined in the previous Chapter) is the following: The pulp densities in different regions inside a refiner should tend to equalize among the three regions around the steady state of refining. If one region has a higher locally averaged pulp density, it is more likely that pulp flocs are going to end up in the region with the lower locally averaged pulp density. For example, when the density is high

in the stator compared with that in the gap, there is little chance for a floc in the gap to go to the stator, but there is a high chance for a floc in the stator to go to the gap. With this principle in mind, we try to put the mechanism into formulas.

6.2 First Version of the Probability Expressions

We define probability parameters as functions of β_r, β_s and β_g, and choose an exponential profile to start with, where all the probabilities (except maybe P_{gg}) are between 0 and 1. We assume that when the steady state in refining is reached the probability parameters will have equal values with respect to the three regions. We also assume that the locally averaged densities of pulp tend to equalize in steady state. In order to satisfy the conditions that when variables are equal to 1 (corresponding to the equal density situation) the probabilities tend to certain specific values, the expressions need to be adjusted by the following.

Now let us consider a special case that all the densities are the same, or the steady state. In this situation, according to our assumption, we obtain that $P_{sg} = P_{rg} = 1/2$ and $P_{gr} = P_{gs} = 1/3$. We have to reflect this situation in the probability expressions:

$$P_{sg} = \exp(-\ln(2)\frac{\beta_g}{\beta_s}) \tag{6.1}$$

$$P_{gs} = \exp(-\ln(3)\frac{\beta_s}{\beta_g}) \tag{6.2}$$

$$P_{gr} = \exp(-\ln(3)\frac{\beta_r}{\beta_g}) \tag{6.3}$$

$$P_{rg} = \exp(-\ln(2)\frac{\beta_g}{\beta_r}). \tag{6.4}$$

We can see that these expressions will satisfy the conditions when variables are equal to 1. For example, when $\beta_s/\beta_g = 1$, $P_{gs} = e^{-\ln(3)} = 1/3$. The 'ln' terms in the expressions only affect the slopes of the profiles, not the values of the end points.

Equations (6.1) and (6.4) are right now, but there are still some problems for Equations (6.2) and (6.3). Notice that both P_{gs} and P_{gr} will be close to 1 when both β_s and β_r are much smaller than β_g, which will lead to P_{gg} negative. This is because we have ignored the special situation in the gap so far, where there are *three*

possibilities instead of *two* as in the stator or the rotor. In other words, we have to take into account the influence of the third density when considering P_{gs} or P_{gr}. Equations (6.2) and (6.3) can be improved by introducing a linear combination in term of ratio of the third density to the density in the gap:

$$P_{gs} = k_r(\frac{\beta_r}{\beta_g})\exp(-\ln(3)\frac{\beta_s}{\beta_g}) \tag{6.5}$$

$$P_{gr} = k_s(\frac{\beta_s}{\beta_g})\exp(-\ln(3)\frac{\beta_r}{\beta_g}), \tag{6.6}$$

where

$$k_r(\frac{\beta_r}{\beta_g}) = \begin{cases} \frac{1}{2}(1+\frac{\beta_r}{\beta_g}) & \text{if } \frac{\beta_r}{\beta_g} < 1 \\ 1 & \text{otherwise} \end{cases} \tag{6.7}$$

and,

$$k_s(\frac{\beta_s}{\beta_g}) = \begin{cases} \frac{1}{2}(1+\frac{\beta_s}{\beta_g}) & \text{if } \frac{\beta_s}{\beta_g} < 1 \\ 1 & \text{otherwise.} \end{cases} \tag{6.8}$$

The above equations for introducing the effect of the third density reflect the assumption that when the ratio of the third density to the density in the gap is greater than 1, the effect on the probabilities is the same as that when the ratio is equal to 1 as far as the particular probability is concerned. However, the higher ratio of the third density to the density in the gap will reduce the other independent probability in the gap. Here we treat the dependence of the third density only up to the point where the third density and the density in the gap are equal.

Now let us check the general trend of Equations (6.5) and (6.6). First, we see that the maximum values for Equations (6.5) and (6.6) are still in the left boundary, but in general will be smaller than one. Secondly, we observe that the influence of the third density has been included in the expressions. For instance, as β_r/β_g increases between 0 to 1, P_{gs} will increase due to increasing of the third density β_r. Lastly, Equations (6.5) and (6.6) go to zero as β_r/β_g and β_s/β_g tend to ∞.

In addition, we can check some special values of probabilities using Equations (6.5) and (6.6) listed in Table 6.1. We see clearly that for most of the cases Equations (6.5) and (6.6) predict the two independent probabilities in the gap correctly. There are still some cases, however, such as those shown in the last two rows in Table 6.1, that

Table 6.1: Some special values of probabilities predicted using P_{gs} and P_{gr} expressions with k_r and k_s factors.

P_{gs}	P_{gr}	β_s/β_g	β_r/β_g
0	1	∞	0
1/3	1/3	1	1
1/2	1/2	0	0
1	0	0	∞
0	0	∞	∞
1	1/6	0	1
1/6	1	1	0

cannot completely satisfy the boundary conditions imposed by rule of probability, namely $P_{gr} + P_{gs} + P_{gg} \leq 1$. This is the result of using a linear combination to approximate the effect of the third density on the probabilities. There seems to be no such a simple form of equations to satisfy all the conditions. It should also be noted that these values predicted by the equations are small deviation from the conditions imposed, and these situations are very rare in the simulation (like β_s/β_g close to 0).

The locally averaged density was averaged again over refining zone to limit the possible unstable components. The above expressions were found to be unstable in the simulations.

6.3 Second Version of the Probability Expressions

We found that the reason for the probability expressions being unstable is the false assumption used that probabilities go to certain values when it is in steady state, and that equal *mass flux* should be demanded in the steady state instead. It does indeed make sense physically that the *mass flux* be related to the density rather than the probability of floc exchanges alone, because it is the product of probability and the number of flocs in one region that controls the total number of flocs out of that region.

We also modify the exchange mechanism that the relative locally averaged density compared to the maximum density of pulp will be the control factor for floc exchanges. We argue that the room availability in different regions inside a refiner plays an important rule in determining the probabilities of floc exchanges. To illustrate the point, let us see two extreme situations:

1. Volumes of the three regions are nearly fully packed with flocs.

   In this situation, a flux of flocs out of that nearly fully packed region is possible only if there is space available in the target region where the flux is going to, i.e., it does not matter how strong the driving forces are, and the pulp flocs can only move if they have room to move to. Thus the densities in the target regions control the flux, regardless of the *ratio* of the density differences of the two regions. Therefore, the densities in source regions are not important.

2. Volumes of the three regions are sparsely packed.

   Then the first category of the factors, such as turbulence, pressure difference between the regions and so on, is probably the mechanism that governs the floc exchanges. In this case, the densities in the target regions are irrelevant, only the densities in the source regions are responsible for the floc exchanges.

In general for the in-between situations, the above two mechanisms apply. So we believe that it is the ratios of the densities to the maximum pulp density that control the probability for floc exchanges among the three regions.

Now we put the new mechanisms into probability expressions:

$$P_{sg} = k_1[\frac{\beta_s}{\beta_{max}}(1 - \frac{\beta_g}{\beta_{max}})] \tag{6.9}$$

$$P_{rg} = k_2[\frac{\beta_r}{\beta_{max}}(1 - \frac{\beta_g}{\beta_{max}})] \tag{6.10}$$

$$P_{gr} = k_3[\frac{\beta_g}{\beta_{max}}(1 - \frac{\beta_r}{\beta_{max}})] \tag{6.11}$$

$$P_{gs} = k_4[\frac{\beta_g}{\beta_{max}}(1 - \frac{\beta_s}{\beta_{max}})]. \tag{6.12}$$

where β_{max} is maximum density of pulp, and k_i are constants.

If we assume that when steady state is reached, the densities tend to equalize and the mass flux into a region is equal to the flux out of that region, then we obtain the following relations:

$$\beta_s = \beta_g = \beta_r \tag{6.13}$$

and,

$$N_s P_{sg} = N_g P_{gs}, \qquad \text{or} \qquad N_s k_1 = N_g k_4 \tag{6.14}$$

$$N_r P_{rg} = N_g P_{gr}, \qquad \text{or} \qquad N_r k_2 = N_g k_3. \tag{6.15}$$

Using the definition of the locally averaged density for pulp flocs described in Chapter 5, we can obtain in the steady state:

$$\frac{N_s}{N_g} = \frac{A_s}{A_g} \tag{6.16}$$

$$\frac{N_r}{N_g} = \frac{A_r}{A_g}. \tag{6.17}$$

Therefore, we can get the connections among 4 coefficients in the probability expressions:

$$k_1 = \frac{A_g}{A_s} k_4 \tag{6.18}$$

$$k_2 = \frac{A_g}{A_r} k_3. \tag{6.19}$$

If we further assume that the probabilities for flocs to go to the stator or to go to the rotor from the gap are equal when densities in the three regions tend to equalize, we can reduce the number of the coefficients to one, i.e., $k_3 = k_4 = k$. The range of k can be estimated from examining the probability expressions in the steady state. For example, from $P_{gr} = k\beta_e(1 - \beta_e)$ where $\beta_e = \beta_s/\beta_{max} = \beta_g/\beta_{max} = \beta_r/\beta_{max}$, we see that P_{gr} reaches a maximum $k/4$ when $\beta_e = 1/2$. Therefore, if we restrict $P_{gr} \leq 1/2$, then we can take $0 < k \leq 2$ in any case.

6.3.1 Testing of the probability expressions

The above probability expressions were tested using the same program described in the previous Chapter (time-dependent model), in which the constant probabilities

Table 6.2: Values of probabilities predicted using the third version of the probability expressions for $k = 1$.

Time(s)	β_s/β_{max}	β_g/β_{max}	β_r/β_{max}	P_{sg}	P_{gs}	P_{gr}	P_{rg}
t=0.60	0.049	0.064	0.078	0.009	0.06	0.059	0.015
t=4.40	0.155	0.139	0.173	0.027	0.118	0.124	0.019

were replaced by these formulas. The probabilities were first given a set of constant values to start the calculation when the refiner is empty, otherwise zero probabilities would have been predicted due to no floc present in any regions. This set of constant values of probabilities was replaced by the formulas when time $t = 0.50$ s, and the probabilities were updated using the expressions after every time step Δt until the second steady state is reached. Note that we still used the averaged pulp densities over refining zone to improve the stability of the probabilities calculated using the formulas. The cross sectional areas used in the program were the same as before, i.e., $A_s = A_r = 9 \times 10^{-6}$ m^2, $A_g = 1.8 \times 10^{-6}$m^2, so that $A_s/A_g = 5$. The maximum density of pulp was chosen to be the density of fibre wall, which is usually considered to be $\beta_{max} = 1500$ kg/m^3 [64]. The number of flocs into the refiner in Δt was $N = 40$, and the dynamic change of flocs was a 10% increase, or 4. All of the other parameters were the same as described in the previous Chapter.

It was turned out that the expressions are quite stable for a wide range of k, like from 0.1 to 5, for this particular set of parameters. When k is very small, say $k = 0.1$, all the probabilities are proportionally smaller, as a result, the exchange among the three regions is very small, and the steady state cannot be reached because of the large difference of the averaged densities for the three regions. The steady state can be achieved when $k \geq 1$. The coefficient k can even be taken as high as 5 because in this case the highest densities predicted by using this set of parameters is about 200 kg/m^3, well lower than the $\beta_e = 1/2$, or 750 kg/m^3. In the Tables 6.2 and 6.3, some typical sets of probabilities and the averaged densities calculated for the cases of $k = 1$ and $k = 4$ are listed.

Table 6.3: Values of probabilities predicted using the third version of the probability expressions for $k = 4$.

Time(s)	β_s/β_{max}	β_g/β_{max}	β_r/β_{max}	P_{sg}	P_{gs}	P_{gr}	P_{rg}
t=0.60	0.057	0.06	0.07	0.043	0.225	0.221	0.053
t=3.50	0.128	0.121	0.110	0.09	0.422	0.431	0.078

The general trend of these expressions is well behaved. In other words, the probabilities grow slowly from the lower values at the time of start of kicking in to some steady values near the first steady state, then to the second. No obvious oscillations were observed for all the cases of using different values of k's.

These sets of probabilities, for example listed in Table 6.3 for $t = 3.50$ s, were also tested as constants using the first stochastic model described in Chapter 3, because we never tried these combinations of the probabilities before. The results are quite similar to those obtained using variable probability parameters.

6.4 Final Version of the Probability Expressions

Based on the experience gained on developing the previous versions of the probability formulas, we want to further improve the formulas in the following aspects:

1. when no floc is in the refiner, the probabilities should not be zero;
2. when densities are small, their effect on the probabilities are also small;
3. when target density is close to maximum, the probability for flocs to go to that region is close to zero.

We also introduce a constant portion A in the probability expressions to explicitly represent the stochastic factors discussed at the beginning of the Chapter. Here are the latest expressions:

$$P_{sg} = k_1[(\frac{\beta_s^2}{\beta_{max}^2} + A)(1 - \frac{\beta_g^2}{\beta_{max}^2})] \tag{6.20}$$

$$P_{rg} = k_2[(\frac{\beta_r^2}{\beta_{max}^2} + A)(1 - \frac{\beta_g^2}{\beta_{max}^2})] \quad (6.21)$$

$$P_{gr} = k_3[(\frac{\beta_g^2}{\beta_{max}^2} + A)(1 - \frac{\beta_r^2}{\beta_{max}^2})] \quad (6.22)$$

$$P_{gs} = k_4[(\frac{\beta_g^2}{\beta_{max}^2} + A)(1 - \frac{\beta_s^2}{\beta_{max}^2})]. \quad (6.23)$$

Using the same principle, we can reduce the number of the constants to 2, k and A, where $k = k_3 = k_4$ and $k_1 = k_2 = (A_g/A_s)k$. If we again limit P_{gr} or P_{gs} to $\leq 1/2$, we can use different combinations of k and A to see the influence of the two categories of controlling factors on the probabilities. The square of the ratio of the densities to the maximum density in the expressions is just one of the simplest choices for the non-linear profiles required by 2). We first used the densities averaged over the refining zone, i.e., over $r_2 - r_1$. Then we also tested the above expressions using the locally averaged densities in δr=4Δr in the gap to calculate the probabilities (denoted by $prob.(r,t)$ to indicate $\beta = \beta(r,t)$), because if we use a single Δr, the fluctuations would be too large to define a steady state as explained in Chapter 5.

6.5 Results and Discussions

We reexamined the maximum density of pulp used in calculating the previous version of the probability expressions. It is more likely that the maximum density of pulp is less than the fibre wall density adopted earlier, because there might still be some spaces among packed fibres due to the random nature of fibre distribution in the form of fibre network. From the experimental data obtained in a laboratory press for static pulp pad [46], we found that the extrapolated maximum density of pulp pad is about 400 kg/m^3, which is much lower than the fibre wall density 1500 kg/m^3. Therefore, a middle value between the two seemed to be a better choice, and we chose the maximum density of pulp as β_{max} = 1000kg/m^3 for the subsequent simulations. But again, the exact value of the maximum density of pulp inside a refiner must be determined by relevant experiment.

Some typical results using the latest version of the probability expressions are shown in the following figures for k=1 and A=0.25. In each figure, a comparison is

given between using the averaged densities over $r_2 - r_1$ and using the locally averaged densities in $\delta r = 4\Delta r$ to calculate the probabilities. And the two cases are represented by $prob.(r,t)$ and $prob.(t)$ respectively in the graphs. Figure 6.1 shows the locally averaged densities in all three regions against the refining radius. While Figure 6.2 illustrates the residence time and the treatment time distributions for the two cases. In Figure 6.3, the fluctuations in the averaged density over the refining zone with respect to time are plotted. And in Figure 6.4, the fluctuations in the number of floc out of the refiner predicted are shown.

In general, the residence time distribution predicted is very non-symmetrical, the trend being close to that shown in Figure 3.13 for using the first stochastic model. And the treatment time distribution is much sharper and closer to the origin. All the above observations reflect the fact for using these sets of probability parameters, the chances for the flocs to go to the gap are much smaller than using the different combinations of probability parameters used before. As a result, the treatment time is much shorter, and there is fairly amount of flocs staying either in the stator, producing a wide spread of distributions ahead of the peak, or in the rotor, producing a sharp concentration of the peak of the residence time distribution.

We see that the difference between using $prob.(r,t)$ and $prob.(t)$ is quite minor, except near the entrance r_1. But it took long time for the case of using $prob.(r,t)$ due to extra loops needed to calculate the locally averaged densities in the program. From the experiences of using both the averaged density and the locally averaged density to calculate the probability expressions $prob.(t)$ and $prob.(r,t)$, it may not be necessary to go back to the locally averaged density (in $4\Delta r$) to calculate the probabilities for the following reasons: First, there is no dramatic changes in the overall density in r direction, although the locally averaged densities fluctuate in a slightly greater scale than that of the counterpart, and these greater fluctuations in the locally averaged density may result in temporary instability in the simulations. Secondly, Δt is the time unit that we actually assign the probabilities for the flocs to switch regions, thus the update of the probabilities should keep the same rate as that of the flocs to switch the regions. So we concluded that there is no need to use the locally averaged

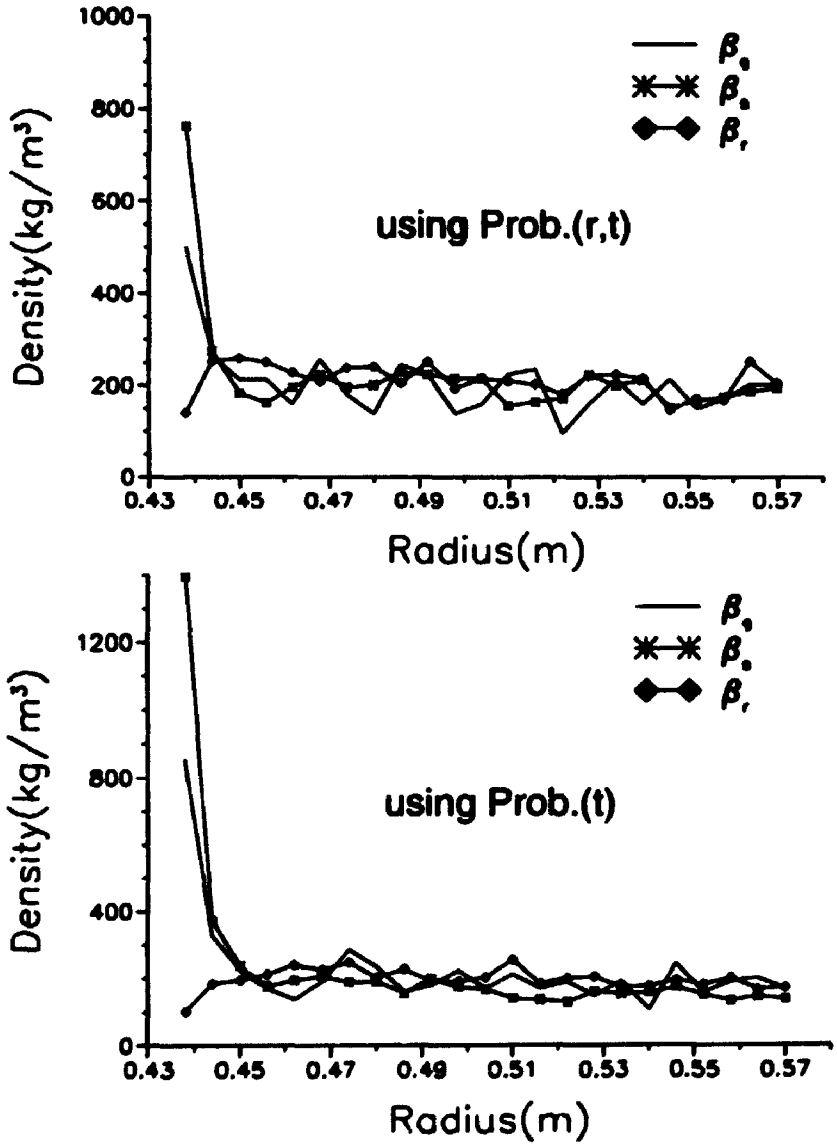

Figure 6.1: Locally averaged densities against radius for using $prob.(r,t)$ and using $prob.(t)$.

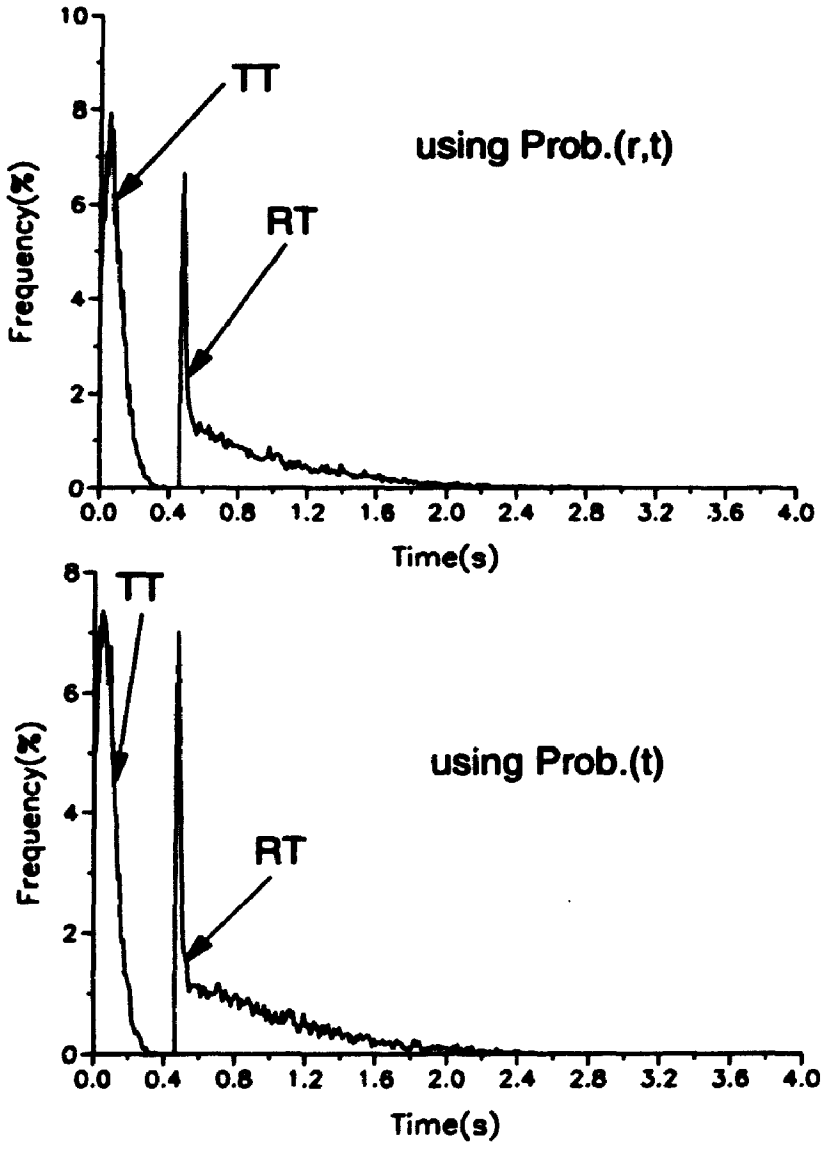

Figure 6.2: Residence time and treatment time distributions for using $prob.(r,t)$ and using $prob.(t)$.

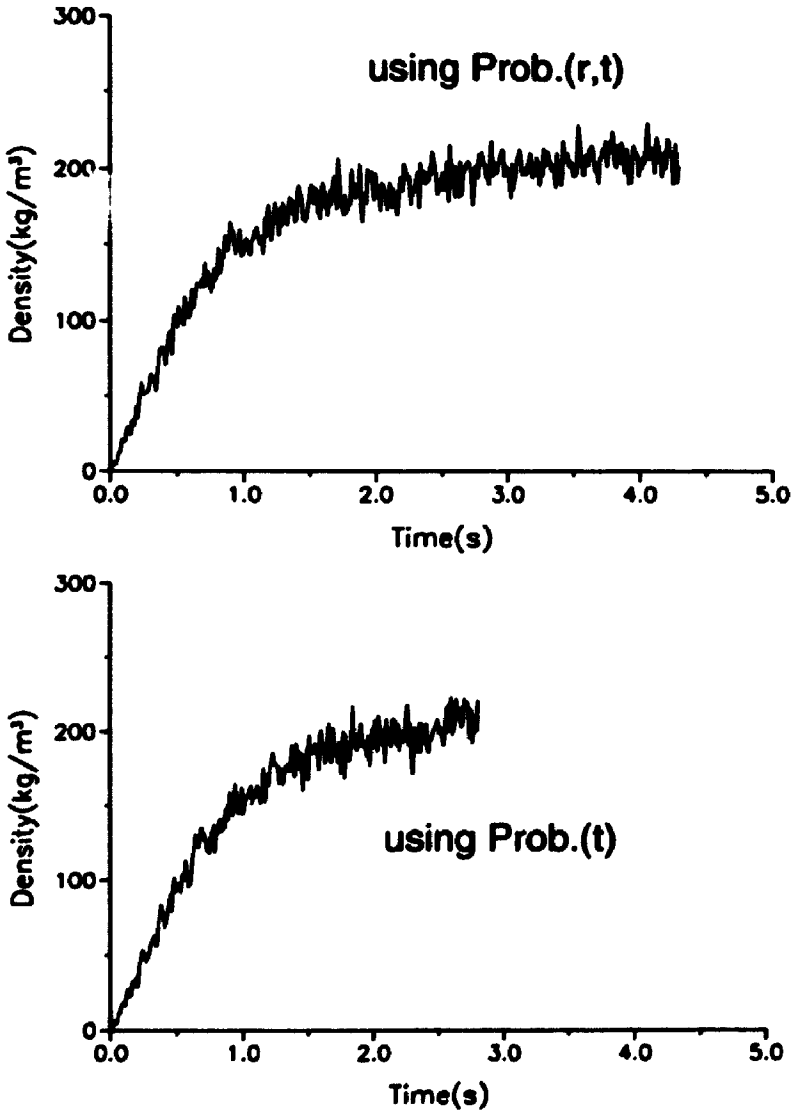

Figure 6.3: Averaged pulp densities against time for using $prob.(r,t)$ and using $prob.(t)$.

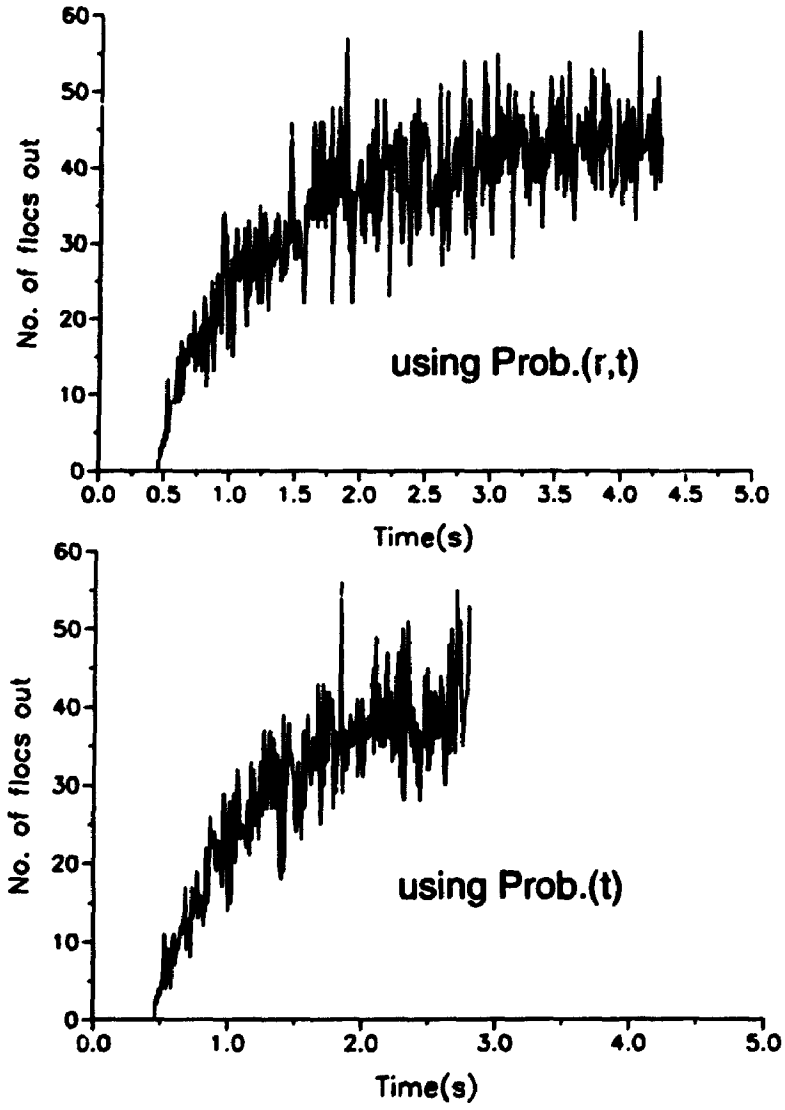

Figure 6.4: The number of flocs out of the refiner against time for using $prob.(r,t)$ and using $prob.(t)$.

densities to calculate the probabilities, unless we study the local property changes, for example, the effect of local dams in the plate grooves.

Next, we want to study the effect of different combinations of k and A in the probability expressions on the results, so that the relative importance of stochastic factors to the density difference factor that control the floc exchange mechanisms can be established. We first find out the range that k and A can take without violating the rule of probability. For example, for P_{gr}, we require that $P_{gr} \leq 1/2$. For the densities around the steady state we have $\beta_g^2/\beta_{max}^2 \approx \beta_r^2/\beta_{max}^2 = \beta_e^2$. Then we rearrange Equation (6.22) to obtain:

$$\beta_e^2(1-\beta_e^2) + A(1-\beta_e^2) \leq \frac{1}{2k}. \tag{6.24}$$

We see that the first term on the L.H.S. of the above inequality condition has a maximum 1/4 when $\beta_e^2 = 1/2$, and the highest value for the second term is A, so that we can derive the condition for k and A:

$$A \leq \frac{1}{2k} - \frac{1}{4}. \tag{6.25}$$

For k between 0 and 2, we have a range of A that can be selected to perform the numerical simulations. Here we chose to show only two typical cases to illustrate the point: case one is $k = 0.5$ and $A = 0.4$ for representing more stochastic effect; and case two is $k = 1.5$ and $A = 0.08$ for emphasizing more density difference effect.

The results are shown in Figures 6.5 to 6.8 in the same sequence as before, i.e., the locally averaged density against radius, the residence time and the treatment time distributions, the averaged density over refining zone against time, and the number of flocs out of the refiner against time. We see that the locally averaged densities in the three regions are only marginally closer to follow the equal density assumption for the case of $k = 0.5$ and $A = 0.4$ than the other case shown in Figure 6.5. In Figure 6.6, only a subtle difference can be observed between the two cases for the residence time and the treatment time distributions. And no obvious difference is seen through Figures 6.7 to 6.8 for the scale of the fluctuations in the averaged densities and the number of flocs out of the refiner between the two cases.

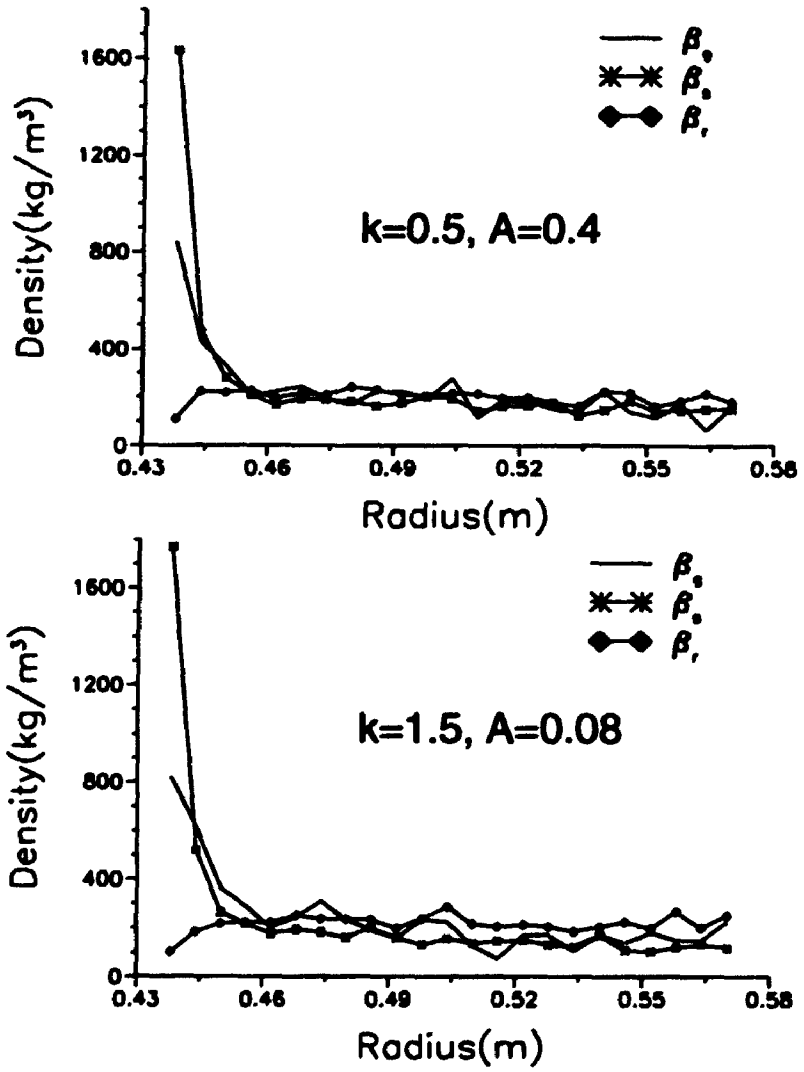

Figure 6.5: Locally averaged densities against radius for the case of $k = 0.5$, $A = 0.4$ and the case of $k = 1.5$, $A = 0.08$.

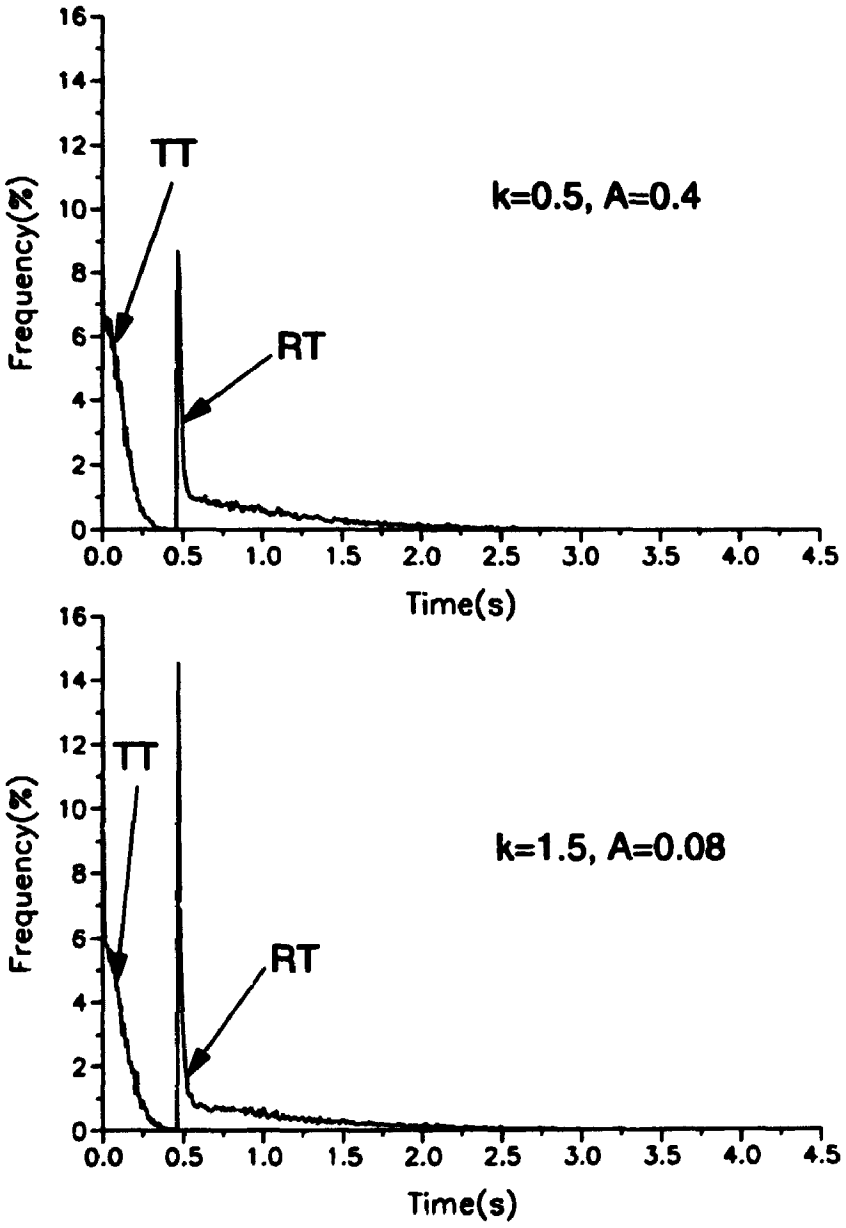

Figure 6.6: Residence time and treatment time distributions for the case of $k = 0.5$, $A = 0.4$ and the case of $k = 1.5$, $A = 0.08$.

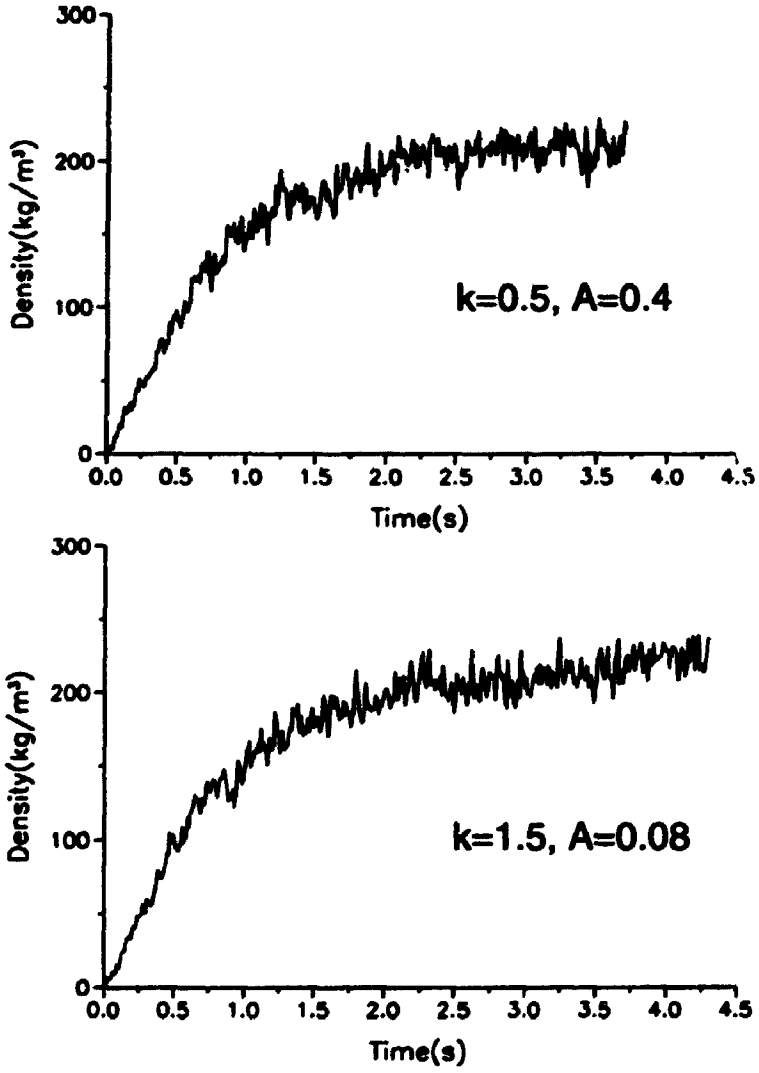

Figure 6.7: Averaged pulp densities against time for the case of $k = 0.5$, $A = 0.4$ and the case of $k = 1.5$, $A = 0.08$.

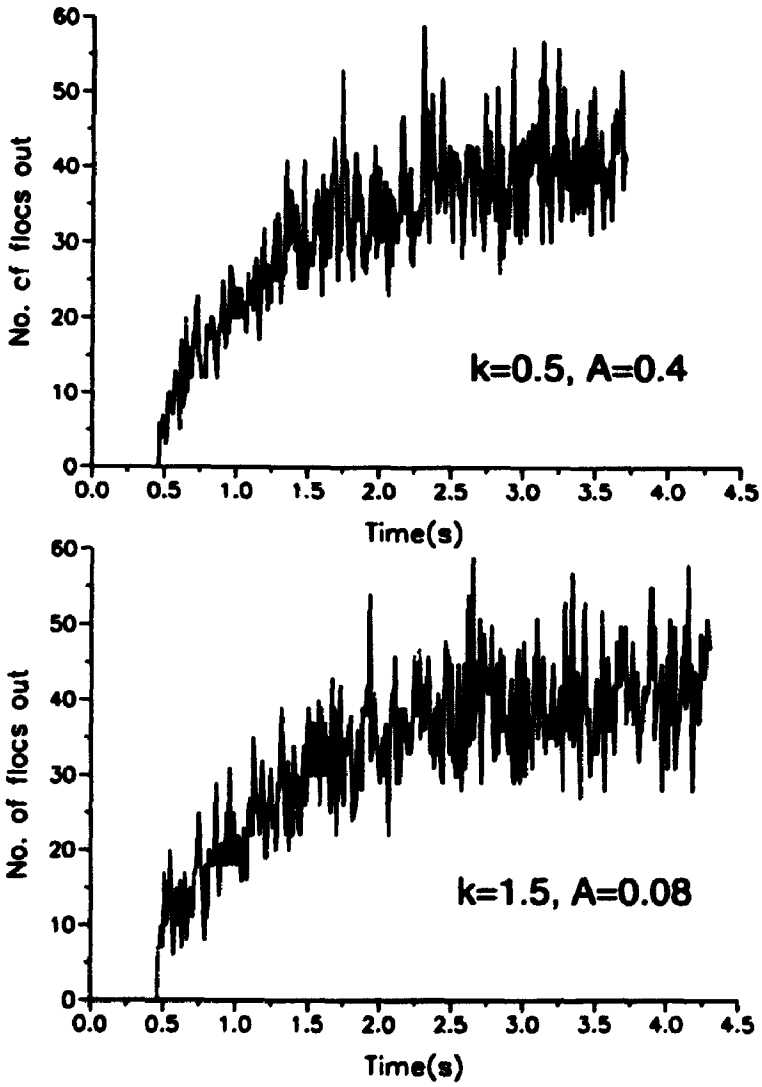

Figure 6.8: The number of flocs out of the refiner against time for the case of $k = 0.5$, $A = 0.4$ and the case of $k = 1.5$, $A = 0.08$.

The results suggest that both categories of the factors which are supposed to influence the floc exchanges may not be as important as we originally thought to be. In other words, if we substitute the probability expressions with constants but keeping the coefficients k_i $(i = 1, 2, 3, 4)$ the same, the results will be quite similar. And this was confirmed by the simulations. The key is the ratio of the cross sectional areas connecting the coefficients k_i, like in $k_1 = k_2 = (A_g/A_s)k = (A_g/A_r)k$. It is the cross sectional area in the probability expressions that guarantees the equal mass flux near the steady state. As a matter of fact, by observing the output step by step during the simulations, we found that in most of cases the averaged densities of pulp calculated are not too far from the steady state. Also the averaged densities predicted are mostly in the sparsely packed state discussed before.

Therefore, we concluded that the primary factor to influence the probability parameters is the cross sectional area which almost warrants the equal densities among the three regions. The density difference is at most secondary, and the extent of the exchanges also depends on the stochastic factors. At present, due to lack of any experimental data about the extent of floc exchanges among the regions inside a refiner, we have to content with an estimation again for the probability parameters. But the values of the probability parameters were found to be not too sensitive to the model from the simulations, as long as the cross sectional areas factors are included in the probability expressions. Furthermore, the significance of relating the probability parameters to cross sectional area of the different regions is that it gives us the crucial connection between the plate gap and the probability parameters, which will be needed for calculating the forces later. Thus for the subsequent simulations, we only use constant probability parameters with cross sectional area factors.

Chapter 7

RELATIONS AMONG OPERATING VARIABLES

7.1 Motivation

One of the main purposes of developing new mathematical models for refining is to predict the relations among the operating variables in refining, so that we can control the refining process better and improve the quality of the product. For example, as shown in Figure 7.1 [65], the relation between the motor load and the plate gap is widely used for refining process control, which is purely obtained by empirical methods. So far no theoretical models can predict a similar trend, and there are only some qualitative explanations, which are not adequate for process control. Although there is some experimental work about the relations among operating variables in steady state [11, 66], very little has been done in the theoretical front, partly due to a lack of understanding of the mechanisms, about how pulp behaves under compression, and partly due to the dependent nature of the variables involved. Recently, Miles and May [51], using their theoretical model for steady state, predicted some relations among the operating variables such as specific energy versus plate gap, throughput versus plate gap and so on. But as we discussed in Chapters 2 and 3, this continuum approach to pulp flow cannot be readily extended to study the time-dependent aspect of refining. Thus we have to derive the forces supported by individual flocs, then develop the mechanism to predict the total load supported by pulp flocs collectively. Here, by the total load we mean the total mechanical load, since we have not put the effect of steam into the model yet.

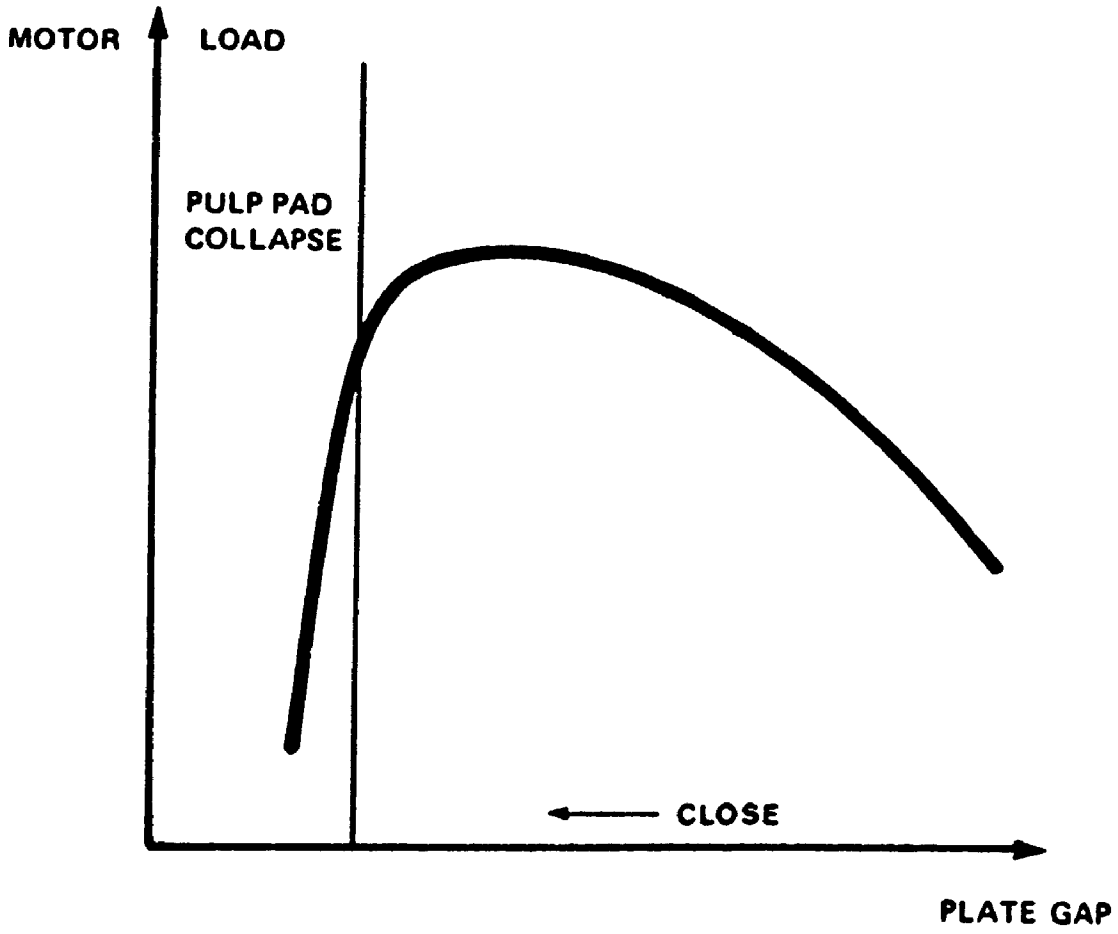

Figure 7.1: A typical curve for the motor load versus the plate gap obtained in refining production to be used for refining process control.

7.2 Conversion of the Experimental Data for Pulp Pad

We started by reexamining the experimental results for a static pulp pad in a laboratory press reported by Miles *et al.* [46]. First we converted their results, which are shown in Figure 7.2 [46], into a plot of pulp density versus applied load by the following means. As seen in the graph, the results were originally presented with pulp pad thickness (or the gap) against applied load which is used to obtained the data for different mass concentrations of pulp per unit area of one press jaw. We calculated the pulp density ρ by using the following equation:

$$\rho = \frac{M_c}{g}, \tag{7.1}$$

where M_c is mass concentration of pulp fibres per unit area of the press jaw, and g is the pulp pad thickness or the gap between the two jaws. Then we marked the applied load to 0, 25, 50, ..., 175, 188 kPa, or 9 groups in Figure 7.2. After that we took the readings of the gap g against mass concentration M_c from the graph for each group. In other words, we took 6 pairs of readings (g versus M_c) for each marked value of the applied load. These 6 pairs of readings were converted to pulp density ρ by using Equation (7.1), and then were further averaged to obtain the averaged pulp density ρ_m for each marked applied load. After completing the calculations, we have 9 converted averaged pulp densities corresponding to the 9 marked applied load selected. These new pairs of averaged densities versus applied load are plotted in Figure 7.3. Between the neighbouring converted data points represented by stars, a straight line was used to connect them in the graph. Given the fact that a wide range of mass concentrations M_c was used in the experiment, we see that the fit of all the data is quite remarkable, that almost a straight line is formed for the relation between the averaged pulp density and the applied load. The ranges of the 6 converted pulp densities used to calculate the averaged pulp densities are also indicated by the vertical bars on each of the marked applied load. And these ranges are pretty consistent with one and another. Note though, in Figure 7.3, that the data for applied load beyond 188 kPa are extrapolated in the conversion, and that the data near 0 applied load are extrapolated by the authors [46].

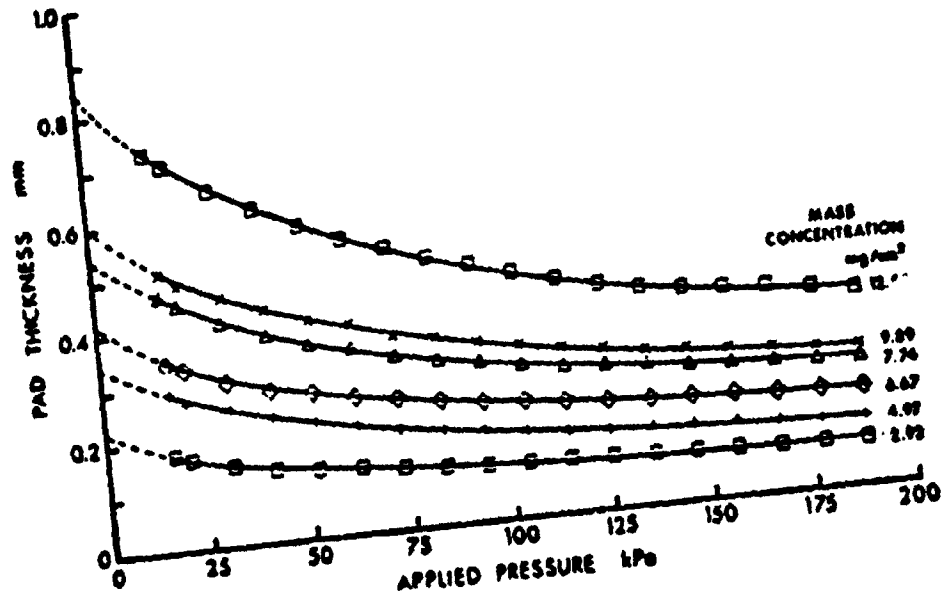

Figure 7.2: Curves of pulp pad thickness versus applied stress obtained from the laboratory press form a family in which the thickness at a given stress is proportional to the mass concentration.

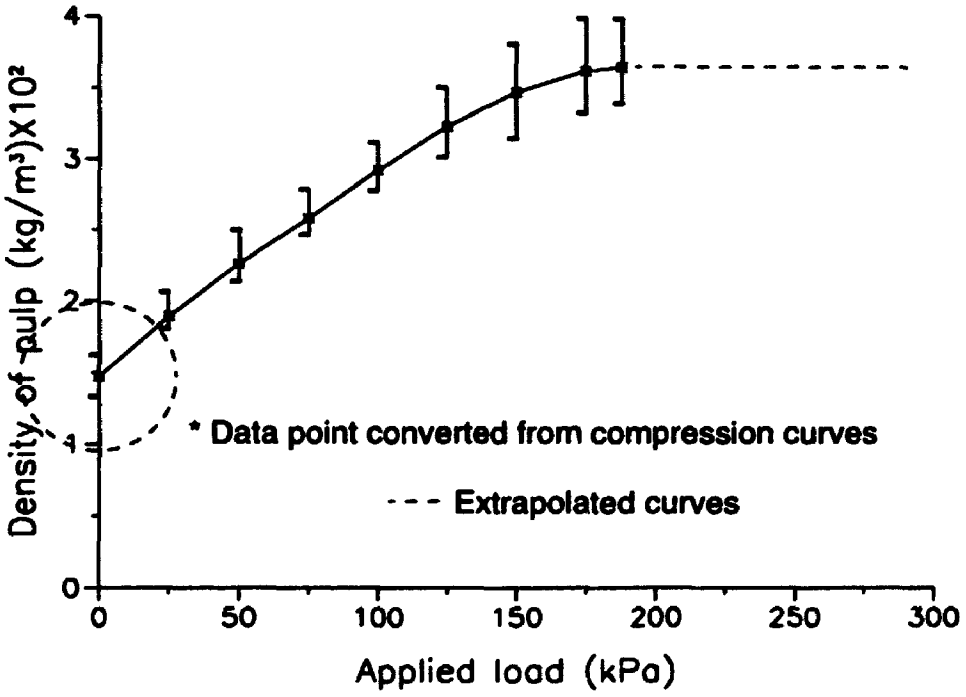

Figure 7.3: Averaged pulp density versus applied load converted from the experimental data for pulp pad in the laboratory press.

7.3 Assumptions for Flocs to Behave in the Gap

The first thing we need to address is how to predict the forces that a single floc can support based on the experimental data obtained in a layer of the static pulp pad. We know already from the experiment observations, that there is fairly large amount of empty spaces between the pulp flocs in the gap, and these void spaces certainly prevent us applying the load versus pulp density relation to the flocs. But if we assume that each pulp floc has a uniform distribution of fibre material inside, plus the assumption of equal mass for each floc made before, we can equivalently use the load versus pulp density relation for within each floc. In other words, we treat the floc in the gap as an evenly distributed pulp pad only within its boundary.

In order to calculate the pulp density within each floc in the gap, we have to know the general shape of a single floc in zero load and how it behaves under compression. Since no experimental data available from the literature for this information, we simply assume that the shape of a floc is a ball under zero load, the reason being that it is likely that there are motions in both radial and tangential directions for flocs in this situation, and a ball offers the least resistance to motion. We also assume that for a single floc in the range of normal compression below the maximum load, the compression will be responded by the floc with a height reduction only (or the radius of the floc ball is approximately the same). The rational behind this is that under such a compression (happens in a very short period of time between the moving bars), there is a tendency that the floc boundary is probably frozen momentarily. And this offers one of the possible explanations why the observed covered bar area by pulp in refiners is only a percentage of the total area of the bars.

Next, we need a mechanism for the load development of the pulp flocs in refiners collectively. It is unlikely that the flocs in the stator or the rotor contribute much of the load, owing to the larger space available there. Thus, we neglect these contributions to the total load. For the flocs in the gap, we assume there are two basic factors contributing to the total load that all the flocs carry:

1. the forces that an individual floc supports;

2. the total number of the flocs that are in the gap in the time period of Δt.

The product of the two should determine the total load of the refiner.

Finally, the behaviour of pulp flocs under the maximum applied load is a critical point for our model. From Figure 7.3, we see that as pulp density approaches the maximum density in the graph, there is not much further increase of the pulp density as the applied load increases. The gap remains approximately the same regardless of how large the applied load is, which is also evidenced in Figure 7.2. We believe this phenomenon is only associated with the evenly distributed and static pulp pad, because the pulp pad has nowhere to escape under compression. In other words, the lateral constraint around any small section within the pulp pad network prevents any further spread of the network. Thus the network essentially remains intact under compression. That is not the case, however, for the pulp flocs under repeated compression and relaxation. First, as we discussed earlier, there are amble spaces between the flocs, or the lateral constraint between the flocs is weak; Secondly, any load exceeding the maximum load (corresponding to the maximum density shown in Figure 7.3) will definitely increase the chance of breakdown of a floc network, because the load has already well passed the elastic deformation zone (the range for a linear relation between load and pulp density); And thirdly, any breakdown or spread of the floc network under this maximum load will reduce the pulp density for a single floc, and in turn reduce the capacity of the floc to support the forces. Based on these arguments, we propose that when pulp density for a floc in the gap exceeds the maximum density (indicated in Figure 7.3), the load that the floc can support is a flat maximum applied load, which is illustrated in Figure 7.4 by a dotted line. We have to bear in mind though, that this is by no means an precise prediction, but rather a first attempt to correctly predict the confirmed industrial trend by using new theoretical models. Any quantitative prediction of the load will depend heavily on a well designed and relevant experiment about the load carrying capacity of the pulp flocs.

So our conceptual picture for floc behaviour in the gap is the following: The total

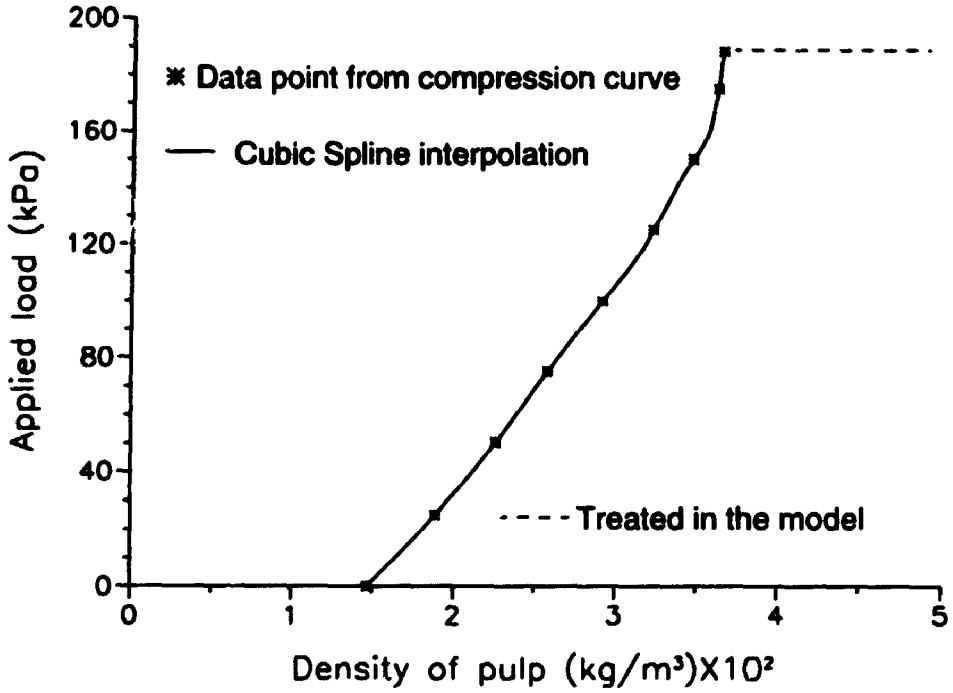

Figure 7.4: Applied load versus averaged pulp density converted from the experimental data for pulp pad in the laboratory press.

load is shared evenly by each floc that is in the gap. Each floc under compression in the gap follows the relation between the load and the pulp density obtained experimentally. Thus for a given plate gap and feed rate, the pressure supported by a single floc, the area of the single floc to support the pressure, and the total number of flocs in the gap will all control the total load that the flocs can carry. For example, when the plate gap is decreased in the normal range of refining, the total number of flocs will be smaller as a result of the smaller cross sectional area available for flocs in the gap. On the other hand, the smaller gap will demand a higher pulp density within each floc that is in the gap, then the forces supported by each floc will go up in the normal range of load versus pulp density. Therefore, the total load will go up as the plate gap is decreased until the point of the maximum load that a floc can carry is reached. Any further decrease of the gap after that will further reduce the total number of the flocs present in the gap, and because the load that a single floc can support is already the maximum load, the total load will go down dramatically as a result of this combination of the two factors.

7.4 Calculation of the Load Supported by Flocs

We assume that there is only one layer of flocs in the gap, and all the flocs have the same average floc size. We now start the calculation by considering a floc ball in general before and after compression, shown in Figure 7.5. Let R ($R = h_0$) be the radius of a floc ball under zero compression, ρ_{min} be the minimum pulp density corresponding to the zero load situation illustrated in Figure 7.4, h be the half gap after compression, R_c be the radius of the area to support the applied load after compression for a floc, and ρ_f be the density for the floc within its boundary after compression. Following the assumptions made earlier about the behaviour of a floc under compression, we can derive the density for the floc after compression as:

$$\rho_f = \frac{m}{V} = \frac{m}{2\pi h(R^2 - \frac{h^2}{3})} \tag{7.2}$$

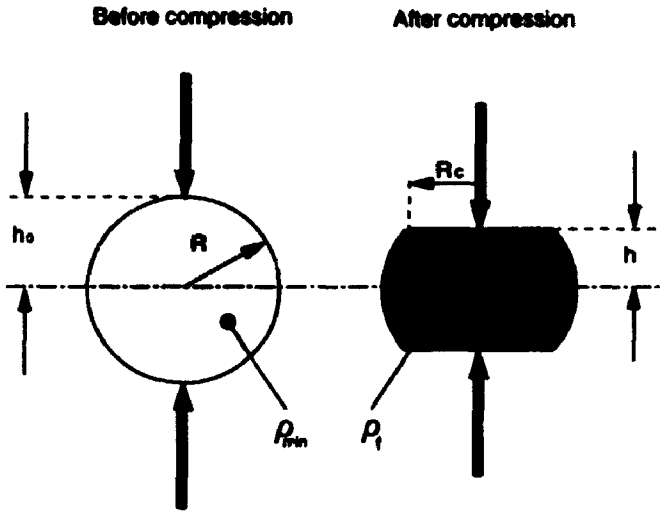

Figure 7.5: Schematic of a floc ball before and after compression.

where m is the mass for a single floc. We can also obtain the floc radius R in terms of m and ρ_{min} from the definition of density:

$$R = \sqrt[3]{\frac{3m}{4\pi\rho_{min}}}. \tag{7.3}$$

Once the mass of a single floc is known (or can be converted from the feed rate and the assumed number of flocs entering the refiner in Δt), we know R from ρ_{min} indicated in Figure 7.4. Thus, for a given plate gap value $g = 2h$, we can calculate the density for a single floc using Equation (7.2). Treating ρ_f as input in Figure 7.4, we can obtain the interpolated value of the applied load corresponding to each value of the input according to the curve. In the program, we used the Cubic Spline interpolation method to get the applied load, which is also indicated by an arc line in Figure 7.4.

Next, we need to calculate the total area to support the load for all the flocs in the gap under compression. First, we see from Figure 7.5, that there is a simple relation among R, h and R_c so that $R_c = \sqrt{R^2 - h^2}$, and also the one side area for a single floc is $A_c = \pi(R^2 - h^2)$. Notice that R_c the radius of the area to support the load for a single floc shrinks to 0 for the case of zero load, and approaches to maximum R theoretically. But because we assumed that the load can only be up to

the maximum load for a floc shown in Figure 7.4, we simply use the maximum load when the calculated density of a floc exceeds the corresponding maximum density. Also, we have to stop somewhere near a small value of h when R_c is close to R since ρ_f will blow up for $h = 0$ according to Equation (7.2). Secondly, we calculate A_t the total areas of all the flocs in the gap inside a refiner to support the total load:

$$A_t = SA_cN_gn, \tag{7.4}$$

where N_g is the total number of flocs in the gap during time Δt, and n is the total number of the grooves or the bars in refiner plates used to convert the feed rate to one groove or one bar as discussed in Chapter 5. The factor S is used here to take into account the situation that the moving bar is aligned with the stator bar for the calculation of the forces, and this consideration is consistent with our earlier assumption made in defining the gap region that the gap region is the average state of bar to bar and bar to groove situations. For simplicity, we took the factor S as 1/2.

Finally, we have to put these factors together to derive the formula for calculating the total mechanical thrust force that all the flocs in the refiner can support. The total thrust force L_t takes the following form:

$$L_t = P_a(\rho_f)A_t, \tag{7.5}$$

where $P_a(\rho_f)$ is the applied load interpolated from the Figure 7.4 using ρ_f calculated as input. We can also derive the motor load of the refiner based on the friction force, the radius for each floc, and the angular velocity of the disc. If we assume that the friction force which every floc exerts on the discs is the same, and that μ_t the friction coefficient in the tangential direction between the flocs and the discs is a constant, then we obtain the following equation for the motor load M_t:

$$M_t = \sum_{i=1}^{N_g} \mu_t \frac{L_t}{N_g} \omega r_i, \tag{7.6}$$

where ω is the angular velocity of the rotating disc, and r_i represents the radius r of the ith floc that is in the gap. In addition, we can get another very important

operating variable for refining, 'specific energy', E by a simple relation:

$$E = \frac{M_t}{F}, \tag{7.7}$$

where F is the feed rate in refining.

7.5 Simulation Procedures

We modified the program used in the previous Chapter for testing the probability expressions to do the simulations. We first adopted the constant probability expressions with cross sectional area factors as discussed in the end of Chapter 6. In particular, we used A=1 and k=0.25-0.5, and the value of k had to be adjusted in the range to accommodate different plate gap settings in the simulations. For example, when an extreme small plate gap is used in the simulation, the number of flocs going into the gap region is dramatically reduced, then a higher k has to be used to encourage the exchanges with the gap so that a steady state can be reached, but we found that the value of k is not too sensitive to the total mechanical thrust predicted. A similar modification had to be made to the criteria that are used to define the steady state, because the relative fluctuations are larger when very few flocs are in the gap region.

We also added some sections to the program to implement the formulas for the calculations of the total mechanical thrust load, motor load, and specific energy. We took the minimum density of floc ρ_{min} as 146 kg/m^3, and the maximum applied load P_a as 188 kPa as shown in Figure 7.4. For a small plate gap setting in the simulations, the density of the flocs ρ_f calculated using Equation (7.2) may exceed the density corresponding to the maximum applied load. We simply assigned the maximum applied load to all the higher densities ρ_f in the calculation, because only the applied load is involved in Equation (7.5). For the case of very large plate gap, when the total thrust predicted is close to zero, the total number of flocs in the gap may be more than the one layer of flocs that the gap region can accommodate. In this case, we simply took into account the total number of the flocs in the gap as far as calculating the thrust is concerned, because the large gap situation is not of interest in refining control due to the poor quality of the product associated with it.

The subroutines 'SPLINE' and 'SPLINT' from Numerical Recipes [67] were appended to the main program to perform the Cubic Spline interpolation for $P_a(\rho_f)$ as indicated in Figure 7.4.

In the simulations, we used the plate gap $g = 2h$ =0.3 mm and the number of flocs entering the refiner in Δt $N = 40$ as the values in the standard set of the parameters, and the rest of the parameters were the same as before. The friction coefficient μ_t was chosen to be 0.75 as explained in [24], and the angular velocity of the rotating disc was 188 s^{-1}.

7.6 Results and Discussions

Some typical results are shown in Figures 7.6 to 7.11. In most of the graphs for the relations between the loads and the plate gap, the calculated data points are indicated by asterisks, and the arc lines connecting the neighbouring points are generated using Cubic Spline interpolation method for plotting.

In Figure 7.6, the relation between the total mechanical thrust load and the plate gap is plotted. The thrust load is calculated with the formula using the standard set of parameters. In each calculation, the value of the thrust is recorded upon reaching the first steady state. Figure 7.7 shows the motor load and the specific energy against the plate gap with the same conditions as in the case of the thrust load. While in Figure 7.8, a comparison is given for using the different number of flocs entering the refiner in Δt for the relation between the thrust load and the plate gap. The effect of the plate gap on the fluctuations in the thrust versus time is illustrated in Figure 7.9, and the time scale is from the start of the refiner to the time that the second steady state is reached, with a 10% increase of the feed rate given at the end of the first steady state. In Figure 7.10, the development of the thrust load against time is presented for $g = 0.3$ mm, but a 25% increase is given to the feed rate instead. The relation between the thrust and the throughput (feed rate) is plotted in Figure 7.11 with a constant plate gap setting.

First, we see that the general trend predicted by the model is similar to that

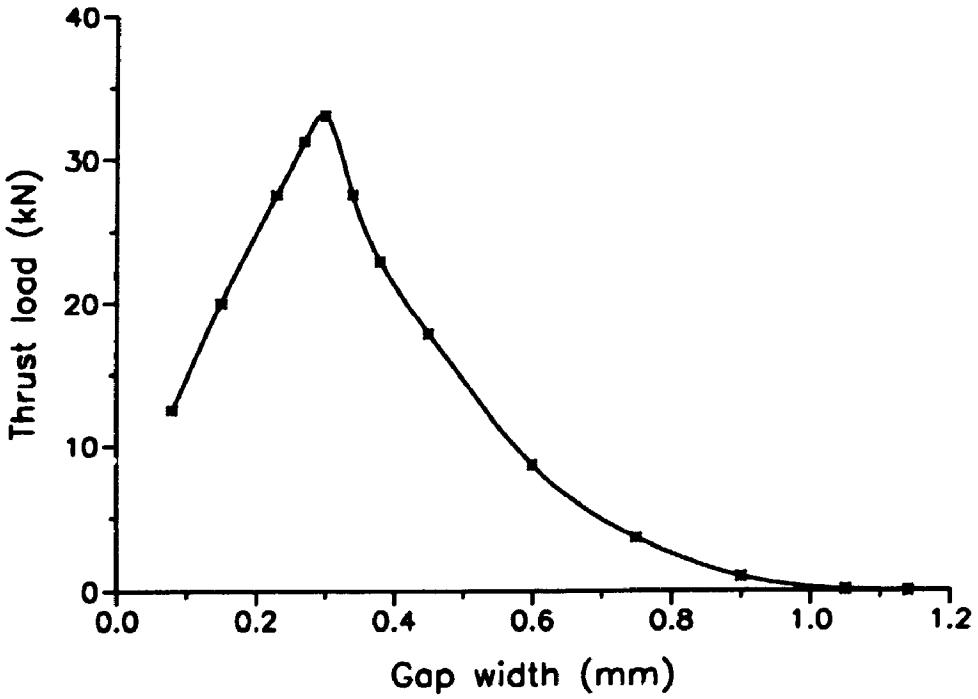

Figure 7.6: The total mechanical thrust load versus the plate gap calculated from the model for $N = 40$.

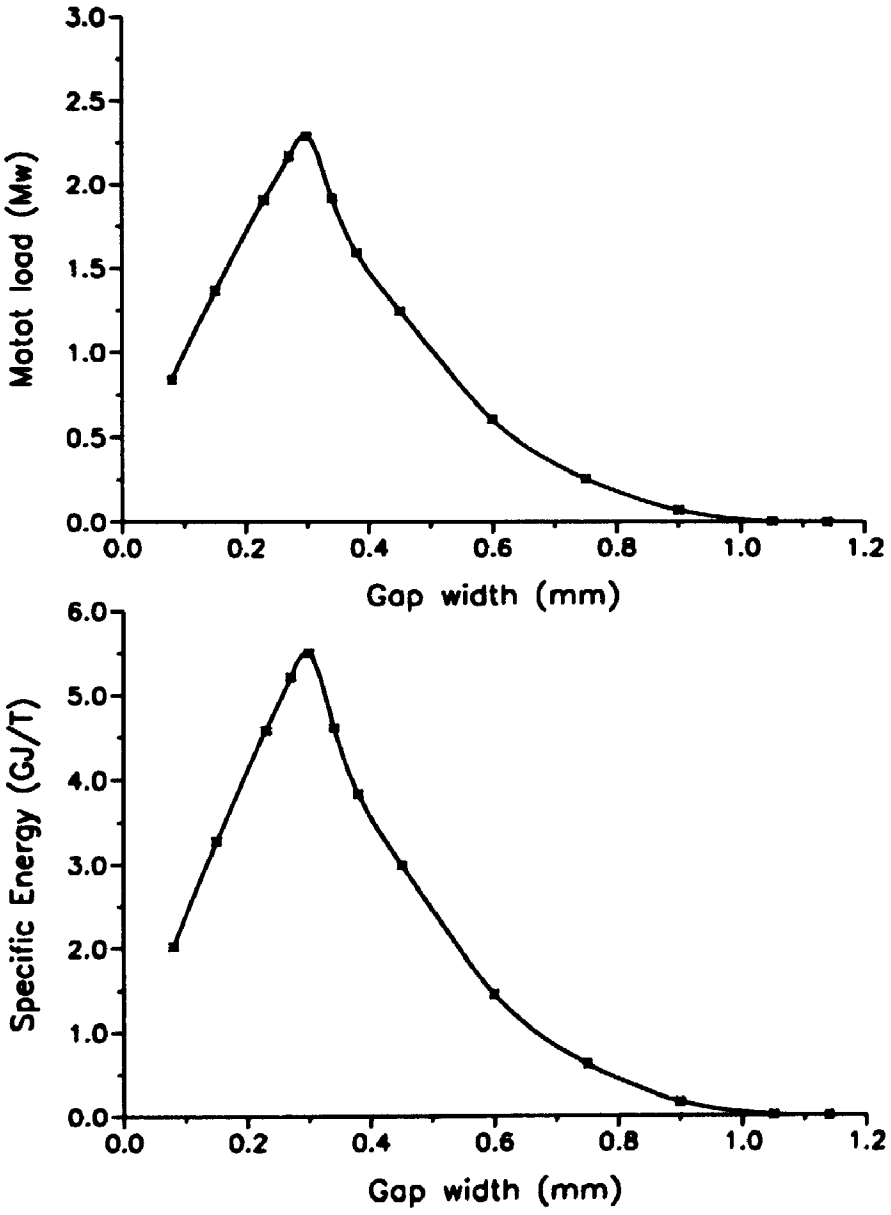

Figure 7.7: The motor load versus the plate gap and the specific energy versus the plate gap calculated from the model for $N = 40$.

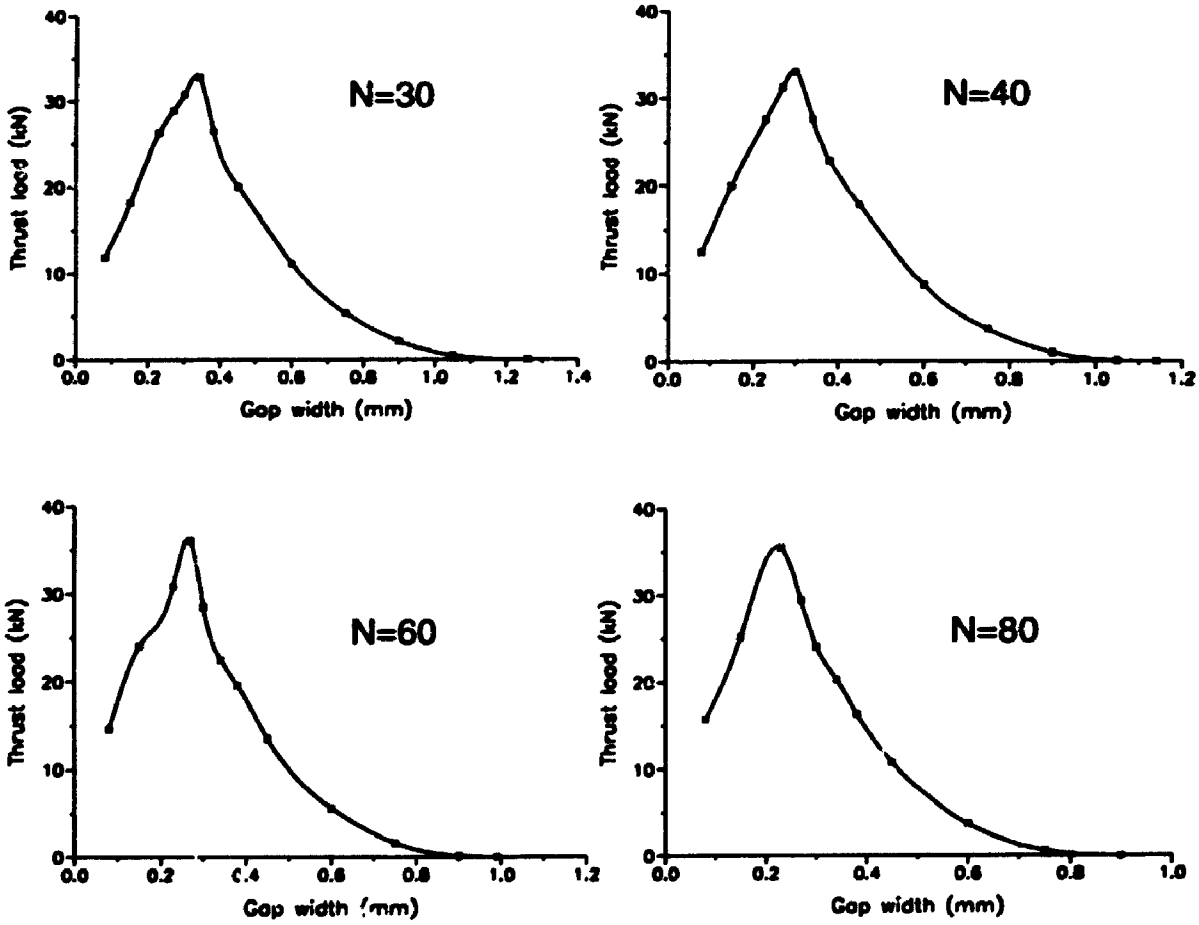

Figure 7.8: Comparison between using the different number of flocs entering the refiner in Δt for the total mechanical thrust load versus the plate gap calculated from the model.

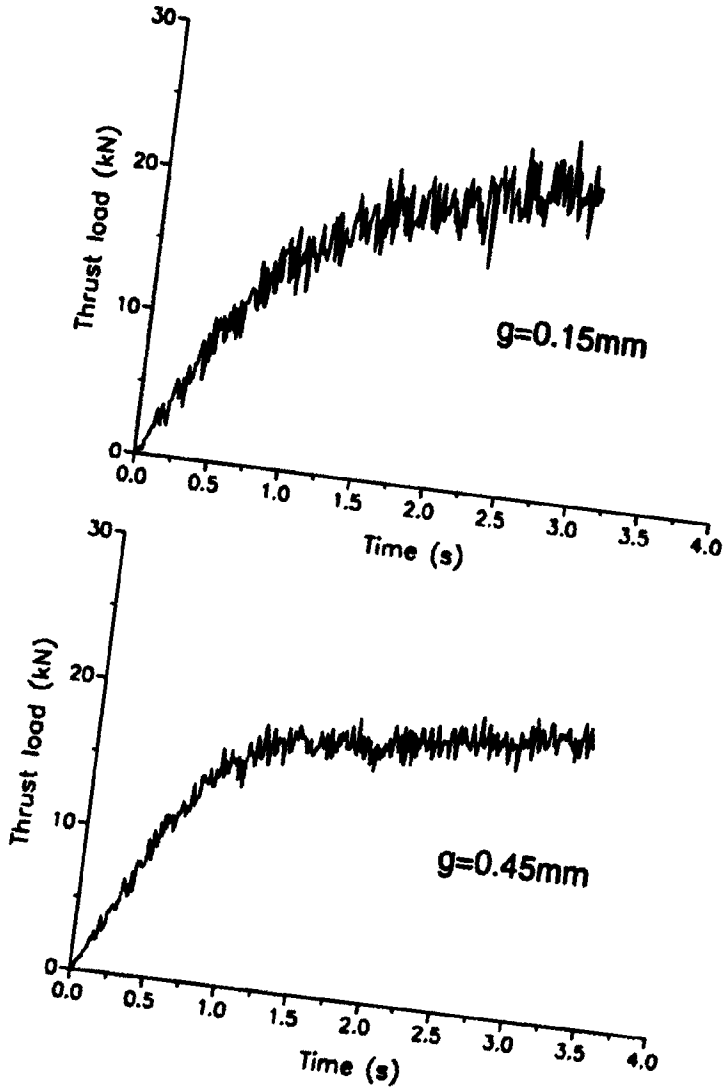

Figure 7.9: Comparison of the scale of the fluctuations in the total mechanical thrust load versus time for the two plate gap settings on both sides near the maximum total thrust predicted.

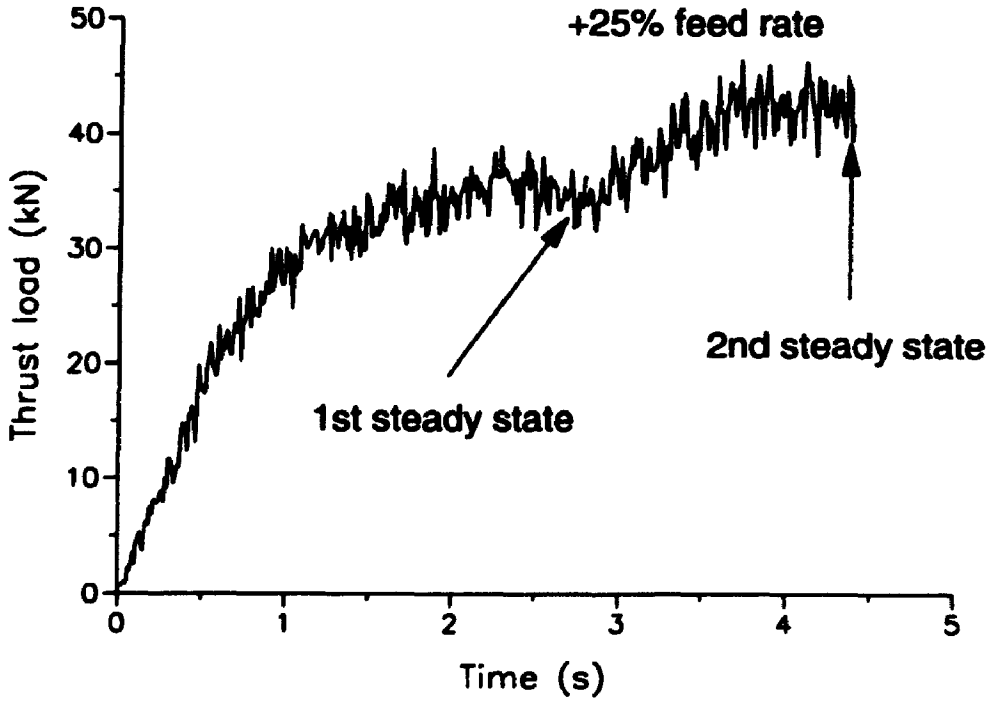

Figure 7.10: The fluctuations of the total mechanical thrust load against time for both the first and the second steady state.

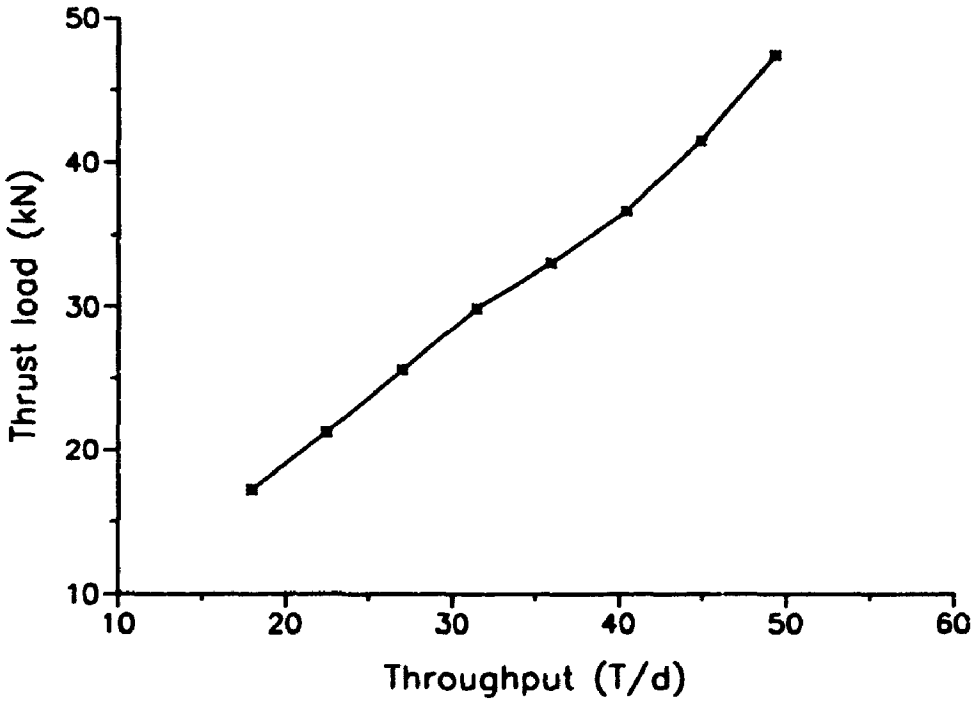

Figure 7.11: The total mechanical thrust load versus the throughput (feed rate) calculated from the model for $N = 40$.

accepted in the industry, for example, compare Figure 7.6 with Figure 7.1, with a peak around some value of the plate gap in the relation between the load and the plate gap. As a matter of fact, this is probably the first theoretically predicted curve that significantly follows those used in controlling industrial refiners. In addition, the values of the loads predicted are comparable with those in the working range of the refiner simulated. Furthermore, our model can predict the approximate time delay that is needed between the different operating set points in normal refining process, though more studies have to be carried out before we can apply the results to refining process control. By breaking away from the traditional methods of modelling pulp movement in refiners, we have successfully introduced the relations between the plate gap and some crucial operating variables, and eliminated the source of instability for time-dependent modelling.

Secondly, we see that the floc size under zero load is not too sensitive to the level of the total thrust load predicted with the model. This floc size is directly related to the number of flocs entering the refiner in Δt through m for a given feed rate F and the minimum pulp density ρ_{min}, which is reflected in Equation (7.3). In particular, as shown in Figure 7.8, both the levels and the distribution of the thrust are not significantly different than one another for a wide range of the N's used in the simulations. Also from the same Figure, we can see that our assumption for the size of the flocs (with a radius R) under compression, represented in the maximum plate gap $g = 2h = 2R$ in the graphs (such as in Figure 7.6), is in line with the experimental evidence found in the literature: It has been found that a floc has a dimension of the order l^2 where l is fibre diameter (about 2 mm) [61], and that the ratio of length (along r direction) to width of a floc is usually about 2:1 [68], which is about the size of two flocs after compression that are aligned in r direction.

Next, the scale of the fluctuations in the thrust is predicted to be related to the plate gap, which is illustrated in Figures 7.9 and 7.10. In general, the smaller the gap, the larger the scale of the fluctuations. This provides some insight for explaining the phenomenon of plate clashing that when the plate gap gets progressively smaller, any adjustment to counter the greater fluctuations in load will be likely to encourage the

gap to pass the peak load position. From the simulations, we also found that there is no significant difference for the times needed from the first to the second steady state, whether a 10% increase or a 25% increase is given to the feed rate. And the thrust load is approximately proportional to the throughput if the steam effect is ignored as shown in Figure 7.11.

Finally, the averaged density of pulp in the gap can be close to that in the stator or the rotor as predicted in the model, because the following reasons: When the moving bars align with the stationary bars, the flocs are compressed. But there are still some void spaces between the flocs in the gap. Thus even though the density of the compressed flocs is higher than the average density of pulp in the stator or the rotor, it is possible that the overall density of all the flocs in the gap remains close to those of the other two regions, owing to the empty spaces between the flocs in the gap. In other words, the higher density of the compressed flocs in the gap is somehow compensated by the empty spaces in the gap. As a result, the averaged densities in the three regions can be similar. But again, the validity of the model and the predictions have to be tested vigorously against carefully designed experiments, in order to establish the foundation for any industrial usage of the model.

Summary and Suggestions for Further Work

The pulp movement model for steady state of refining was first extended to include the time-dependent variables to study the dynamic aspect of refining, but the numerical instability hampered the solution of the hyperbolic system derived. Therefore, a new direction in modelling pulp in refiners was initiated, in which pulp movement is modeled as a stochastic process with individual pulp flocs. The first test of the new model was to predict a distribution of the residence time for steady state refining. The numerical simulations showed that the time step, the probabilities and the pulp velocity are important parameters for the residence time distribution, and in most of the cases the distribution is symmetrical. The treatment time, the time pulp flocs spend in the gap only, can also be predicted using the model But one interesting phenomenon was found in the simulations that the treatment time distribution is non-monotonic. A simplified model was developed to study the behaviour, and a theoretical explanation was found which was also confirmed by numerical simulations. The stochastic model for steady state was then extended to a time-dependent stochastic model by keeping track of all the flocs inside refiners at all the time. The locally averaged densities of pulp were chosen to be the output for the model to reflect the fluctuations in local property changes. The results showed that there is a direct relation between the locally averaged densities and the feed rate, and the number of flocs into the refiner influences the fluctuations. The factors to control the floc exchanges were identified in order to derive the probability expressions that were treated as constants before. The expressions worked fine after several versions of the probability expressions were tested. But the results indicated that it is the cross sectional area of refining zone that controls the floc exchanges. Based on the understanding of floc behaviour and some assumptions, the formulas to calculate the

forces supported by a single floc were derived. Then the total mechanical thrust load was predicted by considering the area to support the load and the number of flocs in the gap contributing to the load. The predicted relation between the total thrust load and the plate gap was similar in trend to that obtained from refining production in mill. The relations between the motor load, specific energy and the plate gap can also be predicted.

Many aspects of the model can be further improved. Until now the velocity field for the three regions is assigned for simplicity, which can be improved by considering the following work: Determine the friction and centrifugal force on floc level in the three regions; Introduce the steam drag on floc level. Energy distribution can be predicted based on the assumption that a bar crossing can transfer certain level of energy to pulp flocs. Some effects on energy distribution can be simulated using the model, such as: number of bar crossings; speed of bar crossings; angle of bars; energy concentrations on different sections of the refining zone. The influence of grooves and bars on refining can also be simulated: Angle of grooves changes the direction of pulp flow in the stator and rotor, in turn, ffects the residence time and the treatment time distributions; Dam effect can be tested by setting the probabilities and the locally averaged densities to zero locally.

Appendix A

Some Additional Results for Chapter 2

The following graphs are some additional results described in Chapter 2 for the solution of the hyperbolic system of the equations. And the figures are in the same sequence as those shown in the text of Chapter 2.

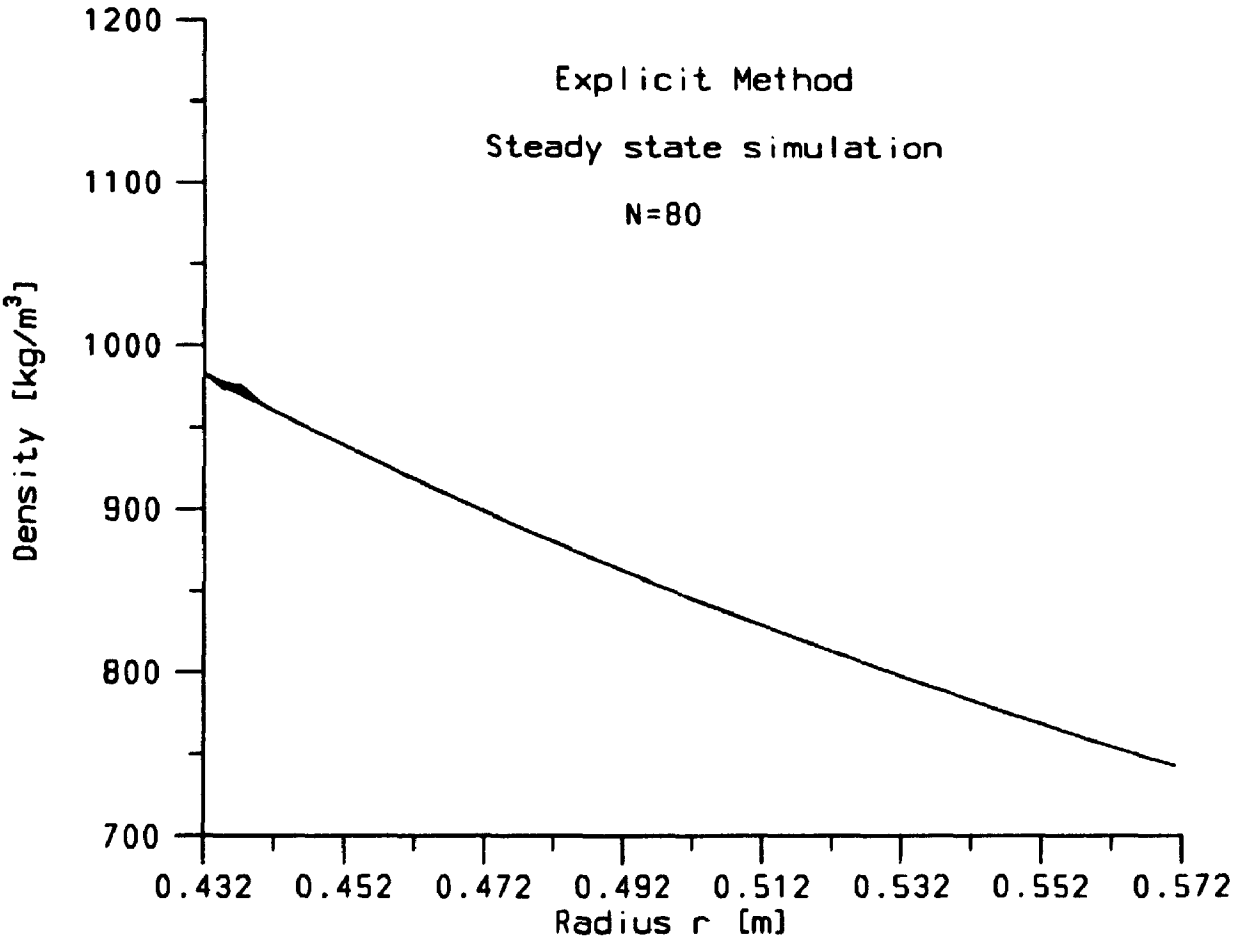

Figure A.1: Steady state simulation using explicit numerical scheme with total number of time steps $N = 80$.

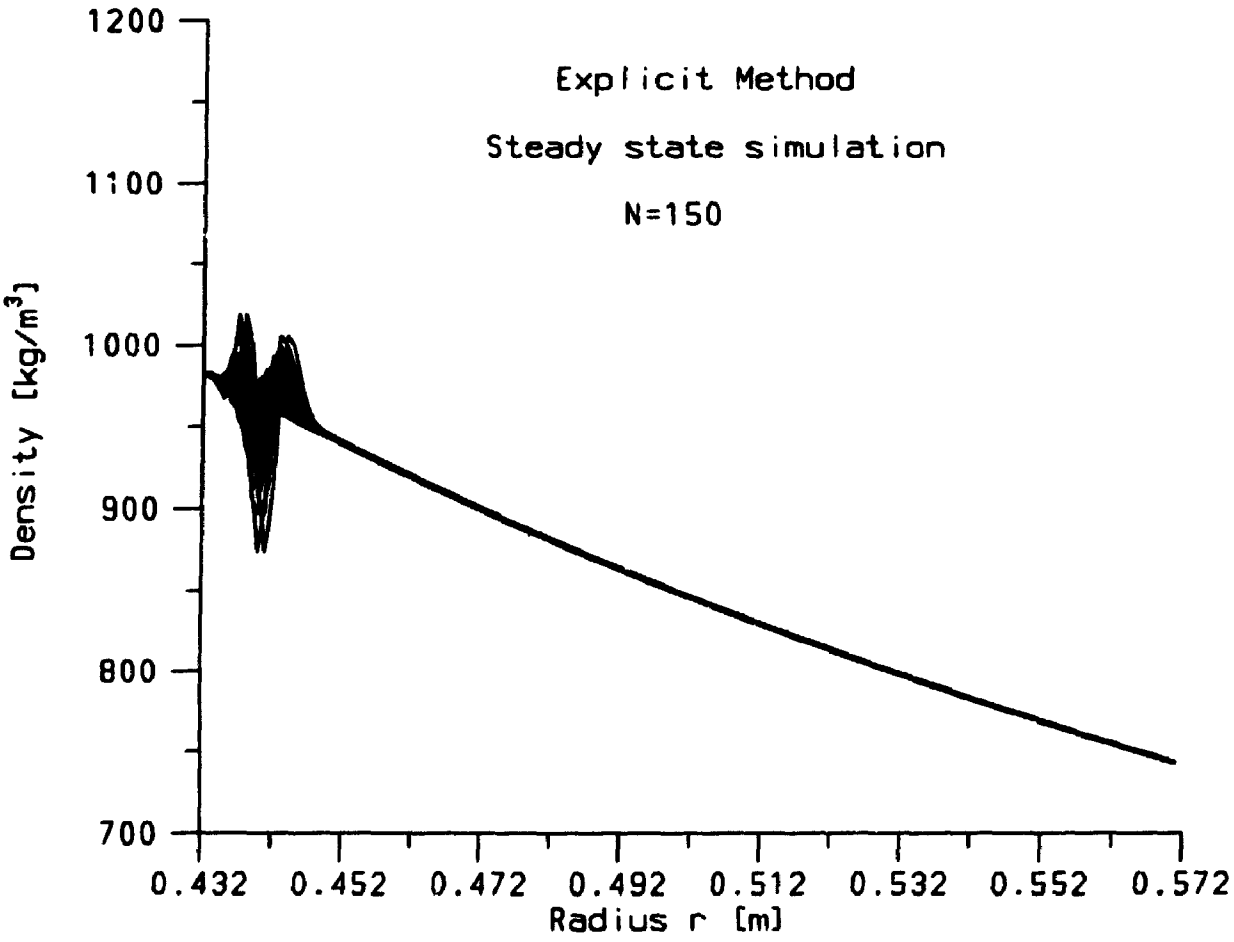

Figure A.2: Steady state simulation using explicit numerical scheme with total number of time steps $N = 150$.

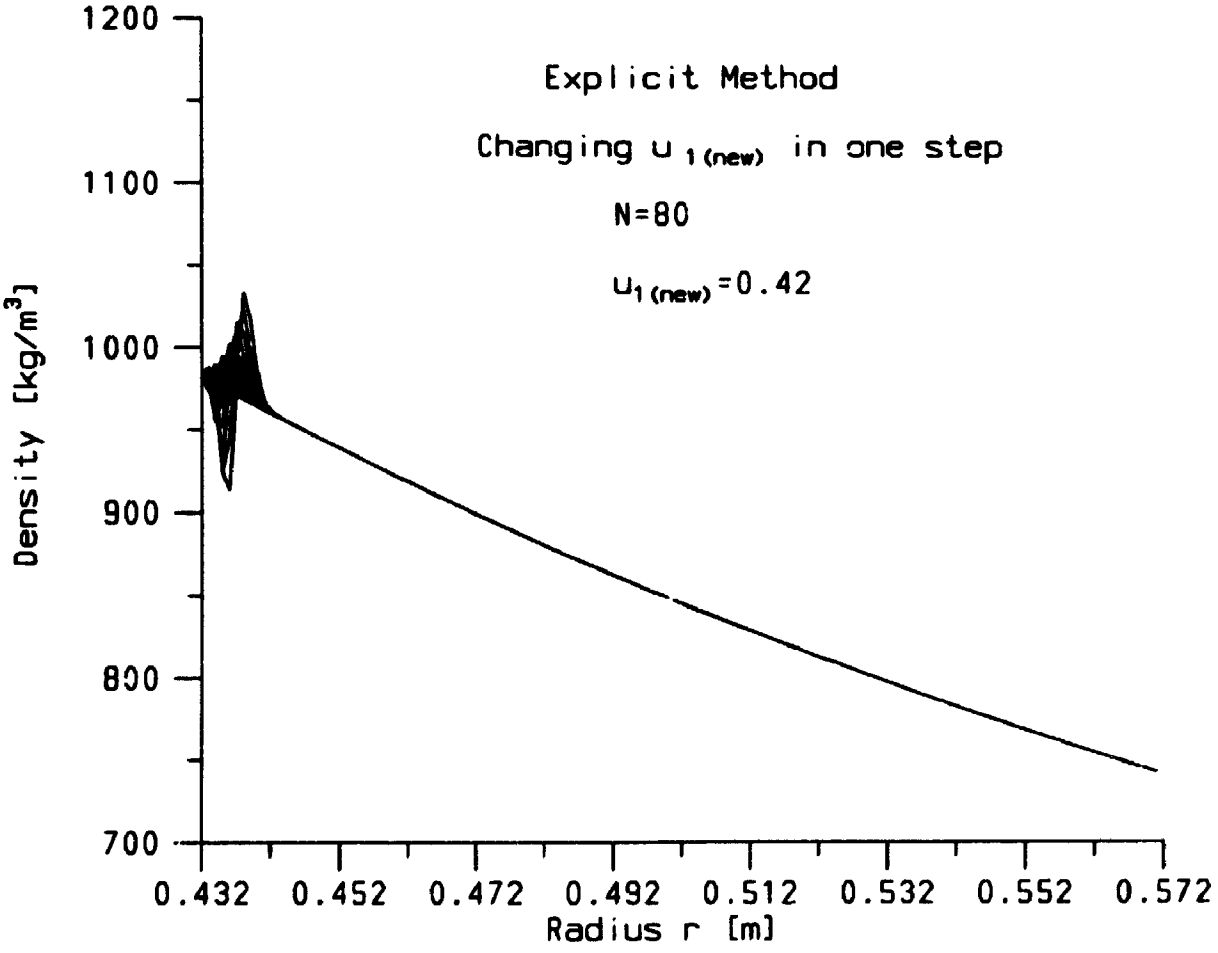

Figure A.3: Dynamic state simulation using explicit numerical scheme with $u_1 = 0.39$ changed to $u_{1new} = 0.42$ in one step.

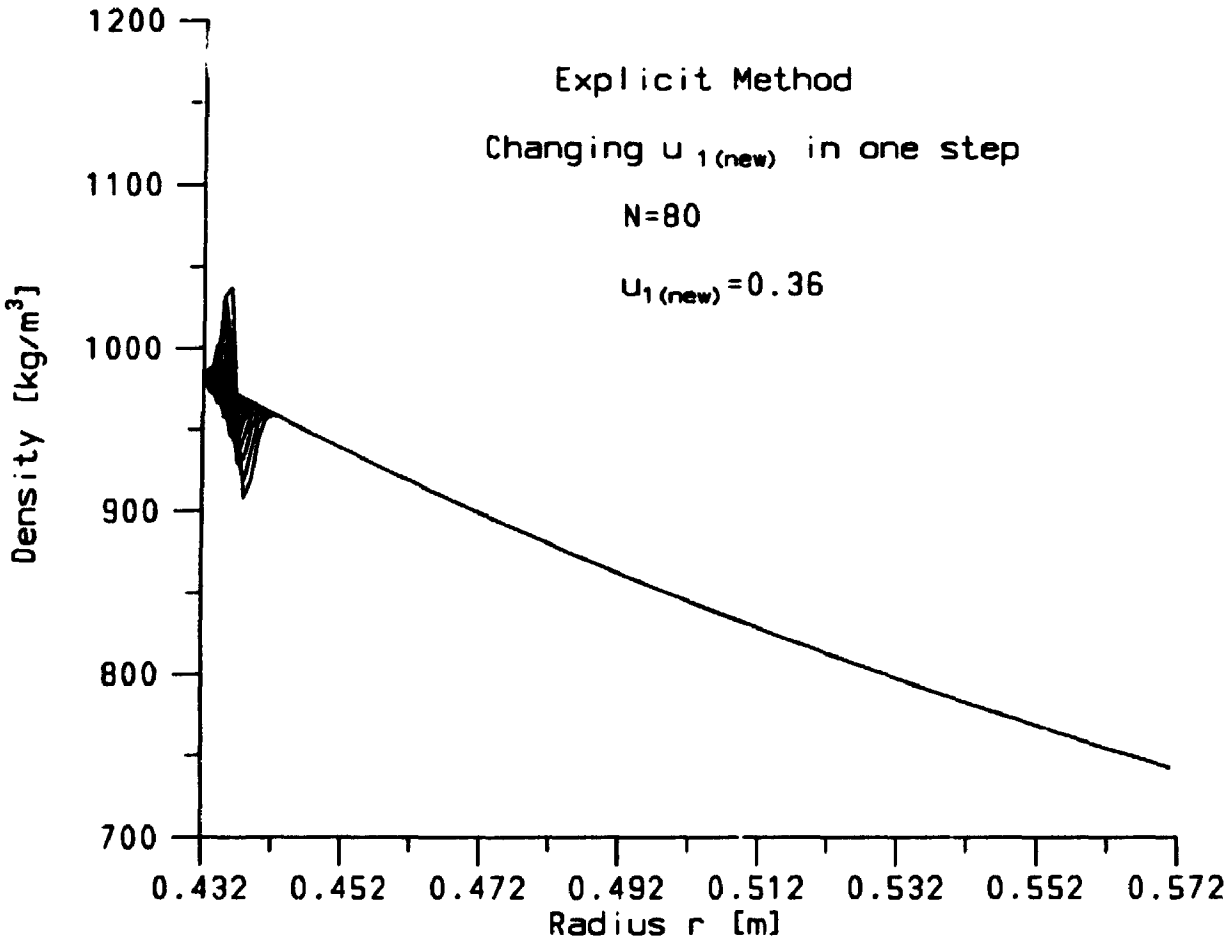

Figure A.4: Dynamic state simulation using explicit numerical scheme with $u_1 = 0.39$ changed to $u_{1new} = 0.36$ in one step.

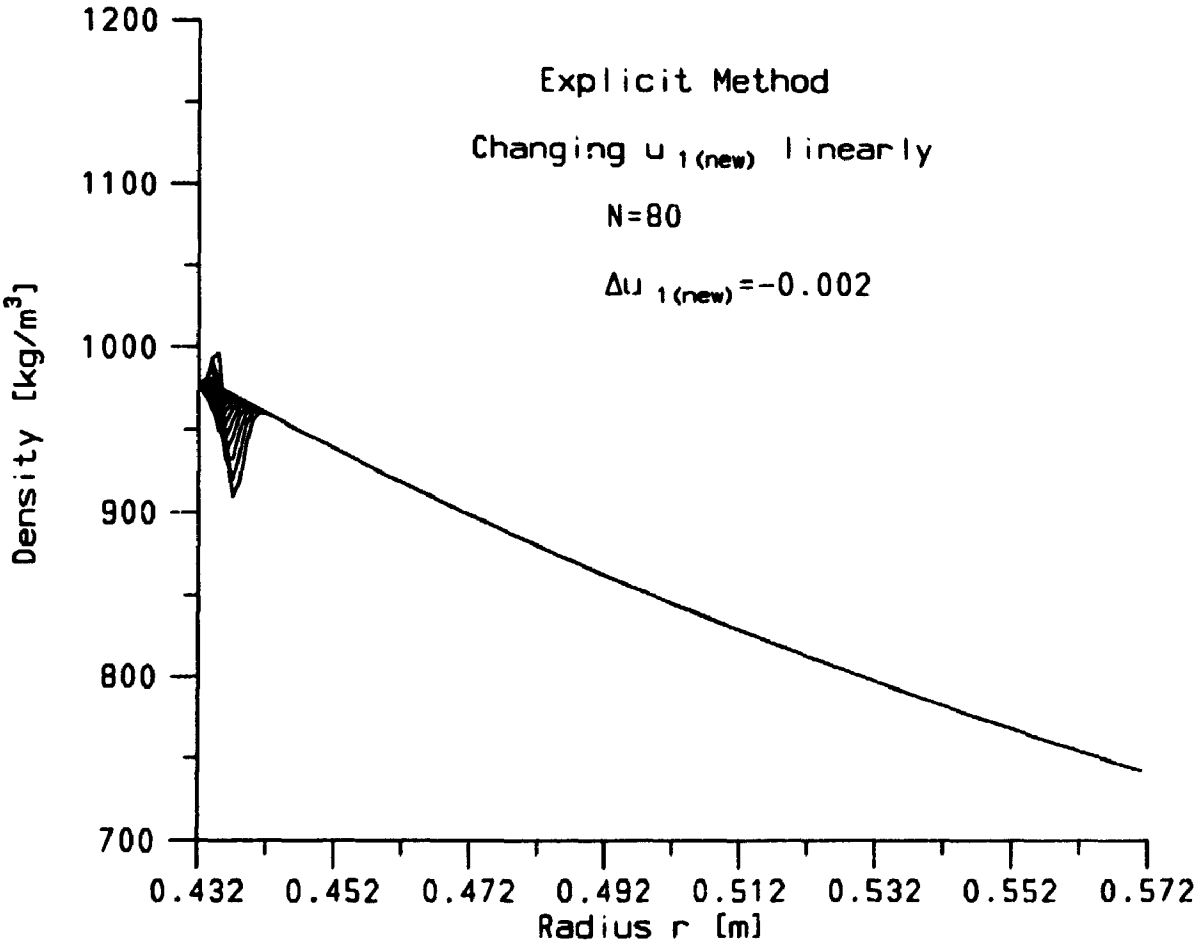

Figure A.5: Dynamic state simulation using explicit numerical scheme with $u_1 = 0.39$ changed to $u_{1,new} = 0.23$ linearly.

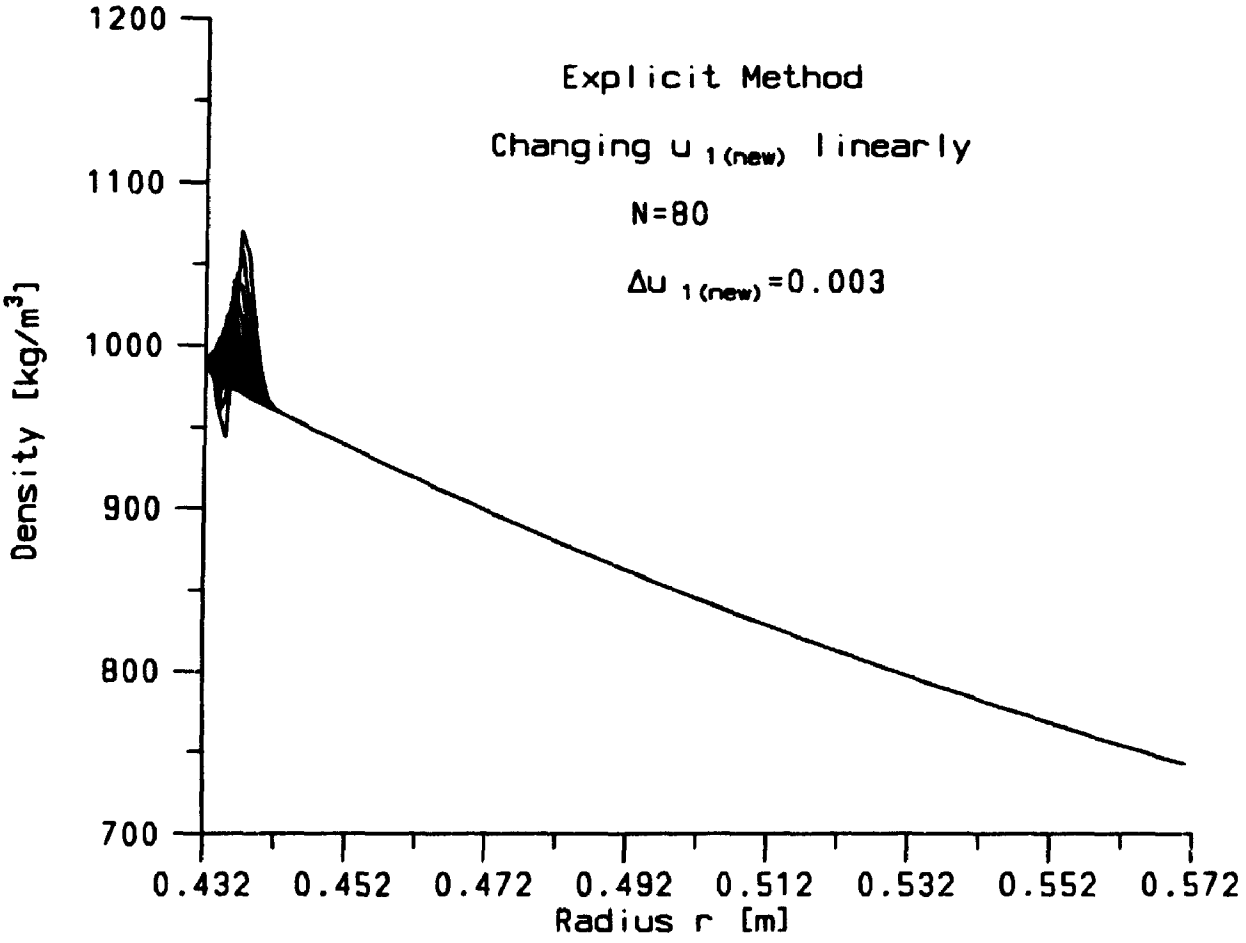

Figure A.6: Dynamic state simulation using explicit numerical scheme with $u_1 = 0.39$ changed to $u_{1new} = 0.63$ linearly.

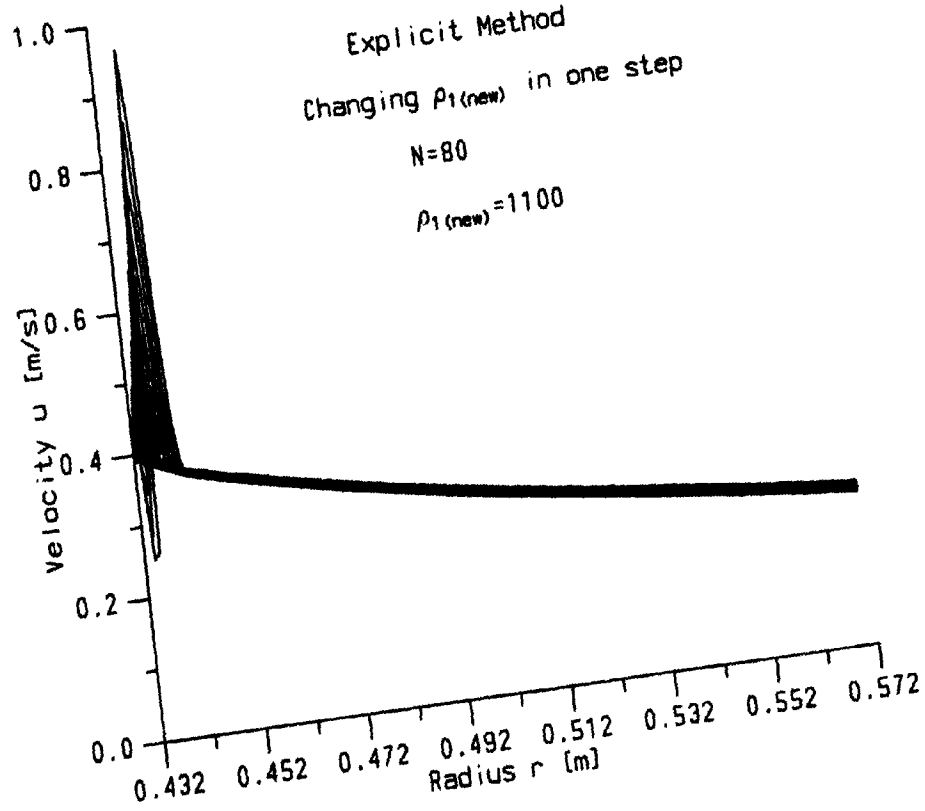

Figure A.7: Dynamic state simulation using explicit numerical scheme with $\rho_1 = 982$ changed to $\rho_{1new} = 1100$ in one step.

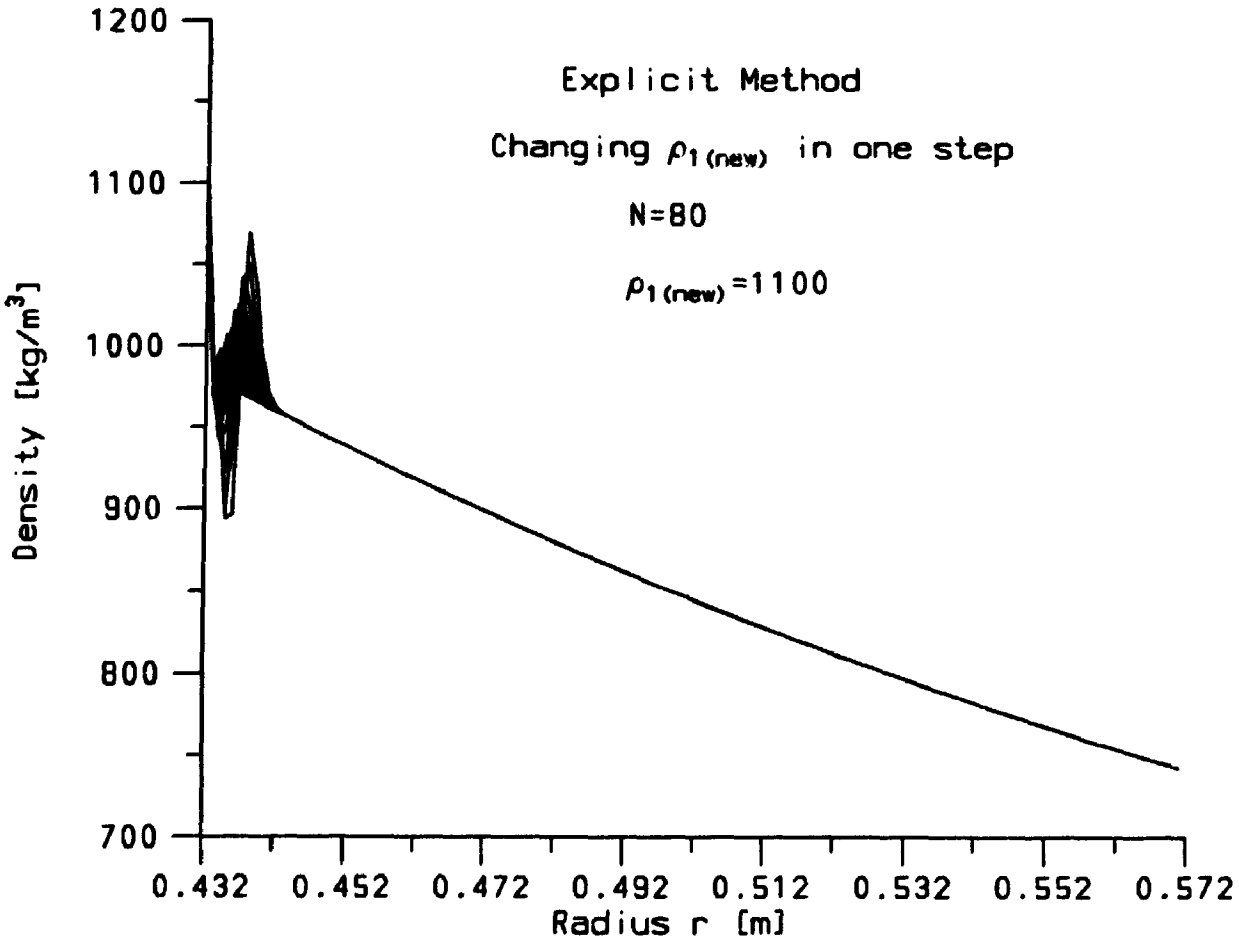

Figure A.8: Dynamic state simulation using explicit numerical scheme with $\rho_1 = 982$ changed to $\rho_{1new} = 1100$ in one step.

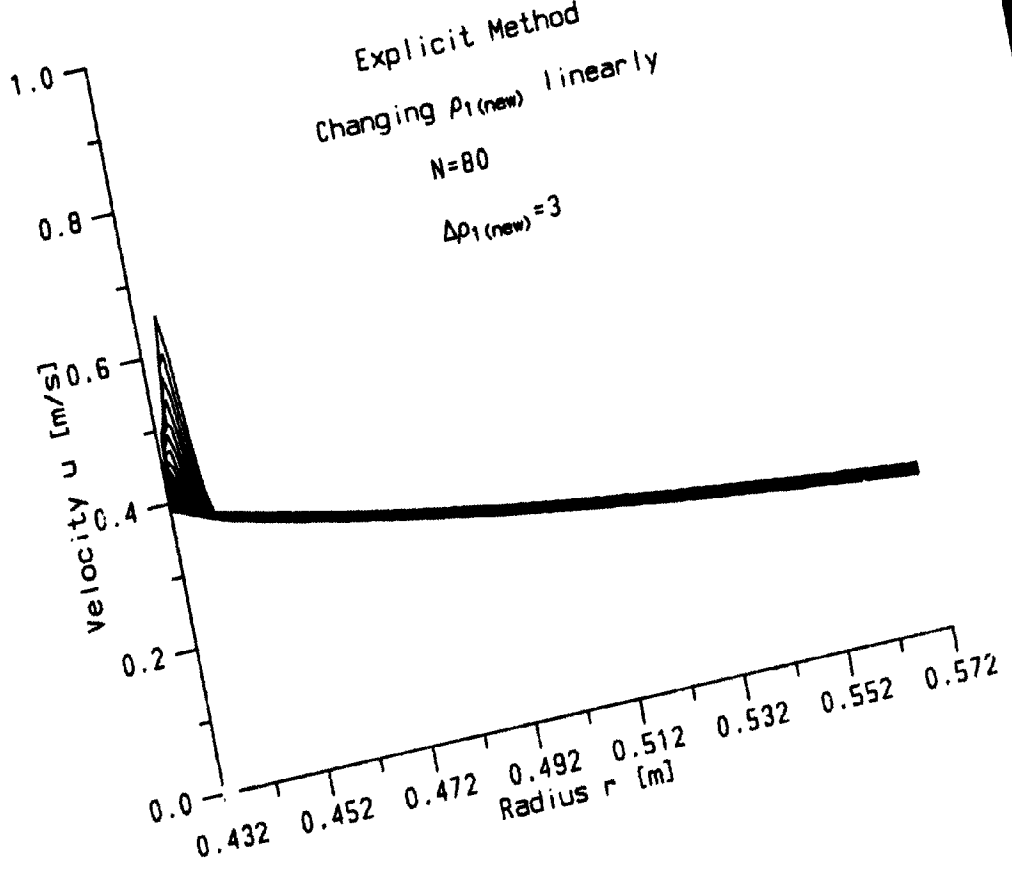

Figure A.9: Dynamic state simulation using explicit numerical scheme with $\rho_1 = 982$ changed to $\rho_{1new} = 1222$ linearly.

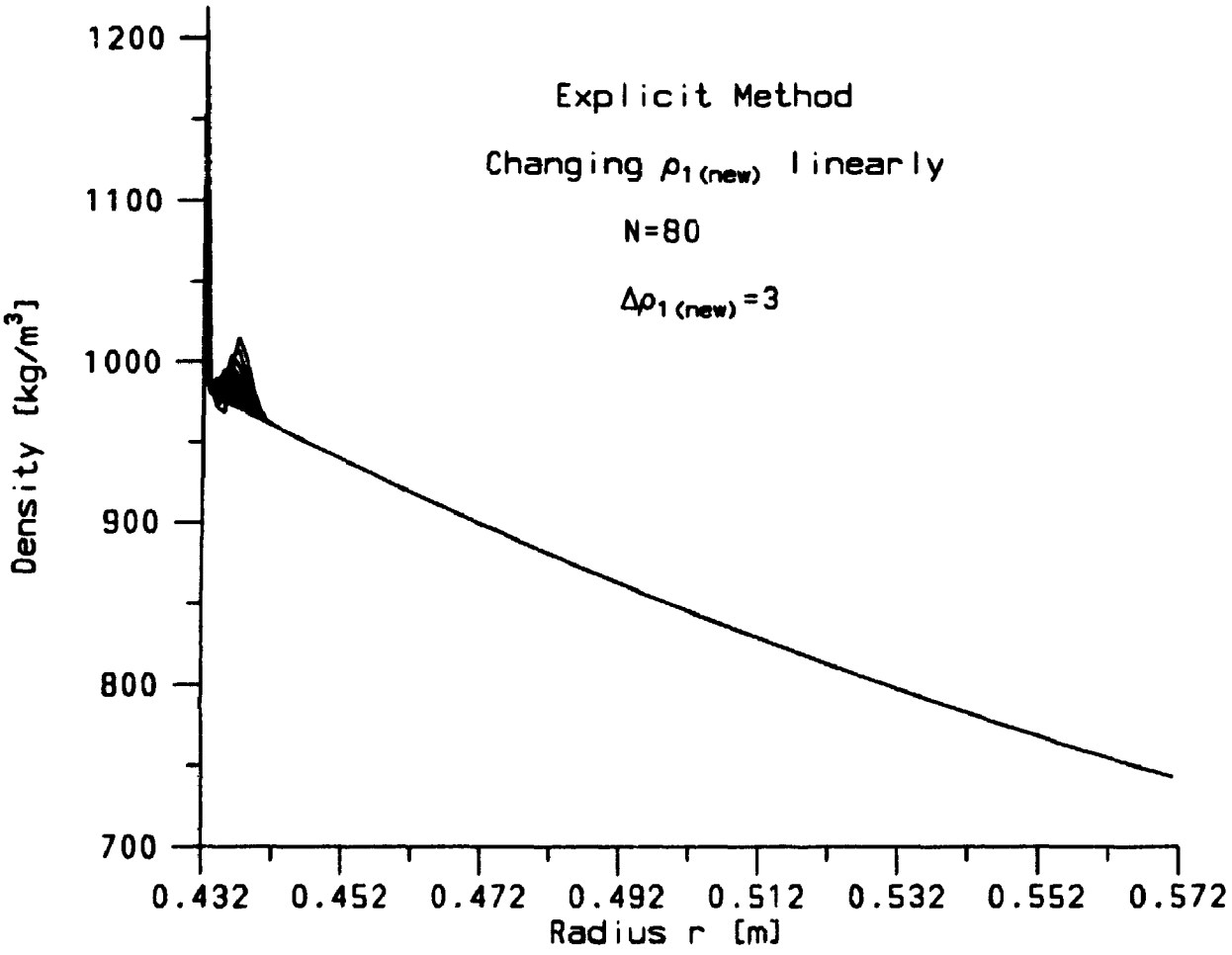

Figure A.10: Dynamic state simulation using explicit numerical scheme with $\rho_1 = 982$ changed to $\rho_{1new} = 1222$ linearly.

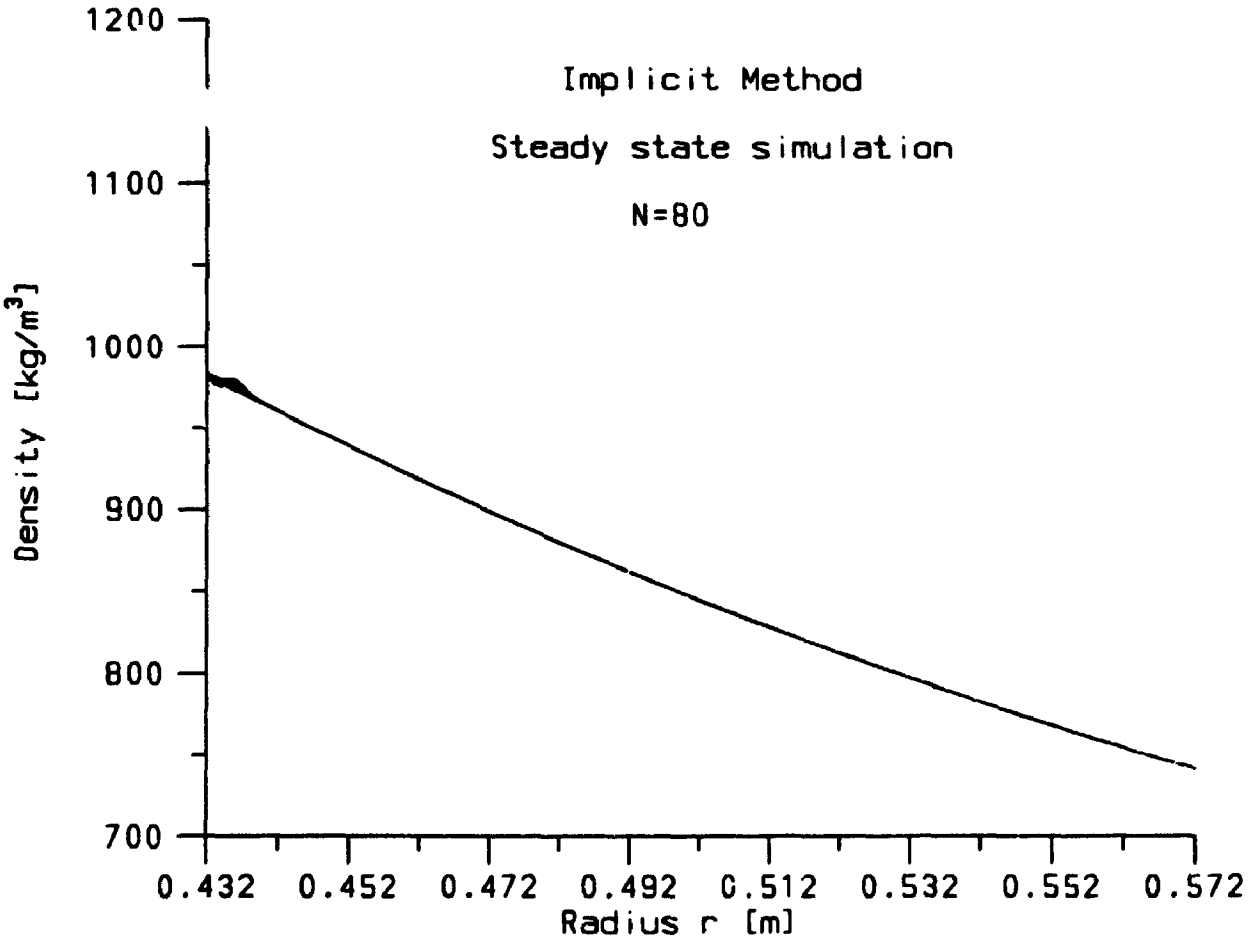

Figure A.11: Steady state simulation using implicit numerical scheme with total number steps $N = 80$.

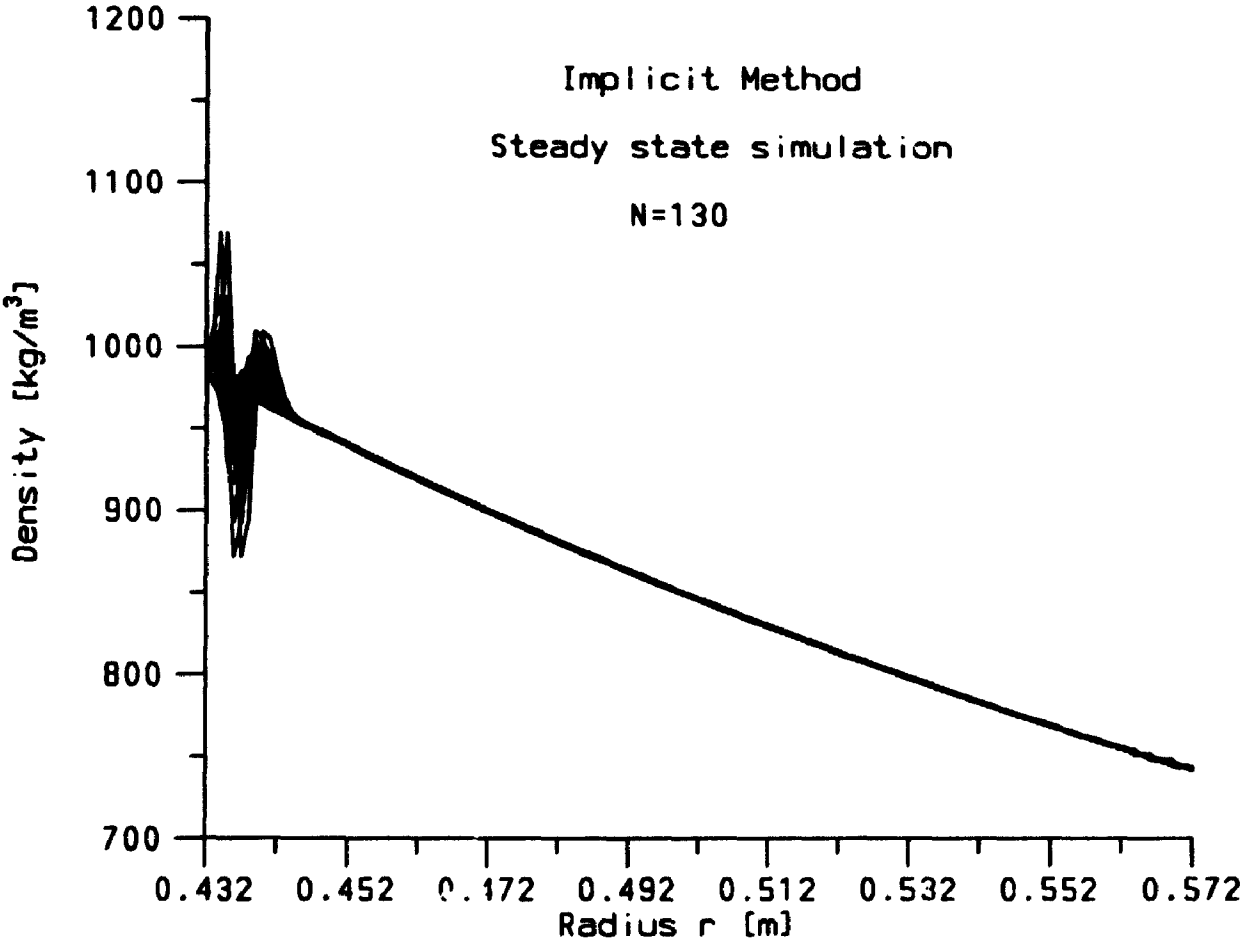

Figure A.12: Steady state simulation using implicit numerical scheme with total number steps $N = 130$.

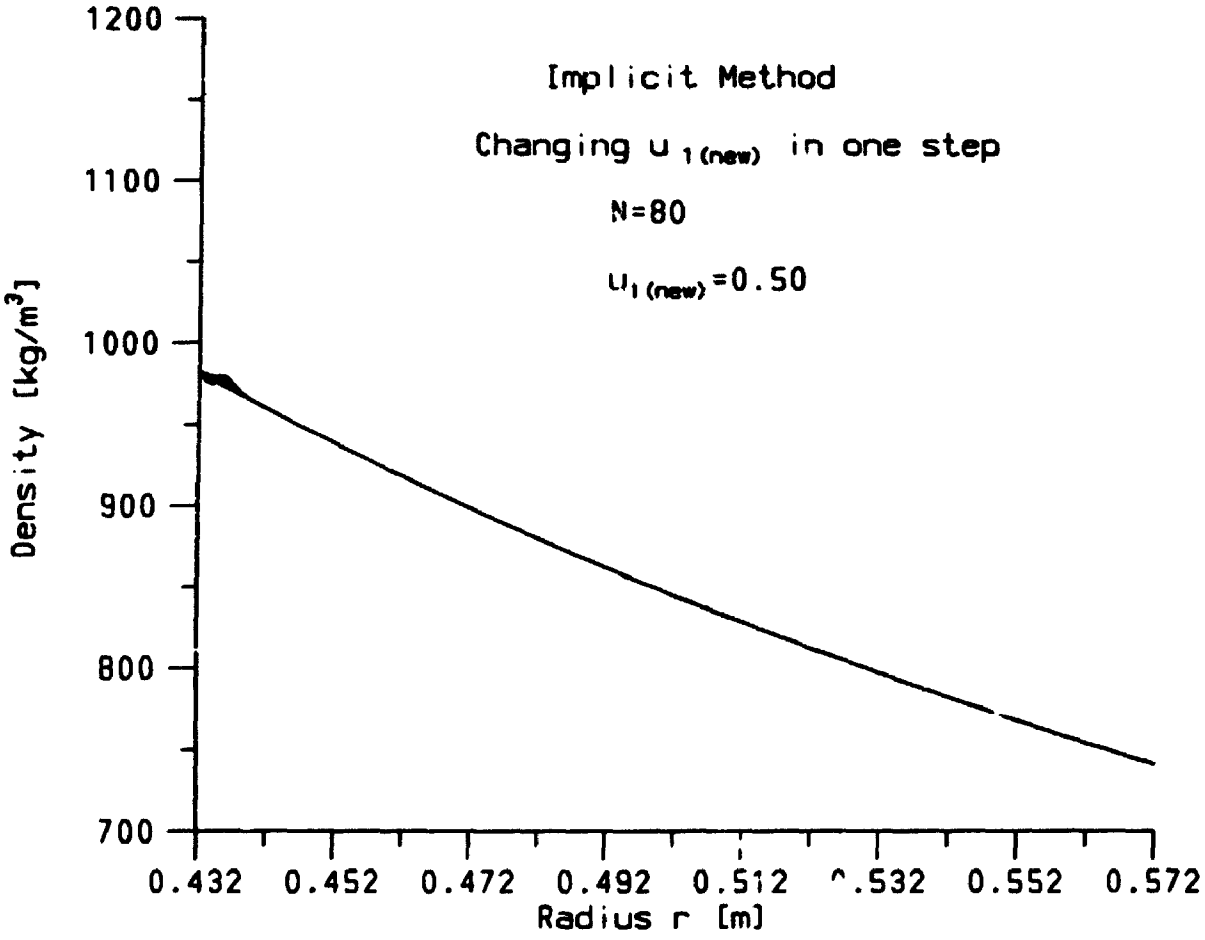

Figure A.13: Dynamic state simulation using implicit numerical scheme with $u_1 = 0.39$ changed to $u_{1new} = 0.50$ in one step.

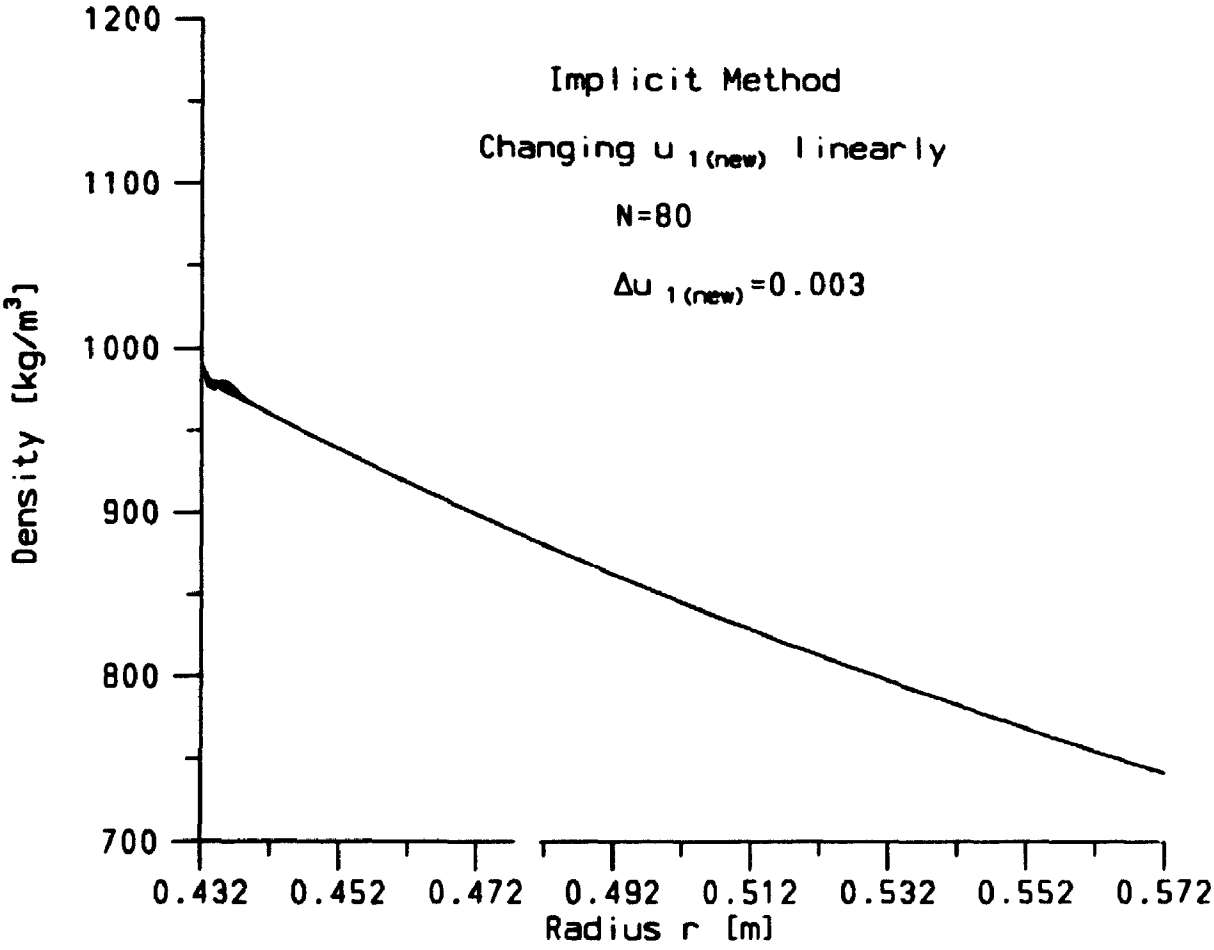

Figure A.14: Dynamic state simulation using implicit numerical scheme with $u_1 = 0.39$ changed to $u_{1new} = 0.63$ linearly.

Appendix B

Definition of Pulp Flocs

The definition of a pulp floc is based on a number of observations, some general and some specific to refiner mechanical pulping. Since the division of a spatial distribution of fibres into entities called flocs must contain some uncertainty, it is important to note at the outset that the results reported in this thesis are insensitive to the exact definition used. Thus the model would give similar results if a different definition resulted in twice as many flocs of half the average size. Simple observations can be made without special equipment that suggest the existence of flocs in pulp. If one observes pulp collected from refiners, it forms clumps spontaneously. A handful of pulp is similar to a mass of cotton-wool balls. The clumps observed are much larger than the floc sizes proposed in the thesis, but they illustrate the tendency of pulp fibres to entangle and form clumps.

The high-speed photographs and films of pulp inside a refiner show pulp that is very sparsely distributed. Visual inspection of the pictures shows easily identifiable regions of high fibre concentration that are well separated from each other. The situation is quite different from the virtually continuous distribution of pulp that is found outside the refiner. Therefore the division of pulp into flocs is much more straightforward and unambiguous than in other situations. As a result of these observations, flocs are defined as collections of pulp fibres that satisfy the following conditions.

1. The fibres occupy a finite volume.

2. A simple convex surface, roughly spherical with a radius of 1–2 mm, can be drawn around the floc such that it contains almost all of the fibres. Because

of the dilute nature of the pulp in the refiner, it is usually the case that the surface does not cut any pulp fibres, but it is not an important exception if a particular collection of fibres is separated into two flocs with only a few fibres joining them. Clearly, this definition will result in flocs having a distribution of sizes. For the model described in this thesis, a single size was used. This simplification, as noted above, does not materially affect the predictions.

3. Although not necessarily permanent, a floc must retain its identity for a finite period of time, such time period being determined by the application of the apparatus that the pulp is subjected to.

4. The floc must exhibit some degree of coherence. In other words, there must exist forces with which the floc resists rupture, and change of shape.

We determine the floc properties mainly by using experimental observations and the physical restraints of refining zone geometry. For example, the size of pulp flocs in disc refiners was estimated by examining the high-speed video frames and drawing contours around coherent, isolated clumps of pulp. Usually, we found that they are of the order 1–3 mm. Also the maximum size of pulp flocs was limited by refining zone local conditions such as the bar width of refiner plates (typically 3 mm). The time scale for the identify of pulp flocs was estimated by observing that they persist at least for one bar passage during refining. This period of time translates about the order of 10^{-4} s for a typical industrial disc refiner. The coherence of the pulp flocs has also been measured experimentally by Martinez [54] using a single-bar laboratory disc refiner.

Appendix C

Calculation of Amount of Pulp in the Gap

Suppose the throughput of a typical refiner is Q t/d (or kg/s). For example, from Table I of Reference [22] for a 45-1B refiner, the throughput is $Q = 36$ t/d (or 0.416 kg/s). From either Reference [25] or [24] we can estimate the residence time in a refiner, which we denote by T seconds. An estimate for T is obtained by using Reference [25] to calculate the average pulp radial velocity for the refiner, obtaining $u = 0.3$ m/s, and thus giving $T = 0.43$ s. The quantity of wood in the refiner must therefore be greater than QT kg. A similar method was used to estimate residence time from the amount of wood in a refiner by May *et al.* [46]. The volume available between the plates is approximately $V = \pi(r_2^2 - r_1^2)g$ (where g is gap width) and so if all the pulp were there, the pulp density would be QT/V provided that water and steam do not take additional space (if they do, the pulp density would be even higher than QT/V). For the example we have been using, the volume is $V = \pi(0.572^2 - 0.432^2)0.15 \times 10^{-3} = 6.6 \times 10^{-5}$ m^3. Thus the pulp density is $QT/V = 2.71 \times 10^3$ kg/m^3 which is about three times higher than the density expected for pulp in this range of consistencies [55]. The pulp density would be even higher if we took into account the fact that the space between the plates is not fully covered by pulp. Stationwala *et al.* [49] reported that bar coverage in an industrial refiner could range from 50% to 85% for different refiner radial positions.

REFERENCES

[1] Smook, G. A., *Handbook for Pulp & Paper Technologists*, 1982.

[2] Rydholm, S. A., *Pulping Process*, 1st Ed., Interscience, 1959.

[3] Casey, J. P., *Chemistry and Chemical Technology*, Vol.1, 3rd. Ed., 1980.

[4] Atack, D., "The Current Status of Mechanical Pulping", Preprints, *Seventh Invitation Symposium*, Oct., 1983, Canberra, Australia, No.11.

[5] Leask, R. A., *Pulp and Paper Manufacture*, Vol.2, 3rd. Ed., 1987.

[6] Keays, J. L. and Leask, R. A., "Refiner Mechanical Pulp - Past Present and Potential", *Paper Trade Journal*, 157(35): p.20-29, 1973.

[7] Nordman, L., Levlin, J. E., Makkonen, T. and Jokisalo, H., "Conditions in an LC-refiner as Observed by Physical Measurements", Preprints, *International Symposium on Fundamental Concepts of Refining*, Appleton, Wis., USA, Sept. 1980, p.121.

[8] Wultsch, F and Flucher, W., *Papier*, 12(1958):13/14, p.334-342.

[9] Konachi, T. and Young, J. H., Preprints, *International Symposium on Process Control*, CPPA Technical Section, Vancouver, BC, Canada, May 1977, p.24-30.

[10] Rance, H. F., Proceedings, *In Symposium on Beating*, Technical Section of the British Paper & Board Makers' Associations, 32(1951):2, p.360-370.

[11] Stationwala, M. I., Atack, D., Wood, J. R., Wild, D. J. and Karnis, A., "The Effect of Control Variables on Refining Zone Conditions and Pulp Properties", Preprints, *1979 International Mechanical Pulping Conference*, Toronto, Ont., Canada, p.93-109.

[12] Jack., J. S., Mills, C. and Baas, P. H., "A Device for Detection and Prevention of Plate Clash in Disc Refiners", *Pulp and Paper Canada*, 82(9): T311-314, 1981.

[13] Leider, P. A. and Nissan, A. H., *Tappi*, 60(1977):10, p.85-89.

[14] Maslakov, V. G., "Some Features of Bar Filling Action on Fibres During Refining", Preprints, *the Soviet-Finnish Symposium of Fundamental Research in the Field of Cellulose Fibre Beating*, Moscow, Jan. 1978, p.7.

[15] Lewis, J. and Danforth, D. W., *Tappi*, 45(1962):3, p.185-188.

[16] Banks, W. A., *Paper Technology*, 8(1967):4, p.363-369.

[17] Clark, J. d'A., *Pulp Technology and Treatment for Paper*, Miller Freeman Publns. Inc., San Francisco, 1978, p.752.

[18] Atack, D. and May, W.D., "Mechanical Reduction of Chips by Double-disc Refining", *Pulp Paper Mag. Can.*, 64(1963):C, T75.

[19] Strand, B. C. and Hartler, N., "Modelling and Optimization of Full Scale Chip Refining", Preprints, *International Mechanical Pulping Conference*, 1985, Stockholm, Sweden, p.46.

[20] Dana, H. K., May, W. D., Miles, K. B. and Newman, B. G., "A Study of Steam Flows and Self-pressurization in Chip Refiners", *Transactions of Technical Section of CPPA*, Vol.1, No.3:p.82-88, Sept. 1975.

[21] Miles, K. B., Dana, H. K. and May, W. D., "The Flow of Steam in Chip Refiners", Preprints, *International Symposium on Fundamental Concepts of Refining*, 1980, Appleton, Wis., USA, p.30.

[22] Newman, B. G., Stationwala, M. I. and Atack, D., "Analysis of Steam Flow in Disc Refining", Preprints, *International Mechanical Pulping Conference*, 1985, Stockholm, Sweden, p.60.

[23] Aarni, I. and Virkkunen, J., "Modelling and Simulation of the Thermomechanical Pulping Process", Proceedings, *4th International IFAC Conference on Instrumentation and Automation in the Paper, Rubber, Plastics and Polymerization Industries*, June 1980, p.219-226.

[24] Miles, K. B. and May, W. D., "The Flow of Pulp in Chip Refiners", *Journal of Pulp and Paper Science*, Vol.16(1990), No.2, J63-72.

[25] Fan, X., "Material Flow in a Wood-chip Refiner", Chapter 4, *M. Eng. Thesis*, McGill University (1988), Montreal, Canada.

[26] Guthrie, W. E., "An Apparent Viscosity for Use in the Application of Reynolds Numbers to the Flow of Dilute Pulp Suspensions", *Tappi*, Vol.42, No.3(1959): p.232-235.

[27] Fox, T. S., Brodkey, R. S. and Nissan, A. H., "Inside a Disk Refiner", Proceedings, *Papermakers Conference*, Chicago, USA, April 6-8, 1981, II, p.135-149.

[28] Atack, D., "Towards a Theory of Refiner Mechanical Pulping", *Appita*, 34(3): p.223-227, 1980.

[29] Atack, D., Stationwala, M. I. and Karnis, A., "What Happens in Refining - Part I", *Pulp Paper Mag. Can.*, 85(12):p.119, 1984.

[30] Colton, D., *Partial Differential Equations, An Introduction*, 1st. Ed., The Random House/Birkhäuser Mathematics Series, New York, 1988, p.92.

[31] Whitham, G. B., *Linear and Nonlinear Waves*, John Wiley & Sons Inc., 1974, p.113-117.

[32] Coulson, C. A. and Jeffrey, A., *Waves*, 2nd. edition, Longman Mathematical Textes, 1977, p.178-188.

[33] Ames, W. F., *Numerical Methods for Partial Differential Equations*, 1st. edition, NELSON, 1969, p.180-184.

[34] *Ibid*, p.209-212.

[35] Ames, W. F., *Nonlinear Partial Differential Equations in Engineering*, Academic Press Inc., 1965, p.437-448.

[36] Jeffrey, A. and Taniuti, T., *Nonlinear Wave Propagation*, Academic Press Inc., 1964, p.65-71.

[37] *Ibid*, p.141-148.

[38] Courant, R., Isaacson W. and Rees, M., "On the Solution of Nonlinear Hyperbolic Difference Equations by Finite Differences", *Communications of Pure & Applied Mathematics* 5(1952), p.243-255.

[39] Jeffrey, D. J., "Plotting Subroutines in Fortran", *unpublished work*, Department of Applied Mathematics, The University of Western Ontario, Canada, 1992.

[40] Hoffman, J. D., *Numerical Methods for Engineers and Scientists*, Mcgraw-Hill, Inc., 1992, p.42-46.

[41] VonNeuwmann, J. and Richtmyer, R. D., "A Method for the Numerical Calculation of Hydrodynamic Shocks", *Journal of Applied Physics*, Vol.21(1950), p.232.

[42] Arjas, A., "Residence Time Distribution in Conical Refiners and Refining Systems", Preprints, *International Symposium on Fundamental Concepts of Refining*, Appleton, WI, USA, Sept. 1980, p.8-20.

[43] Groome, E. J. and Gerhardt, T. D. , "Fiber Retention Time in a Disc Refiner", *ibid*, p.21-29.

[44] Arjas, A., "Influence of Residence Time Distribution on Pulp Properties", *ibid*, p.139-148.

[45] Fox, T. S., "Inside a Disk Refiner", *ibid*, p.281-313.

[46] May, W. D., Mcrae, M. R., Miles, K. B. and Lunan, W. E., "An Approach to the Measurement of the Residence Time in a Chip Refiner", *Journal of Pulp and Paper Science*, 14(3), J47-52, 1988.

[47] Stationwala, M. I., Miles, K. B. and Karnis, A., "The Effect of First-Stage Refining Conditions on Pulp Properties and Energy Consumption", *Journal of Pulp and Paper Science*, 19(1), J12-18, 1993.

[48] Miles, K. B., Lunan, W. E. and May, W. D., "Abrasive-Filled Refiner Plates in Thermomechanical Pulping", *Journal of Pulp and Paper Science*, 15(2), J66-71, 1989.

[49] M. I. Stationwala, D. Atack and A. Karnis, "Distribution and Motion of Pulp Fibres on Refiner Bar Surface", *Journal of Pulp and Paper Science*, 18(4), J131-137, 1992.

[50] Atack, D., Stationwala, M. I., Huusari, E., Ahlqvist, P., Fontebasso, J. and Perkola, M., "High Speed Photography of Pulp Flow Patterns in a 5MW Pressurized Refiner", *Paperi ja Puu* 6:p.689-695, 1989.

[51] Miles, K. B. and May, W. D., "Predicting the Performance of a Chip Refiner: A Constitutive Approach", Preprints, *International Mechanical Pulping Conference*, 1991, p.295-301.

[52] Ouellet, D and Bennington, C. P. J., *Unpublished Work*, Pulp and Paper Centre, University of British Columbia, Canada, 1993.

[53] Miles, K. B., "A Simplified Method for Calculating the Residence Time and Refining Intensity in a Chip Refiner", *Paperi ja Puu*, 73(1991):9, p.852-857.

[54] Martinez, D. M., *Ph.D. Thesis*, Pulp and Paper Centre, The University of British Columbia, Canada, submitted on June 1994.

[55] *Engineering Data Sheet Z-1*, Technical Section, CPPA, 1970.

[56] Mcleod, A. I., "Efficient Fortran Coding of a Random Number Generator", *Technical Report*, Department of Statistical and Actuarial Sciences, The University of Western Ontario, Canada, Nov. 1982.

[57] Mcleod, A. I., "A Remark on Algorithm AS 183. An Efficient and Portable Pseudo-random Number Generator", *Applied Statistics*, Vol.34, No.2, p.198-200, 1985.

[58] Wichmann, B. and Hill, I. D., "Algorithm AS 183. An Efficient and Portable Pseudo-random Number Generator", *Applied Statistics*, Vol.31, p.188-190, 1982.

[59] Fournier, M., Ma, H., Shallhorn, P. M. and Roche, A. A., "Control of Chip Refiner Operation", *Journal of Pulp and Paper Science*, 18(5), J182-187, 1992.

[60] Fan, X., Jeffrey, D. J. and Ouellet, D., "A Stochastic Model for the Residence Time of Pulp in a Single Disc Chip Refiner", *Journal of Pulp and Paper Science*, 20(11), J343-349, 1994.

[61] Kerekes, R. J., "Characterization of Pulp Refiners by a C-factor", *Nordic Pulp & Paper Research Journal*, No.1, 5(1990): p.3-8.

[62] Miles, K. B., "Refining Intensity and Pulp Quality in High Consistency Refining", *Paperi ja Puu*, 5(1990):p.508.

[63] Fan, X., Jeffrey, D. J. and Stanford, D., "Analysis of a Pulping Process: Non-monotonic Characteristics", paper submitted to *Information Systems and Operations Research: INFOR* on May 1994.

[64] Bennington, C. P. J.. Kerekes, R. J. and Grace, J. R., "The Yield Stress of Fibre Suspensions", *The Canadian Journal of Chemical Engineering*, Vol.68(1990), p.748-756.

[65] Dumont, G. A., Legault, N. D. and Rogers, J. H., "Computer Control of a TMP Plant", Preprints, *International Mechanical Pulping Conference*, Oslo, June 16-19, 1981, Session III, No.1, p.1-19.

[66] Franzen, R. and Sweitzer, R., "Refining Forces in High Consistency Refining", Proceedings, *Northeast Regional Conference*, Boston, MA, USA, March 27, 1980, p.314-323.

[67] Press, W. H., Flannery, B. P., Teukolskey, S. A. and Vetterling, W. T., *Numerical Recipes*, FORTRAN Version, Cambridge University Press(1990), p.86-89.

[68] Bank, W. A., "Design Consideration and Engineering Characteristics of Disc Refiners", *Paper Technology*, Vol.8, No.4(1967), p.363-369.